UNIVERSITY OF NOVA GORICA
GRADUATE SCHOOL

ASPECTS OF MICRO BLACK HOLE EVAPORATION

DISSERTATION

Saeede Nafooshe

Mentor: prof. dr. Martin O'Loughlin

Nova Gorica, 2015

UNIVERZA V NOVI GORICI
FAKULTETA ZA PODIPLOMSKI ŠTUDIJ

ASPEKTI IZHLAPEVANJA MIKROSKOPSKIH ČRNIH LUKENJ

DISERTACIJA

Saeede Nafooshe

Mentor: doc. dr. Martin O'Loughlin

Nova Gorica, 2015

Abstract

Considering the existence of the large extra dimensions, creation of the micro black holes during the high energy collisions is unavoidable. Having formed in these kind of process, these tiny objects won't have chance to live for long and they evaporate instantly after formation. Different aspects of evaporation of micro black holes have been discussed in this dissertation.

In this dissertation we reviewed the importance of the grey-body factors as well as the existing techniques for their derivation. We also investigated an alternative way for calculation of the grey-body factors which simplifies the wave equations drastically and gives us the opportunity to have analytical form of these factors even in the high energy ranges. We used the large-D limit of general relativity to calculate the graviton grey body factors for a non-rotating micro black hole and we found exactly the same analytical expression for tensor and vector type gravitational perturbations as it was in the literature. We also investigated the properties of possible signals of micro black hole decay that might be seen in the detectors using most recent Monte-Carlo micro black hole event generators.

We investigated the wave equations of a perturbed dynamical space time, out-going Vaidya space-time with linear mass function, in details. Using both numerical and analytical techniques we calculated the quasi-normal modes of an evaporating black hole in the out-going Vaidya background.

Keywords: micro black holes, evaporation, gravitons, grey-body factors, large dimensions, quasi-normal modes,Vaidya metric

Povzetek

Nastanek mikroskopskih črnih lukenj pri visokoenergijskih trkih je, ob upoštevanju velikih dodatnih dimenzij, neizogiben. Tako nastale mikroskopske črne luknje so kratkožive in izhlapijo takoj po svojem nastanku. V tej disertaciji smo obravnavali različne vidike njihovega izhlapevanja.

V sklopu disertacije smo pregledali pomen faktorjev sivih teles, kot tudi že obstoječe načine njihove izpeljave. Pri tem smo raziskali alternativni način za njihov izračun, kar drastično poenostavi valovne enačbe in omogoča analitično izpeljavo faktorjev pri visokih energijah. Pri izračunu faktorjev sivih teles za primer nevrteče mikroskopske črne luknje smo uporabili večdimenzijsko limito splošne relativnosti, tako imenovano veliko-D limito, ter pri tem našli povsem enake analitične izraze za tenzorsko in vektorsko gravitacijsko motnjo, kot ju zasledimo v literaturi. Prav tako smo raziskali lastnosti morebitnih detektorskih signalov razpada mikroskopskih črnih lukenj z uporabo najsodobnejših Monte-Carlo generatorjev dogodkov črnih lukenj.

Podrobno smo raziskali valovne enačbe dinamičnega perturbiranega prostor-časa izhodni Vaidya prostor-čas z linearno masno funkcijo. Z uporabo numeričnih in analitičnih metod smo izračunali kvazinormalne načine izhlapevanja črnih lukenj v izhodnem Vaidya ozadju.

Ključne besede: mikroskopske črne luknje, izhlapevanje, gravitoni, faktor sivega telesa, visokodimenzionalni prostori, kvazinormalna stanja, Vaidya metrika

To my parents

Acknowledgements

Throughout my studies at University of Nova Gorica, there have been many people who have supported me kindly, for which I am very grateful. First I would like to thank my supervisor, prof.dr. Martin O'Loughlin, without whom, this research would not end to the place that has ended today. During my studies, he has provided valuable guidance and advices, and I have learned much from him. Next, I would like to thank my family and friends for being there during the good times and the bad, and for always standing by my side. I would like to thank the office staff as well as Astroparticle physics laboratory members for the information and support that they have continuously provided. I also thank the members of my defense committee for reading this dissertation. I would like also to thank the Slovenian Research Agency for their financial support.

Contents

List of Figures

1

Introduction

1.1 Motivations for physics beyond the Standard Model

The effort of thousands of physicists over time has resulted in a remarkable insight into the fundamental structure of matter. The Standard Model (SM) of particle physics explains how the building blocks of matter interact. All interactions are governed by four force; the electromagnetic, strong, weak and gravitational forces. The SM includes all of these forces and all their carrier particles except gravity. Gravity, the most familiar force in our everyday lives, is not part of the SM because to describe the interactions between particles at very high energies of the order of Planck mass, $M_{Pl} \sim 10^{16}$ TeV, a theory of quantum gravity is required. While the SM is an effective field theory that is valid up to some certain energy scale, $M_{EW} \sim 1$ TeV. There are also some other issues like dark matter and dark energy, matter-antimatter asymmetry, neutrino masses and the quantum instability of the Higgs mass that cannot be explained in the context of the SM. The study of physics Beyond the Standard Model (BSM) is motivated by the desire to have a more complete fundamental model.

The main theme of this dissertation is the study of the final stages of tiny black holes evaporation. These tiny black holes are hypothetical black holes that can be classified in two different families. The astrophysical black holes with masses much smaller than the solar mass belong to the first family and micro black holes

(μBH) can make the second family. Regarding the μBHs, our will be on the study of the grey-body factors. Moreover by study the quasi-normal modes of an evaporating black hole we will provide a strong reason for the validity of a new model for the end point of black hole evaporation. This latter scenario can be applicable to any type of black hole including the tiny astrophysical black holes that might be evaporating in our era.

1.2 General relativity and Einstein equations

In general relativity, in contrary with Newtonian mechanics, space and time are not absolute concepts. In a given system, space-time is related to the matter distribution on that system. In other word details of the space-time that is encoded in the metric are determined by this matter content. The relation between the matter content and the geometry of the space-time is given by the Einstein equations,

$$R_{\mu\nu} - \frac{1}{2}Rg_{\mu\nu} = 8\pi G T_{\mu\nu}. \tag{1.1}$$

where $R_{\mu\nu}$ is Ricci tensor and R is Ricci scalar. The geometry of the space-time is described by the metric $g_{\mu\nu}$, all the information related to the geometry and casual structure of the space-time is encoded in it. $T_{\mu\nu}$ is the energy momentum tensor that describes the amount of mass-energy at a given event. Finally, G is Newton's constant in four dimensions and it determines the strength of the gravitational coupling.

It is possible to define a surface gravity, κ, for black holes that are the solutions of (1.1). Recalling that the event horizon is a Killing horizon, which means the null horizon generators are orbits of a Killing field, χ^a, then κ can be defined as the magnitude of the gradient of the norm of the horizon generating χ^a, evaluated at the horizon

$$\kappa^2 = -(\nabla^a|\chi|)(\nabla_a|\chi|). \tag{1.2}$$

Equivalently one can say that the surface gravity is the magnitude of the acceleration of a stationary particle with zero angular momentum just outside the

horizon. This is the same as the force per unit mass that must be applied at infinity in order to hold the particle on its path. For a given energy-momentum tensor one can use equation (1.1) to find the solutions for the corresponding metric.

1.2.1 Black holes in 4 dimensions

In this section we discuss three different solutions to the Einstein equations upon which the major part of discussion of black hole physics fundamentally depends. These solutions are the vacuum solutions to the Einstein equations. Study of these solutions may give us a general overview of black hole physics. The First solution is vacuum solution for $T_{\mu\nu} = 0$ which is called Schwarzschild solution. Next solution is when the source of radiation, energy-momentum, is electromagnetic source. This solution is called Reissner-Nordstrom solution. The last one that we discus here is the Kerr vacuum solution, which models space-time outside a rotating body such as a star or a black hole.

1.2.1.1 Schwarzschild solution

A few months after publishing the Einstein equations in 1916, Karl Schwarzschild surprised the physics community by publishing the first non-trivial exact solution of these equations. This solution describes the gravitational field around a chargeless, static spherically symmetric body with mass M in the Vacuum. Since $T_{\mu\nu} = 0$

$$R_{\mu\nu} - \frac{1}{2}Rg_{\mu\nu} = 0, \tag{1.3}$$

solution to this equation is the Schwarzschild metric

$$ds^2 = -(1 - \frac{r_s}{r})dt^2 + (1 - \frac{r_s}{r})^{-1}dr^2 + r^2 d\Omega^2 \tag{1.4}$$

where $d\Omega^2 = d\theta^2 + \sin^2\theta d\varphi^2$ is the line element on the 2-sphere and r_s is the Schwarzschild radius and for $G = c = 1$ this radius is equal to $2M$. This solution is also called Schwarzschild black hole.
By calculating an invariant factor like Kretschmann scalar from Riemann curvature tensor, $R_{\mu\nu\rho\delta}$

$$K_s = R_{\mu\nu\rho\delta}R^{\mu\nu\rho\delta} = \frac{12r_s^2}{r^6} = \frac{48M^2}{r^6} \tag{1.5}$$

One can see that the physical singularity is located at $r = 0$, where the curvature of the space-time becomes infinite; while at $r = r_s$, (1.5) is well behaved [8].
For $r \to \infty$ (1.4) becomes like a flat space-time (Minkowski) solution.

1.2.1.2 Reissner-Nordstrom solution

Reissner-Nordstrom solution is a solution of the Einstein equations with the source that is the stress energy tensor, $T^{em}_{\mu\nu}$, for the electric and magnetic field from a point source.

$$R_{\mu\nu} - \frac{1}{2}Rg_{\mu\nu} = 8\pi G T^{em}_{\mu\nu}. \tag{1.6}$$

with the solution

$$ds^2 = -f(r)dt^2 + f(r)^{-1}dr^2 + r^2 d\Omega^2, \qquad f(r) = 1 - \frac{2M}{r} + \frac{q^2}{r^2} \tag{1.7}$$

where q is the total electric and magnetic charge. This solution describes the geometry of the space-time outside of a spherically symmetric charged body with mass M.
Function $f(r)$ in (1.7) has two roots

$$r_\pm = M \pm \sqrt{M^2 - q^2} \tag{1.8}$$

Considering (1.8) there are three different possibilities:

- If $M^2 - q^2 < 0$, $f(r)$ has no real root. There is a curvature singularity at $r = 0$ that is time-like and it is not protected by an event horizon; these kind of singularities are called "naked singularity". This situation may be unphysical due to the conjecture called *Cosmic Censorship Conjecture* [9]. In terms of this conjecture collapse of physically realistic matter configuration will not form a naked singularity.

- If $M^2 - q^2 = 0$, $f(r)$ has a double zero at $r_+ = r_- = M$. This solution is also known as extreme Reissner-Nordstrom solution and it may look also unphysical because for mass M, it contains maximum amount of charge. Though this case is allowed by the Cosmic Censorship Conjecture, one cannot cross the same horizon in two different directions.

- If $M^2 - q^2 > 0$ $f(r)$ has a two real zero. In this case we have two horizons, inner and outer horizon, and outer horizon ($r_+ > M$) is the event horizon which prevents anything to escape from the inner space.

1.2.1.3 Kerr solution

We know that astrophysical stars as well as young black holes rotate, thus it is interesting to study an axially symmetric object in the empty space-time, $T_{\mu\nu} = 0$, with mass M rotating with angular momentum J. In 1963 Kerr suggested the Kerr metric which is an exact solution to Einstein equations and describes the geometry of the space-time around a rotating uncharged axially symmetric isolated object.

$$ds^2 = -\frac{\rho^2\Delta}{\Sigma}dt^2 + \frac{\Sigma}{\rho^2}\sin^2\theta(d\phi - \Omega dt)^2 + \frac{\rho^2}{\Delta}dr^2 + \rho^2 d\theta^2, \tag{1.9}$$

where

$$\begin{aligned} \Delta &= r^2 - 2Mr + a^2 \\ \rho^2 &= r^2 + a^2\cos^2\theta \\ \Sigma &= (r^2 + a^2)^2 - \Delta a^2 \sin^2\theta \end{aligned} \tag{1.10}$$

with $\Omega = \frac{2Mar}{\Sigma}$ that can be interpreted as angular velocity and $a = J/M$ as oblateness. With the condition $|a| < M$ to avoid naked singularities, by calculating Kretschmann scalar one can see that there is a curvature singularity at $(r = 0; \quad \theta = \pi/2)$ [10]. This metric is independent of the angle ϕ and time t which means this is an stationary axially symmetric solution. The presence of off diagonal terms

$$g_{t\phi} = g_{\phi t} = \frac{-2Mra\sin^2\theta}{\rho^2} \tag{1.11}$$

tells us that there is inertial frame dragging. The frame dragging means that any object (or light) that comes close enough to the black hole will participate in its rotation. The region that this co-rotating effect for radially in-falling objects holds is called ergoregion whose boundary being the so called ergosphere. The speed of the dragging space-time along the direction of black hole rotation may vary with respect to its distance from event horizon. To find the position of this

surface for a stationary observer one needs to calculate where the g_{tt} of the metric is zero

$$r^2 - 2Mr + a^2 \cos^2 \theta = 0. \tag{1.12}$$

Solving the above equation for r leads to

$$r_e(\theta) = M + \sqrt{M^2 - a^2 \cos^2 \theta}, \tag{1.13}$$

and regions with $g_{tt} > 0$ and $g_{tt} < 0$ mark the regions inside and outside of this ergosphere respectively. Any object that comes to this sphere and splits to two parts, may have one part falling into the black hole and the other gaining energy at the expenses of the spin of the black hole. As this object is still outside of the event horizon it may be able to escape and carries the energy away. This process is called Penrose process after Roger Penrose suggested it in 1969. This process can simply be explained using figure(1.1). If a particle falls into the ergosphere

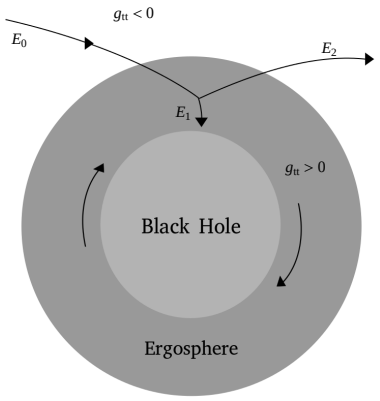

Figure 1.1: The Penrose process

it may split to two particles because of the rotational energy in this region. One of these particles may fall into horizon and the other one travels to infinity. By Momentum conservation

$$p_0 = p_1 + p_2, \tag{1.14}$$

where p is the 4-momentum of the particle and by energy conservation at the point of decay

$$E_0 = E_1 + E_2. \tag{1.15}$$

By considering the Killing vector $\xi_t = (1, 0, 0, 0)$ the energy will be $E = p.\xi_t$. If particle 1 wouldn't fall into event horizon and instead was traveling to infinity then E_1 had to be positive. However inside the ergosphere ($\xi_t.\xi_t = g_{tt} > 0$), which means ξ_t is a space-like vector within the ergosphere. This means that $-E_1$ is a component of spatial momentum inside ergosphere, so it can be positive or negative. If the decay trajectories are arranged such that $E_1 < 0$ then from (1.15) one expect that $E_2 > E_0$, implementing that the particle that crosses the event horizon and falls into black hole adds a negative angular momentum. As a result angular momentum and total energy of the black hole reduces in order to balance the angular momentum and energy that carries away by the particle that escape black hole.

The horizons of the Kerr black hole can be calculated by taking $\Delta \to 0$ which gives us

$$r_\pm = M \pm \sqrt{M^2 - a^2}, \tag{1.16}$$

where r_- marks the Cauchy horizon and r_+ is the event horizon and it is also the surface of the constant t. Comparing (1.13) and r_+ in (1.16) shows that for non-zero a the surface $r_e(\theta)$ lies outside the event horizon r_+, except at the poles, where the two surfaces are coincident and when $a = 0$ both r_+ and $r_e(\theta)$ define the same surface. The Penrose process is reversible if the horizon area doesn't change. This condition can be reached if the incoming particles enters to the black hole on a trajectory tangent to the one of the null generators of the horizon. This behavior of the horizon area which governs on efficiency of energy extraction from black hole is similar to the relation between area and entropy and this analogy was also motivation for study of the black hole thermodynamics.

Since astrophysical black holes are electrically neutral, Kerr's solution can be considered the most general description of astrophysical black holes.

1.2.2 Results from the golden age of general relativity

The next decade after Kerr's discovery was a golden age for general relativity and black hole physics. First the uniqueness theorem [11] was proved by Israel, then in 1973 the four laws of black hole mechanics were proved by Bardeen, Carter and Hawking [12]. Soon after Bekenstein suggested that black holes have entropy [13] and finally in 1975 Hawking showed that black holes evaporate [14]. In the following sections we will explain more about these concepts.

1.2.2.1 The uniqueness theorem

The first uniqueness theorem that was announced by Israel [15] was only the beginning of an approach that continues today. The main motivation behind the uniqueness theorem is answering to the question: how many different types of black holes do exist? Uniqueness theorem for four dimensional black holes guarantees that , the static electro-vacuum, asymptotically flat, black hole solutions to the Einstein equations are presented by the Reissner-Nordstrom metric which can be parametrized by its mass and electric and magnetic charges, whereas allowing for angular momentum the stationary (non-static) and axisymmetric solutions are given by the Kerr-Newman metric. Apart from these solution a number of black hole uniqueness theorems have been proved under various reasonably well motivated assumptions not only for 4 dimensional black holes but also for higher dimensional ones, although one cannot clearly answer to the former question yet.

1.2.2.2 The laws of black hole mechanics

Laws of black hole mechanics have brought out connections between classical general relativity, quantum physics. The key idea in these laws is that the area A of event horizon and the surface gravity κ of the black hole, have analogy with entropy and temperature respectively. Therefore the four laws of black hole mechanics are similar to four laws of thermodynamics [12].

Zeroth law As we mentioned before, surface gravity κ is analogous to temperature, and for a stationary black hole, κ is constant over the event horizon.

First law The first law in thermodynamics is about conservation of energy and the analogous law in black hole mechanics can be stated by

$$\delta M = \frac{\kappa}{8\pi G}\delta A + \Omega \delta J \tag{1.17}$$

where M is mass of black hole, Ω is the angular velocity, J is the angular momentum. Eq. (1.17) shows that the change in the black hole parameter like angular momentum or horizon area cause the change in the energy (mass) of the back hole.

Second law or the area theorem states that the area A of event horizon of each individual black hole should not decrease with time

$$\delta A \geq 0 \tag{1.18}$$

(1.18) reminds us the corresponding law in thermodynamics which states that total entropy does not decrease.

Third law It is impossible, by any procedure no matter how idealized, to reduce κ to zero. In other word it is impossible to form a black hole with zero surface gravity.

It is important to say that at the classical level temperature and entropy are both zero. With considering the quantum mechanical effects, one finds that at some special temperature black holes have thermal radiation.

1.2.2.3 Black hole entropy

The fact that both black hole area and entropy tend to increase irreversibly showed that there are similarities between thermodynamics and black hole physics [13]. Black hole increases its horizon surface area when it makes a transition from one equilibrium state to a nearby one and similarly any changes in a closed thermodynamical system is also in the direction of increasing entropy. From (1.17) one can find that the black hole entropy is $S_{bh} = \frac{1}{4G}A$.
According to classical general relativity when matter drops into a black hole and vanishes from views into the space time singularity, the total entropy of universe will decrease as it is not possible to compensate these lost of entropy and this is

violation of the second law of thermodynamics. To solve this problem, Bekenstein who was inspired by the Hawking area theorem, proposed that black holes have intrinsic entropy. If the black hole had an associated entropy S_{bh} and the mass and energy of the remaining Universe had an entropy S_m, then the total entropy would be,

$$\delta(S_{bh} + S_m) \geq 0 \tag{1.19}$$

Expression (1.19) is non-decreasing, thus, avoiding the violation of the second law of thermodynamics.
Microscopic description of entropy has been found for some special classes of black holes like extremal, stationary black hole in context of string theory [16].

1.2.2.4 Hawking discovery

We mentioned earlier how the energy can be extracted from the rotating black hole by Penrose process. This process together with finding the analogy between black hole and thermodynamics suggest that if a black hole behaves like a thermodynamical system, one would expect it to also radiate were motivations for reconsidering the classical definitions were implementing that nothing can escape from a black hole.
In 1975 Stephen Hawking published a paper in which he described his semiclassical (studying quantum field in a classical black hole background) calculations that showed black holes emit particles with a characteristic black body spectrum

$$\Gamma(\omega) = \frac{1}{e^{\beta\omega} - 1} \frac{d^3k}{2\pi^3}, \tag{1.20}$$

where $\beta = \frac{1}{T_H}$. Therefore black holes were shown to radiate and the emerging radiation was labeled as "Hawking radiation". From (1.20) one can obtain the temperature known as "Hawking temperature" as $T_H = \frac{1}{\beta}$, and relates to the surface gravity, κ

$$T_H = \frac{\kappa}{2\pi} \tag{1.21}$$

Associating the temperature to the black holes was a strong proof that black holes are thermal systems. The discovery of Hawking radiation phenomenon reveals a remarkable connection between thermodynamics, quantum mechanics,

and gravity. The fact that black holes have non-vanishing entropy, tells us that they have microscopic degrees of freedom and to study them one needs to consider the quantum gravitational effects.

1.2.2.5 Black hole evaporation

In a simple word one can say that when a pair of virtual particle is around the event horizon, the negative energy partner might travel cross singularity before being able to recombine and leaving its partner to escape as a real radiation that can be observed at infinity. When these particles fall into the singularity, they decrease the energy and mass of the black hole and make it smaller and smaller. This is the phenomenon known as black hole evaporation.
Hawking's discovery demonstrated that black holes behave like blackbody emitters, possessing a temperature and emitting particles from the event horizon. This was the direct consequence of the gravitational field at the event horizon which forms a surface of infinite redshift in one side while in the far past, the space-time is nearly Minkowski. Hawking assumed that the quantum state is empty of in-particles near past null infinity. After a star collapses and forms a black hole, near future null infinity the vacuum state of in-particles contains a thermal flux of out particles. This means that any outgoing wave with finite frequency that reaches the observer at infinity corresponds to an exponentially high frequency mode near the horizon as he took the early time positive frequency modes to be the solutions of the wave equation that behave exponentially near the past null infinity.
It is worthwhile to review Hawking's original calculations. For the mathematical details we refer to Appendix (A).
If we take ϕ_{in} be a complete basis of the solutions to the scalar wave equation

$$g^{ab} = \nabla_a \nabla_b \psi = 0 \tag{1.22}$$

where g^{ab} is the space-time metric which for Minkowski space-time is $g_{ab} = \eta_{ab}$ and ϕ_{in}s are the positive frequency modes that near past null infinity behave like

$$\phi_{in} \sim e^{-i\omega v}, \tag{1.23}$$

where v is the ingoing null coordinate.The quantum field ψ can be expanded in the basis of ϕ_{in}, ϕ^*_{in} in terms of creation, a^+_ω, and annihilation, a_ω, operators as

$$\psi = \int d\omega (a_\omega \phi_{in} + a^+_\omega \phi^*_{in}) \tag{1.24}$$

where a_ω satisfies

$$a_\omega |0>_{in} = 0 \tag{1.25}$$

and $|0>_{in}$ is the lowest energy state. For the second basis solutions ϕ_{out}, one can take the boundary conditions such that on future null infinity wave is positive frequency

$$\phi_{out} \sim e^{-i\omega u} \tag{1.26}$$

where u is the outgoing null coordinate. The field ψ has an expansion on this basis as well

$$\psi = \int d\omega (b_\omega \phi_{out} + b^+_\omega \phi^*_{out}) \tag{1.27}$$

where

$$b_\omega |0>_{out} = 0 \tag{1.28}$$

and $|0>_{out}$ is the second vacuum state. Hawking studied a wave propagating backwards in time in the collapsing star space-time, means considering this boundary condition one should find out what will be the behavior of the scalar field on the past null infinity. Then ignoring the back reaction effects one relates the ϕ_{in} and ϕ_{out} by a reparametrization

$$\phi_{in}(v) = \phi_{out}(u(v)) \tag{1.29}$$

The (1.26) propagates along a path from future null infinity along u and passes close to black hole horizon and going through the collapsing star, finally propagates out to past null infinity along a geodesic v. Then u takes the form

$$u(v) = \frac{-1}{\kappa} \ln(\frac{v_0 - v}{C^2}) \tag{1.30}$$

where C is a constant and κ is the surface gravity. With (1.30) wave on past null infinity is

$$\phi_{out} \sim e^{\frac{i\omega}{\kappa} \ln(\frac{v_0 - v}{C^2})}, \quad \text{for} \quad v < v_0, \tag{1.31}$$

while for $v > v_0$ the wave vanishes. Therefore the Bogoliubov coefficients which in terms of the inner product of basis functions are

$$\alpha_{\omega\omega'} = (\phi_{out_\omega}, \phi_{in_{\omega'}}), \qquad \beta_{\omega\omega'} = -(\phi_{out_\omega}, \phi^*_{in_{\omega'}}) \tag{1.32}$$

can be written as

$$\alpha_{\omega\omega'} = \frac{(i\omega')^{(-i\omega/\kappa)}}{i\pi\sqrt{\omega\omega'}}\Gamma(1 + i\frac{\omega}{\kappa}) \tag{1.33}$$

$$\beta_{\omega\omega'} = -i\alpha_{\omega,-\omega'} \tag{1.34}$$

Using (1.34) the spectrum of produced particles is[1]

$$\int d\omega' |\beta_{\omega\omega'}|^2, \tag{1.35}$$

and this integral will result in (1.20). One should note that at very large values of ω' this integral is divergent [14]. But using the normalized wave packets one can find a finite number of particles produced in a given frequency per unit time.

1.3 A motivation for the presence of large extra dimensions

One of the open questions of SM physics is related to the hierarchy of the scales: the fact that the electroweak scale is much lower than the Planck scale. More technically, one loop corrections to the Higgs mass are quadratically divergent and to regulate the divergence a cut off (Λ) must be introduced in the loop momentum integral and in the SM a natural value for Λ would be the Planck mass implying that the bare Higgs mass should also be of this order. However, after the discovery of the Higgs boson we know that the Higgs mass is around 125 GeV and this either demands extreme fine tuning of the bare parameters of the Lagrangian to give loop cancelation or a cut off less than 1TeV.
One way to resolve this problem is by considering the presence of the additional symmetries like conformal symmetry or supersymmetry. The other solution has been suggested by introducing a brane world model (motivated by string theory)

[1]For more details see (A).

with large, flat, extra dimensions that can result in low scale gravity.
The fundamental objects in string theory are vibrating strings that are living in more than three space-like dimension that we experience everyday. SM interactions are like open strings which start and end on a brane but gravitons that are considered as closed strings can propagate in all the spatial dimensions. In the brane world models our Universe is considered as a slice lying inside an extra dimensional space-time that is called bulk. One of the key features of this model is that the SM particles and forces are confined to live just on the brane however gravitational degrees of freedom can travel into the bulk. This means that gravity can see the higher dimensions and the reason why it looks like so much weaker than any other forces is because it gets diluted by traveling to extra dimensions.

1.3.1 Extra dimensional model: ADD

One of the models that may provide a resolution of the hierarchy problem is the "large extra dimensions" model that was introduced by Arkani, Dimopoulos and Dvali (ADD model) in 1998 [17]. In this model all the SM particles are confined to a 3-dimensional brane that is located in a higher dimensional bulk. The graviton can propagate in the compactified d-extra spatial dimensions through the bulk. The 4-dimensional Planck scale and the $4+d$-dimensional gravity scale M_D are related via

$$M_{\mathrm{Pl}}^2 = V_d M_D^{2+d}, \tag{1.36}$$

where V_d is the volume of the compactified dimensions. The ADD model assumes that M_D is of the order of a few TeV so that the hierarchy between M_D (the fundamental gravity scale) and $\mathrm{M_{EW}}$ is due to the large volume of the higher dimensional space. Although in this model the electroweak scale is the only fundamental energy scale, LHC results from the first run showed that this fundamental scale is larger than 1 TeV [18] and is at least around 3 TeV and increases as the number of extra dimensions increase.

1.3.2 Trans Planckian energy domain

If one considers M_D as the fundamental scale of gravity, depending on the center of mass energy of the collision, $\sqrt{s}$, one can have black hole production in elementary particles collisions. We may define three different energy domains; the Planck domain ($\sqrt{s} \sim M_D$), trans-Planckian domain ($\sqrt{s} \gg M_D$) and sub-Planckian domain ($\sqrt{s} \ll M_D$). This gives us the opportunity to study the formation and evaporation of the micro black holes that may form during the high energy processes in which the center of mass energy of the colliding particles is much higher than the higher dimensional Planck scale. So in this sense one can say that trans Planckian energy domain may be accessible in man made colliders like LHC or free colliders where the high energy cosmic rays (UHCRs) hit the Earth's atmosphere. Thus if the Planck scale is in the TeV range μBHs might be created at the Large Hadron Collider (LHC) [19] or by the collision of ultra high energy cosmic rays with the Earth's atmosphere [20]. When these micro black holes evaporate, they may reach the Planck domain at the end stage of their evaporation. The Planck domain is the most unknown energy domain and the knowledge of quantum gravity is essential to study it. On the contrary, it is possible to apply perturbative quantum field theory and Einstein gravity for trans-Planckian domain. One can investigate this domain using the semiclassical approximations where the knowledge of quantum gravity in not required.

1.3.2.1 Micro black hole formation

One way to reveal extra dimensions would be through the production of microscopic black holes (μBH). If the centre-of-mass energy of two colliding particles is higher than the fundamental Planck scale, and their impact parameter b is less than the Schwarzschild radius R_S, in terms of the hoop conjecture a black hole should be produced. The number of black hole signals that might be produced at LHC can be calculated using LHC luminosity, $\mathcal{L}_{LHC}$, and production cross section,$\sigma(pp \to \mathrm{BH} + X)$, and the branching ratio of the decaying black hole to the signal, $Br(\mathrm{BH} \to \mathrm{signal})$

$$\mathcal{N}_{BH\ signal} = \sigma(pp \to \mathrm{BH} + X) \times \mathcal{L}_{LHC} \times Br(BH \to signal) \tag{1.37}$$

where the production cross section in the proton-proton collisions can be calculated by integrating over the parton distribution functions (PDF), $f_i(x, \hat{s})$, and parton level cross section, $\hat{\sigma}_{ij\to \mathrm{BH}}$, which is a geometrical cross section

$$\sigma(pp \to \mathrm{BH} + X) = \left(\int_{M_D^2/s}^{1} du \int_u^1 \frac{dv}{v} \sum_{ij} f_i(u, \hat{s}) f_j(\frac{u}{v}, \hat{s}) \hat{\sigma}_{ij\to \mathrm{BH}} \right), \qquad (1.38)$$

the sum runs on $i, j = (q, \bar{q}, g)$, where $q = (u, d, s, c, b)$ are the partons in proton. The partonic level cross-section

$$\hat{\sigma}_{ij\to \mathrm{BH}} = \mathcal{F} \pi r_s (\sqrt{\hat{s}})^2 \qquad (1.39)$$

contains a factor, $\mathcal{F}$, which is called form factor. All the information related energy loss, angular momentum, charge and all other dynamical modification should be considered to calculate this factor.

1.3.2.2 Micro black hole evaporation

The μBH lifetime is very short (for instance, in the ADD model with fundamental Plank scale of order of few TeV the life time is of the order of 10^{-26} s) and its temperature (typically about 100 GeV),

$$T_{\mathrm{H}} \sim \frac{M_D(D-3)}{4\pi} \left(\frac{M}{M_D} \right)^{-1/D-3}, \qquad (1.40)$$

is much lower than that of a black hole with the same mass in a four-dimensional space. Nevertheless, if they do appear in collisions created by the LHC or UHECRs, they will disintegrate rapidly. They would decay into SM or supersymmetric particles, creating events that have a high multiplicity, a large transverse energy, a democratic coupling to all particles and a rapid increase in the production cross-section with energy. The detection of these events would depend on the number of extra dimensions, the mass of the black hole, the size of the extra dimensions and the energy at which the μBH is produced. To distinguish the events that come from μBH decays one needs to simulate all the processes of μBH formation and evaporation. These simulations must be done according to the existing μBH models. However, the existing theoretical models fail to completely explain every aspect of the μBH formation and evaporation processes.

The theoretical model for black-hole evaporation essentially assumes that the Hawking formula for black-hole radiation is valid all the way up to the point at which its mass reaches the Planck mass. This is justified by the fact that the temperature is not very high and the evaporation proceeds slowly (adiabatically) up to this point. The Hawking radiation is modified by grey-body factors which determine how much of the radiation outgoing at the horizon can penetrate the potential barrier which surrounds the black-hole. These factors can be calculated from the absorption cross section of the waves, that scatter off the black hole.

1.3.2.3 Superradiance

The absorption cross section for an incident wave can be calculated by solving the relevant wave equation with appropriate boundary conditions corresponding to an incident wave of amplitude I from spatial infinity scattering to a reflected wave of amplitude R and a transmitted wave of amplitude T at the horizon. If the reflection coefficient is greater than the amplitude of the incident wave, $|R|^2 > |I|^2$, this implies that the energy incident on the black hole can be amplified [21] and this amplification is called super-radiance.
For a charged static black holes the condition that may result in the super-radiance is [22]

$$\omega - qQ/r_+ < 0, \tag{1.41}$$

where ω and q are respectively the frequency and the charge of the wave and Q is the black hole charge. The condition for superradiance amplification from rotating black holes is

$$\omega - m\Omega_H < 0, \tag{1.42}$$

where m is the azimuthal quantum number and Ω_H is the angular velocity. This simply means any wave that satisfies (1.42) can extract energy from the black hole horizon. In the low-frequency regime, condition (1.42) is valid for any field's spin s with $\ell \gg 2s^2$, and the maximum of the amplification occurs for modes with angular momentum quantum number ℓ equal to m.

1.4 Structure of this thesis

In this thesis we will concentrate on different aspects of black hole evaporation. We start with reviewing Hawking radiation and grey-body factors in the chapter 2 and at the end of the chapter we will present the results of our analysis using the most recent micro black hole event generators and finally we investigate how important is to have the exact form of the grey-body factors as the input of the black hole event generators.
In the chapter 3 we explain the quasi-normal modes and their importance in different sectors of astrophysics. This chapter will be an introduction for our final work which is the calculation of the quasi normal mode of out-going Vaidya space-time at the end stage of the black hole evaporation.
In the chapter 4 we review some of the interesting features of the large-D limit of general relativity and in the next chapter we will use this large-D method to calculate the graviton grey-body factors of a non-rotating black hole in order to check if this method can give us the same result as the ones that already exists in the literature.
In the chapter 6 we will explain the out-going Vaidya space-time and after calculating the quasi-normal like modes of a special class of this space-time we present our results. In chapter 7, the last chapter, we discuses about our results.

2

Hawking radiation and grey body factors

Hawking radiation is a thermal radiation that shows black holes are not just perfect absorbers but they can also emit particles. The temperature that is associated to this radiation is proportional to the surface gravity. For instance consider the Schwarzschild black hole space-time, this black hole has a negative specific heat which means that by emitting particles the temperature increases, as the surface gravity $\sim \frac{1}{M}$, and the black hole gets hotter and hotter until finally it explodes/vanishes.

The Hawking radiation is a semi-classical radiation which by semi-classical we mean study of quantum fields in a classical space-time. Although Hawking's original derivation is completely independent of the Einstein equation and only had been performed for the scalar fields, it is possible to perform the calculation for all fields and also for higher-dimensional black holes. We already explained Hawking's original derivation in (1.2.2.4) and we introduced the classical black body spectrum (1.20). Hawking in his calculations never considered the effect of any gravitational potential that arises from the interaction of the considered fields with the space-time geometry. Effect of this interactions are not negligible and considering this effect will modify the classical black body spectrum to a more realistic one and the modification factor is called the "grey-body factor". In spite of the complication and difficulties of doing these kind of calculations grey-body factors have been calculated for almost all the degrees of freedom.

One of the recent motivations for calculating these factors comes from the possibility of detection of micro black holes that may be produced in the high energy process at LHC or by the ultra high energy cosmic rays. If these tiny black holes can be produced, they cannot live for a long time and they evaporate almost instantly after production. The spectrum that one may expect to see in detectors can be predicted by calculating the grey-body factors and subsequently calculating the energy emission rate and the fluxes using these factors. Thus, having this information, one can carry out a detailed experimental study of black hole evaporation and detecting those objects can be possible.

2.1 Decay process

If the theory of large extra dimensions is a correct theory, as a results of this theory one may expect that micro black holes form during the high energy processes either in man made colliders or by collision of high energy cosmic rays with the Earth's atmosphere. If a micro black hole forms in a high energy collision, one can learn about this micro black hole by studying its decay products. The micro black hole after formation spins very fast and it decays immediately after formation. Its decay process can be classified to four stages [23].

Balding phase If a micro black hole forms, at energies well above the TeV scale in hadronic collisions, the intermediate resonance that is created during the parton collision carries the gauge and spin quantum numbers of the parent partons. The initially formed micro black hole, which is more like an excited state, also carries these charges and quantum numbers and its horizon has a very asymmetric shape. Because of the distribution of these gauge charges and energy-momentum, the created multipole moments will add also some extra hairs. Micro black holes quickly become bald by shedding the charges that are associated with the multipole moments by emission of gravitational radiation and classical gauge radiation to the gauge fields on the brane. The frequency of the oscillation of these multipole moments, as well as the

balding time scale, can be explained in terms of the Schwarzschild radius

$$\omega \sim \frac{c}{r_h}, \qquad \tau_b \gtrsim r_h \tag{2.1}$$

If one takes the ratio of the power emissions (energy loss) of the gauge and gravitational radiation, which are respectively dominated by the dipole mode and energy momentum quadruple moments

$$\frac{P_{gauge}}{P_{gravity}} \sim \frac{\alpha}{(r_h M_p)^{D-2}} \tag{2.2}$$

where α is the fine structure constant, one can see that this parametrical calculation shows that the energy loss by gravitational radiation is dominant during the balding phase.

The gauge charges from the initial partons will also be discharged by the Schwinger process [24] both in the balding phase and at the beginning of the evaporation phases. At the end of this stage the micro black hole still rotates but has lost most of its charges. This rotating stationary black hole can be described using the Myers-Perry [25] solution. Because of the high asymmetry during the balding phase, that is a result of the violent formation of micro black hole, the modeling of it is very difficult and most of the studies for understanding this phase are numerical studies.

At the end, evaporation of this micro black hole continues via Hawking radiation which takes place in two stages: spin down and the Schwarzschild phases.

Hawking radiation: spin down phase During this phase the micro black hole loses its angular momentum and becomes more symmetrical. Angular momentum will be shed in quanta with typical energy $E \sim 1/r_h$ which will account for about 25% of the mass loss. The emitted modes will be radiated to both the brane and bulk but the dominant process of mass loss is by radiation along the brane [26]. This can be because of predominant emission of Hawking radiation in the S-wave. Moreover black hole decays mostly to the SM particles that are confined to the brane. This procedure will continue until the micro black hole settles down into a stationary Schwarzschild state. At the end of this stage the micro black hole has zero angular momentum.

Hawking radiation: Schwarzschild phase In the Schwarzschild phase, the micro black hole continues to Hawking radiate and loses its mass until it reaches the Planck scale where $M_{\mu BH} \sim M_D$. One can compute the power spectrum and relative emission rates for this process and this is where the importance of grey body factors emerges. Mostly because for any experimental searches for evaporation signatures of micro black holes one might need to consider the effects of these factors in modifying the emission rate to present a more realistic picture of Hawking radiation process which by including the grey body factors will be different from the black body radiation. This stage together with the spin down phase are expected to be the most dominant stages in the life time of a micro black hole.

Planck phase When the micro black hole mass is close to the fundamental Planck scale it enters the Planck phase. To describe this phase a full quantum gravitational description is required and due to the lack of a theory of quantum gravity the Planck phase is the least understood phase of the decay process. However it is believed that μBH may completely decay to few partons with energies of the order of Planck scale.

2.2 Wave scattering by black hole

Study of scattering problems involving black holes is slightly different from the classical scattering problems. For scattering by black holes the curvature of space-time should be considered in the equations that describe the propagation of different waves (scalar, electromagnetic and gravitational waves) in the space-time under consideration, in addition to taking into account curvature effects, boundary conditions may also be different from the classical scattering problems.
In order to learn more about the different concepts of waves scattering by black holes one can study the scalar field for which all the equations are simpler.

2.2.1 Scalar waves scattering

To have a general overview we will consider a scalar field Φ propagating in a static, spherically symmetric d-dimensional, $d = 4 + n$, space-time like d-dimensional

Schwarzschild space-time [27]. The line element for d-dimensional Schwarzschild is

$$ds_d^2 = -f(r)dt^2 + f(r)^{-1}dr^2 + r^2 d\Omega_{d-2}^2 \tag{2.3}$$

and

$$f(r) = \left(1 - \left(\frac{r_0}{r}\right)^{d-3}\right) \tag{2.4}$$

where the event horizon is at r_0. The evolution of the scalar field is governed by the Klein-Gordon equation,

$$\frac{1}{\sqrt{-g}}\partial_\mu(\sqrt{-g}g^{\mu\nu}\partial_\nu)\Phi(t, r, \theta, \phi) = 0 \tag{2.5}$$

Because of spherical symmetry Φ can be discretized as

$$\Phi = r^{1-\frac{d}{2}}\psi(r)e^{i\omega t}Y_{lm}(\theta, \phi) \tag{2.6}$$

where the Y_{lm}s are the spherical harmonics and ω is the complex frequency of the wave. In the above space-time (2.3), the wave equation for the scalar field reduces to the following Schrödinger-type equation for the radial part

$$\left(\frac{d^2}{dr_*^2} + \omega^2 - V_l(r)\right)\psi(r) = 0 \tag{2.7}$$

where the so-called tortoise coordinate is defined by

$$\frac{d}{dr_*} = f(r)\frac{d}{dr}. \tag{2.8}$$

Using the tortoise coordinate we push the event horizon to $-\infty$, namely we map the semi-infinite interval $(r_0, +\infty)$ that represents space-time external to the black hole into the infinite interval $(-\infty, +\infty)$. The potential $V_l(r)$ is given by [28]

$$V_l(r) = f(r)\left(\frac{l(l+d-3)}{r^2} + \frac{(d-2)(d-3)f(r)}{4r^2} + \frac{(d-2)f'(r)}{2r}\right), \tag{2.9}$$

this potential is like a barrier and its maximum indicates the location of the unstable circular photon orbit. Understanding the behavior of this potential is important for problems dealing with the black hole perturbations. Solutions of (2.7) will tell us how an incoming wave originating at $r_* = +\infty$ or outgoing wave originating at $r_* = -\infty$ is scattered by the potential $V_l(r)$. The potential vanishes

when $r_* \to \pm\infty$, showing that the solutions will behave asymptotically like plane waves, $e^{\pm i\omega r_*}$. This potential is an obstacle for incident waves. Waves with short wave length or high frequency may be transmitted through it easily but those with low energy will be partially transmitted and partially scattered by the black hole barrier, see figure (2.1).

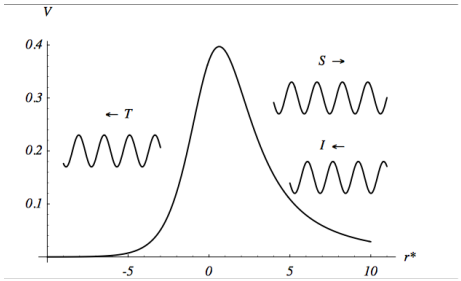

Figure 2.1: A schematic description of the scattering of waves in the Schwarzschild background. The effective potential is shown as a function of r_*. An incident wave I is decomposed into a transmitted component T and a scattered component S

2.2.2 Boundary conditions, reflection and transmission factors

To be able to calculate the reflection and transmission coefficients for a given potential one needs to define proper boundary conditions. Let's consider $\psi_\omega(r_*)$ and $\psi_{-\omega}(r_*)$ as two solutions of the equation (2.7) for an incoming wave originating at $r_* = +\infty$ where both of them satisfy the boundary condition that requires purely ingoing radial wave at the horizon,

$$\begin{aligned} \psi_\omega(r_*) &\sim \begin{cases} e^{i\omega r_*} + Re^{-i\omega r_*} & r_* \to +\infty \\ Te^{i\omega r_*} & r_* \to -\infty \end{cases} \\ \psi_{-\omega}(r_*) &\sim \begin{cases} e^{-i\omega r_*} + \tilde{R}e^{i\omega r_*} & r_* \to +\infty \\ \tilde{T}e^{-i\omega r_*} & r_* \to -\infty \end{cases} \end{aligned} \tag{2.10}$$

Where R and T are respectively reflection and transmission coefficients. If we build the conserved flux and evaluate at $r_* \to \pm\infty$

$$\mathcal{F} = \frac{1}{2i}\left(\psi_{-\omega}\frac{d\psi_\omega}{dr_*} - \psi_\omega\frac{d\psi_{-\omega}}{dr_*}\right)_{r_*\to\pm\infty} \tag{2.11}$$

From the quantum mechanical point of view considering energy conservation law, we know that if a wave of unitary amplitude is incident on one side of the potential barrier, it gives rise to a reflected and a transmitted wave such that the sum of the square of their amplitudes is one. Thus we require that the flux should be the same in both limits, $r_* \to \pm\infty$, and we get

$$R\tilde{R} + T\tilde{T} = 1 \tag{2.12}$$

It should be noted that if we consider outgoing waves which originate at $r_* \to -\infty$, we can write them as linear combination of incoming waves. In this way, after some simple manipulation, one finds that there is no difference between incoming and outgoing transmission coefficients. Namely, one can consider the scattering of the wave by the black hole for either incoming waves that come from spatial infinity or outgoing waves that originate from black hole itself.

2.3 Grey body factors

The spectrum of radiation from the black hole that can be observed at infinity is,

$$\Gamma(\omega)\mathrm{d}\omega = \frac{\gamma(\omega)}{e^{\beta\omega} \pm 1}\frac{\mathrm{d}^3k}{(2\pi)^3}, \tag{2.13}$$

where $\gamma(\omega)$ is the grey body factor. This factor can be defined in terms of the transmission and reflection coefficients of the potential barrier. For generic frequency $\omega \in \mathbb{C}$ using transmission coefficient one can define

$$\gamma(\omega) = T(\omega)\tilde{T}(-\omega). \tag{2.14}$$

In this respect grey-body factor can be considered as the absorption cross section which tells us how much of the incident field is transmitted through the potential and absorbed by black hole. One can also find the grey body factor by comparing the flux that is coming from infinity with the flux of the radiation that originated from black hole horizon, thus we define it as follow,

$$\gamma(\omega) = \frac{\mathcal{F}_{horizon}}{\mathcal{F}_{infinity}}. \tag{2.15}$$

In general depending on the space-time under consideration or the fields that encounter to the space-time potential this factor may change. For instance these factors can be calculated for both bulk and brane emissions as well as for rotating and non-rotating space-times. Thus one can say that this factor depends on the spin and frequency of the field under consideration and also on the angular momentum; for different mode quantum numbers we may have different grey-body factors. However if we want to obtain the flux of particles or angular momentum and energy emission rates we need to sum over all modes. The differential emission rates per unit time and frequency have the following form

$$\frac{\mathrm{d}^2E}{\mathrm{d}t\mathrm{d}\omega} = \frac{1}{2\pi}\sum_j\sum_{\ell=s}^{\infty}\sum_{m=-\ell}^{\ell}\gamma_{s,\omega,\ell,m}\mathcal{N}_{s,\omega,\ell,m}\frac{\omega}{\exp((\omega-m\Omega)/T_{\mathrm{H}})\pm 1}, \tag{2.16}$$

$$\frac{\mathrm{d}^2N}{\mathrm{d}t\mathrm{d}\omega} = \frac{1}{2\pi}\sum_j\sum_{\ell=s}^{\infty}\sum_{m=-\ell}^{\ell}\gamma_{s,\omega,\ell,m}\mathcal{N}_{s,\omega,\ell,m}\frac{1}{\exp((\omega-m\Omega)/T_{\mathrm{H}})\pm 1}, \tag{2.17}$$

$$\frac{\mathrm{d}^2J}{\mathrm{d}t\mathrm{d}\omega} = \frac{1}{2\pi}\sum_j\sum_{\ell=s}^{\infty}\sum_{m=-\ell}^{\ell}\gamma_{s,\omega,\ell,m}\mathcal{N}_{s,\omega,\ell,m}\frac{m}{\exp((\omega-m\Omega)/T_{\mathrm{H}})\pm 1}. \tag{2.18}$$

where s is the particle spin and T_{H} is the Hawking temperature

$$T_{\mathrm{H}} = \frac{(n+1)+(n-1)a_*^2}{4\pi(1+a_*^2)r_{\mathrm{h}}}, \tag{2.19}$$

and Ω is the angular velocity defined by

$$\Omega = \frac{a_*}{(1+a_*^2)r_{\mathrm{h}}}. \tag{2.20}$$

where a_* is a dimensionless spin parameter defined as $a_* = a/r_h$, and r_{h} is the horizon radius. As can be seen, all of these fluxes depend on the grey-body factor as well as the degeneracy factor $\mathcal{N}_{s,\omega,\ell,m}$. The degeneracy factors do not depend on the frequency and the azimuthal quantum number but considering different

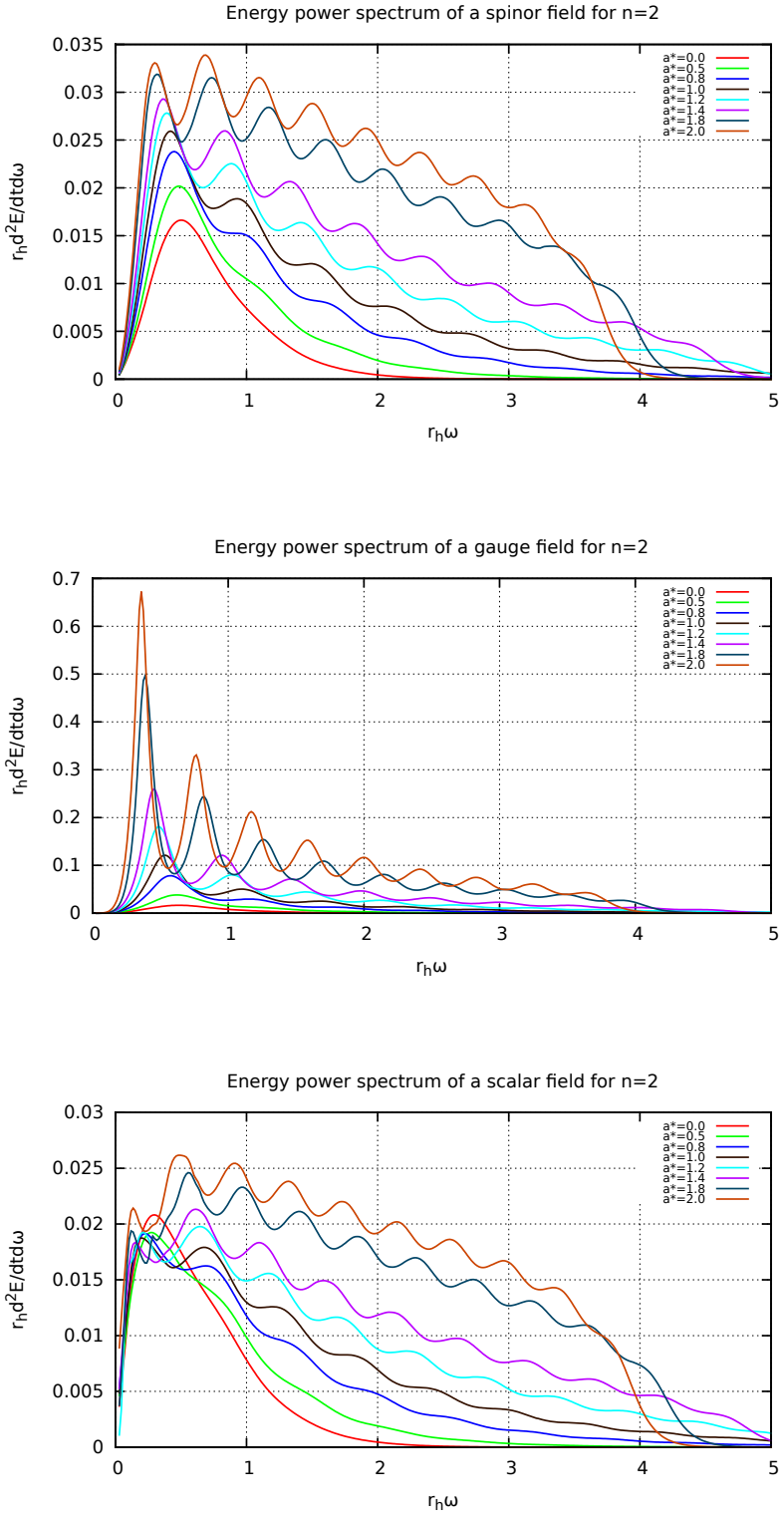

Figure 2.2: Energy power spectrum for spinor, gauge and scalar fields for $n = 2$.

fields they depend on ℓ and j and the number of extra dimensions. They account for the multiplicity of modes with quantum numbers (s, ω, ℓ, m). In (2.16) to (2.18) the sum over j is associated with the hyper-spherical harmonics and is only relevant for the scalar field emission in the bulk and tensor-type graviton emission from a rotating black hole [29]. The energy power spectrum has been presented for different spin parameters in figure (2.2) for spinor, gauge and scalar fields in the presence of two extra dimensions.

2.3.1 Different energy regimes

In order to be able to find any analytical solution to the field equations one can simplify the process by considering different energy regimes by studying the field equations in different frequencies. We can consider two limits of high and low frequency regimes where high and low may be considered relative to the black hole horizon radius r_0. Setting $r_0 = 1$ one can define two frequency regimes:

Low frequency regime In this frequency regime where $\omega \ll 1$, the near horizon and far region can be defined respectively by $r - 1 \ll 1/\omega$ and $r \gg 1$. In this range the wavelength of the wave is much larger than the radius of the black hole. With this approximation one can use the known matching techniques to find a solution on the whole space time. We should mention here that low frequencies give a significant contribution to the total power emission [30]. The procedure of analytical solution in the low frequency is as follows [31]

- Solve the radial equation in the near horizon region and expand the solution as ingoing and outgoing waves
- Implement the boundary condition in near horizon requiring that only purely outgoing wave should be accepted
- Solve the radial equation for the far region and expand the solution as ingoing and outgoing waves
- Match the two stretched solutions in the overlapping region to find the integration constant

- Calculate the absorption cross section using the integration constant that we have already obtained

High frequency regime This frequency regime is relevant when $\omega \gg 1$. In this regime the wavelength becomes almost of the same order as the black hole radius. The waves with high frequency can easily penetrate into the gravitational potential therefore one can use the monodromy matching technique [32] to solve the wave equations with the highest contribution coming from high-ℓ modes.

One should take note that the solution to the wave equations will not depend on the choice of energy regions but by considering different energy regions one can use proper analytical techniques to solve the wave equations. If one wants to solve the wave equations for all the frequencies one can also use the numerical techniques. However as you will see in this chapter this is also not an easy task as depending on the spin of emitted particles one may encounter some difficulties.

2.4 Hawking radiation from non-rotating and rotating black holes in the brane or bulk

As we explained earlier in this chapter, one should start to consider the Hawking emission during spin-down and Schwarzschild phase. The geometry of the space time during these two phases is different; during the spin-down phase the black hole is rotating so its space-time can be described by a Kerr like solution in higher dimensions, for instance Myers-Perry solution. However during the Schwarzschild phase the black hole no longer rotates, so its geometry can simply be described by higher dimensional Schwarzschild metric. The important point is that particle emission should be considered during these two phases separately as their emission rates should be modified by different grey-body factors as a result of having different geometry.

Besides considering whether the particle emission is from a rotating or a non-rotating black hole, it is also important to consider if these particles will be emitted to the brane or to the bulk. Modeling black holes in the ADD scenario,

which is our preferred extra dimensional model to study micro black holes, the forces and particles of the Standard Model are confined on the 3-dimensional brane but gravitational degrees of freedom (gravitons and scalars) can propagate in the bulk. Thus, as much as it is important to study the particle emission into the brane the emission of fields through the higher dimensional bulk may also be important. Although only the propagation of particles into the brane may be detectable for brane localized observers the portion of energy that may be emitted to the bulk can be counted as the missing energy. Knowing about the amount of energy that may be emitted into the bulk will give us the required knowledge to answer the question of energy balance between bulk and the brane. We know that the number of degrees of freedom that propagate into the brane are much larger than those that travel to the bulk, so if one knows how much energy is emitted to the bulk, the missing energy, one can evaluate how much energy should we expect to have during Hawking emission into the brane.

All types of emissions from either rotating or non-rotating black holes have been studied in the literature extensively. However there are some difficulties to calculate the emission of the gravitons from a rotating black hole which we will discuss about them in this chapter. In this section we will review some of the methods and results of Hawking emission from both rotating and non-rotating black holes through bulk and brane. We consider the ADD model in which the extra space-like dimensions are flat and compactified with a compactification radius that is larger than the Planck length $R \gg \ell_p$ and a horizon radius that is smaller than the size of the extra dimensions $r_H < R$; such a higher dimensional black hole will be centered on the brane and it will have some extension into bulk as well. We also consider a tensionless brane and we assume that all the fields that propagate into the brane or bulk are massless. One should note that grey-body factors have also been calculated for some degrees of freedom assuming the tension on the brane as well as for the propagation of massive fields. We may review some of the effects of considering these two issues in the calculation of the grey-body factors at the end of this chapter.

2.4.1 Hawking emission from a non-rotating black hole

One expects that Schwarzschild phase be the longest phase in the black hole evaporation process and black hole losses most of its mass in this phase [31]. To start one should consider the gravitational background that the particles propagate through. For a non-rotating background the proper line element is

$$ds^2 = -f(r)dt^2 + f(r)^{-1}dr^2 + r^2 d\Omega_{2+n}^2, \tag{2.21}$$

where

$$f(r) = 1 - \left(\frac{r_H}{r}\right)^{n+1}, \tag{2.22}$$

and the angular part is

$$d\Omega_{2+n}^2 = d\theta_{n+1}^2 + \sin^2\theta_{n+1}\left(d\theta_n^2 + \sin^2\theta_n\left(... + \sin^2\theta_2(d\theta_1^2 + \sin^2\theta_1 d\phi^2)...\right)\right). \tag{2.23}$$

Depending on the brane or bulk emission different parts of (2.21) should be taken into account. After choosing the proper part one just needs to consider the spin of particles in order to obtain the right formalism. Considering Newman-Penrose formalism [33] for fields with spin $s = 0, 1, 1/2$ for the motion of a particle in the assumed background one needs to obtain (2.5) for spin-0, Dirac equation for spin-1/2 and Yang-Mills equation for spin-1 particles. Then using the relevant field factorization one may obtain radial and angular equations that can be solved either analytically [34, 35] or numerically [31].

2.4.1.1 Brane emission

If we want to calculate the brane emission we need to project the black hole onto our 3-dimensional brane world. To do that we choose $\theta_i = \pi/2$ for $i \geq 2$ in (2.23). By using the following separation of variables [31]

$$\psi_s = e^{-i\omega t}e^{im\phi}R_s(r)S_{s,\ell}^m(\theta), \tag{2.24}$$

in the corresponding equations (namely the perturbation equations for different spins) and separating them into radial and angular equations one then obtains the following equations valid for all spins with $\Delta = f(r)r^2$

$$\Delta^{-s}\frac{d}{dr}\left(\Delta^{s+1}\frac{dR_s}{dr}\right) + \left(\frac{\omega^2 r^2}{f(r)} + 2i\omega sr - \frac{is\omega r^2 f(r)'}{f(r)} + s(\Delta'' - 2) - \lambda_{s\ell}\right)R_s(r) = 0, \tag{2.25}$$

for the radial equation while the angular equation is

$$\frac{1}{\sin\theta}\frac{d}{d\theta}\left(\sin\theta\frac{dS^m_{s,\ell}}{d\theta}\right)+\left(-\frac{2ms\cot\theta}{\sin\theta}-\frac{m^2}{\sin^2\theta}+s-s^2\cot^2\theta+\lambda_{s\ell}\right)S^m_{s,\ell}(\theta)=0, \tag{2.26}$$

where $S^m_{s,\ell}(\theta)$s are spin-weighted spherical harmonics and $\lambda_{s\ell}$ is the separation constant which can be derive from solving (2.26)

$$\lambda_{s\ell}=\ell(\ell+1)-s(s+1). \tag{2.27}$$

Solutions to the radial equation (2.25) have the form (2.10) for the near horizon and far regions. Having this solution one can calculate the grey body factors as explained in (2.2.2). Subsequently one can use (2.16) and (2.17), for rotation parameter a_* equal to zero, to obtain the desired fluxes.
Results of the numerical calculation for the brane channel that is the only observable channel for the brane localized observers have shown that as the number of the extra dimensions increases the energy emission rate also increases and this holds for all types of the brane emissions [31]. The numerical calculation in [31] shows that grey-body factors will decrease by increasing the number of extra dimensions. However the energy emission has an increasing rate and that is because of the black hole temperature that increases as the number of extra dimension increases and this will compensate the suppression of the grey-body factors.

2.4.1.2 Bulk emission

The only particles that can propagate into the bulk are gravitons and scalar fields. To compute the bulk emissions we need to consider the propagation of the scalar fields and graviton on the background of (2.21). We also need to substitute $S^m_{s,\ell}(\theta)$ in (2.24) by $\tilde{Y}_\ell(\Omega)$ which is the generalization of the usual spherical harmonic functions depending on the angular coordinates. Using this new factorization the radial equation for scalar emission into bulk will be [34]

$$\frac{f(r)}{r^{n+2}}\frac{d}{dr}\left(f(r)r^{n+2}\frac{dR}{dr}\right)+\left(\omega^2-\frac{f(r)}{r^2}\ell(\ell+n+1)\right)R=0 \tag{2.28}$$

The solution to this equation has been obtained both analytically for low frequency range and numerically for all frequencies respectively in [31, 34].

For graviton emission one needs to consider the gravitational perturbation in the back-ground (2.21). Computing the graviton emission is more complicated because the perturbation equations that describe the motion of a graviton subjected to the potential of (2.21) will decompose into three parts: a scalar, a vector and a symmetric traceless tensor part. The formalism for the treatment of these three types have been discussed in [36]. All the equations which describe these three gravitational degrees of freedom are separable and the equation of radial part is [36]

$$f(r)\frac{d}{dr}\left(f(r)\frac{dR}{dr}+(\omega-V_{(S,V,T),(\ell,n,\omega)})\right)R(r)=0, \tag{2.29}$$

where $V_{S,V,T}$ is the gravitational potential for scalar, vector and tensor perturbations. This potential for tensor and vector part can be written as

$$V_{T,V}=\frac{f(r)}{r^2}[\ell(\ell+n+1)+\frac{n(n+2)}{4}-\frac{k(n+2)^2}{4}(\frac{r_H}{r})^{n+1}], \tag{2.30}$$

where $k=-1,3$ stands for tensor and vector type respectively and for scalar perturbation

$$V_S=\frac{f(r)}{r^2}\frac{qx^3+px^2+\omega x+z}{4(2m+(n+2)(n+3)x)^2}, \tag{2.31}$$

where

$$\begin{aligned}
&m\equiv\ell(\ell+n+1)-n-2, \qquad x\equiv\left(\frac{r_H}{r}\right)^{n+1}=1-f,\\
&q\equiv(n+2)^4(n+3)^2, \qquad z\equiv 16m^3+4m^2(n+2)(n+4),\\
&p\equiv(n+2)(n+3)[4m(2n^2+5n+6)+n(n+2)(n+3)(n-2)],\\
&\omega\equiv-12m(n+2)[m(n-2)+n(n+2)(n+3)].
\end{aligned} \tag{2.32}$$

It should be noted that the angular functions are simple spin-weighted hyper spherical harmonics. The radial equation (2.29) has been solved using different techniques in the low [7] and intermediate energy regions [37].

The amount of energy which is channeled into the bulk is not observable for us and it can be counted as missing energy. For scalar emission in the bulk the behavior is like brane emission but the suppression of grey-body factor at low energy regime is milder [31] and in contrast with brane emission this won't cause any enhancement in the energy emission rate. However in the high energy limit the increase of the temperature by number of dimensions again cause an enhancement in the energy

emission rate. The analytical solutions to the perturbation equations for graviton emission into the bulk revealed that vector perturbation is the dominant mode emitted in the bulk for all the number of extra dimensions, n, however emission rate of the scalar and tensor modes depends on n and it can be higher for small n for scalar modes and at higher n the emission of tensor modes is prevalent and the energy emission rates of all these three types decreases as the number of extra dimensions increases [7]. Comparing the scalar emission rate with the graviton emission rate for all modes in the low energy limit shows that scalar field emission is dominant and this is due to the absence of the $\ell = 0, 1$ modes for graviton. At intermediate energy [37] the total graviton cross-section, which is the sum of the perturbations (scalar, vector and tensor) is of the same order of magnitude as the scalar case.

2.4.2 Hawking emission from a rotating black hole

Emission of Hawking radiation from a micro black hole during the spin-down phase has been studied in the literature for the case of brane emission regarding scalar and gauge boson as well as for the fermion field [38, 39, 40, 41, 42, 43] and in the case of bulk emission for the scalar fields [44, 45] and partially for gravitons [46]. To study the Hawking emission from a rotating black hole first we need to introduce the proper line element that describes the space-time of a rotating black hole in the bulk. This line-element has been introduced by Myers and Perry (MP)[25]. In general when studying the Hawking emission from the rotating space-time it will be very difficult to deal with the general MP solution. Instead one can consider a relevant sub-class of MP solutions consistent with the conditions under which the micro black hole has been formed. If we assume that the micro black hole formation takes place in the collision of particles in the LHC in which the propagation of colliding particles is restricted to an infinitely-thin 3-brane, thus formed micro black hole will only have one non-zero angular momentum parameter about an axis in the brane and this is because micro black hole has been created by particles that are localized on the 3-brane and have a non-zero impact parameter only along a brane space-like coordinate. In this case

all the rotation parameters a_i are equal to a and the line-element has the form

$$\begin{aligned} ds^2 = (1 - \frac{\mu}{\Sigma r^{n-1}})dt^2 + \frac{2a\mu \sin^2\theta}{\Sigma r^{n-1}} dt d\varphi - \frac{\Sigma}{\Delta} dr^2 - \Sigma d\theta^2 \\ - \sin^2\theta \left(\frac{a^2 \mu \sin^2\theta}{\Sigma r^{n-1}} + a^2 + r^2 \right) d\varphi^2 - r^2 \cos^2\theta d\Omega_n^2, \end{aligned} \tag{2.33}$$

where

$$\Delta = a^2 + r^2 - \frac{\mu}{r^{n-1}}, \quad \Sigma = a^2 \cos^2\theta + r^2, \tag{2.34}$$

and $d\Omega_n^2$ denotes the metric for the unit n-sphere. The parameters μ and a in (2.34) are associated to the micro black hole mass M_{BH} and angular momentum J using the following relations

$$M_{BH} = \frac{(n+2)A_{2+n}\mu}{16\pi}, \qquad \text{and} \qquad J = \frac{2aM_{BH}}{n+2}, \tag{2.35}$$

where A_{2+n} is the area of the (n+2)-dimensional unit sphere

$$A_{2+n} = \frac{2\pi^{(n+3)/2}}{\Gamma[(n+3)/2]}. \tag{2.36}$$

In (2.33) $d\Omega_n^2$ is the part of the metric that comes from the extra dimensions while the rest of the metric describes the space-time of a rotating black hole in the brane.

2.4.2.1 Brane emission

If we are to study the Hawking emission that radiates on the brane we need to consider the proper background which in this case can be obtained by projecting the higher dimensional one (2.33) onto the brane, as in the non-rotating case by fixing all additional azimuthal coordinates to $\pi/2$. Doing so the $d\Omega_n^2$ part of the metric disappears while the rest remains unchanged. The formalism for describing the perturbation of this rotating space time can be deduced from the generalization of Teukolsky equations [47, 48] using Newman-Penrose formalism. This work was first done by Ida-Oda-Park in [38]. The resulting equation for different spins, $s = 0, 1, 1/2$, can be written in one master equation which by using the proper factorization

$$\psi_s = e^{-i\omega t} e^{im\phi} R_\Lambda(r) S_\Lambda(\theta), \qquad \Lambda = \{s, \omega, \ell, m\} \tag{2.37}$$

is separable to the radial and angular equations [43, 49]

$$\Delta^{-s}\frac{d}{dr}\left(\Delta^{s+1}\frac{dR_\Lambda}{dr}\right)+(\Delta^{-1}(K_{\omega m}^2-isK_{\omega m}\Delta')+4is\omega r+s\delta_{s,|s|}(\Delta''-2) \\ -a^2\omega^2+2ma\omega-\lambda_\Lambda)R_\Lambda(r)=0, \tag{2.38}$$

$$\frac{1}{\sin\theta}\frac{d}{d\theta}+\left(\sin\theta\frac{dS_\Lambda}{d\theta}\right)+(-\frac{2ms\cot\theta}{\sin\theta}-\frac{m^2}{\sin^2\theta}+a^2\omega^2\cos^2\theta-2as\omega\cos\theta \\ +s-s^2\cot^2\theta+\lambda_\Lambda)S_\Lambda(\theta) \tag{2.39}$$

where

$$K_{\omega m}=(r^2+a^2)\omega-am \tag{2.40}$$

and λ_Λ is the angular eigenvalue that can be found by numerically solving the angular equation (2.39) which is the spin-weighted spheroidal harmonic equation. The radial equation has been solved analytically in the low energy limit using the matching technique in [38] however for high energy regime this technique doesn't work any more and one needs to use numerical methods to find the solution to (2.38). Solution to the wave equations for different particle species shows that the angular distribution of the total power flux respect to the axis of rotation is different for the scalar, gauge and femionic fields. As can be seen in figure (2.3) the rotating black hole prefers to emit energy in the form of scalars and fermions while fermionic emission is slightly dominant compared to scalar emission. Moreover from (2.3b) it is clear that black hole has to spend large amount of energy in order to emit gauge bosons. The integrated emission rate over all frequency regims shows that this emissivity for all the degrees of freedom enhance respect to increase of n and rotation parameter a_*.

2.4.2.2 Bulk emission

Hawking emission from a rotating black hole into the bulk have been calculated for scalar field in [44, 45] and partially for gravitons in [46]. To calculate the emission of these fields into the bulk one needs to consider the whole metric (2.33), not just a slice like in the case of brane emissions. The perturbation equations for the scalar bulk emission are separable but this is not the case for

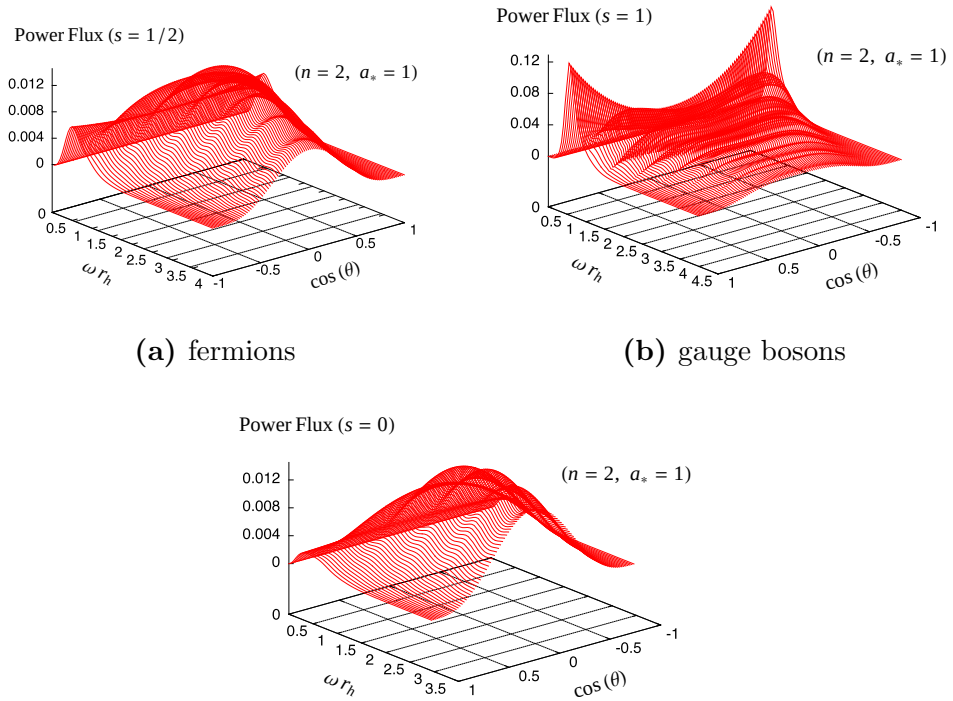

(a) fermions **(b)** gauge bosons

(c) scalars

Figure 2.3: Angular distribution of the power spectra for (a) fermions, (b) gauge bosons, and (c) scalars in the presence of 2 extra dimensions with $a_* = 1$ [1]

gravitons. To obtain the perturbation equations for scalars one needs to include a hyper-spherical harmonic,$Y_{jn}(\Omega)$, in the field factorization (2.37)

$$\psi_0 = e^{-i\omega t} e^{im\phi} R_\Lambda(r) S_\Lambda(\theta) Y_{jn}(\Omega), \qquad \Lambda = \{\omega, \ell, m, j, n\} \tag{2.41}$$

using this factorization in the Klein-Gordon equation for a field that is minimally coupled to the background one obtains three equations, one equation that defines the hyper-spherical harmonics on the n-sphere and two radial and angular equations that are coupled through one angular eigenvalue that can be find using different methods, although it is not possible to find an analytical solution. The equation for $Y_{jn}(\Omega)$ is

$$\sum_{k=1}^{n-1} \frac{1}{\prod_{i=1}^{n-1} \sin^i \theta_i} \partial_{\theta_k} \left[\left(\prod_{i=1}^{n-1} \sin^i \theta_i \right) \frac{\partial_{\theta_k} Y_{jn}}{\prod_{i>k}^{n-1} \sin^2 \theta_i} \right] + \frac{\partial_{\phi\phi} Y_{jn}}{\prod_{i=1}^{n-1} \sin^2 \theta_i} + j(j+n-1) Y_{jn} = 0, \tag{2.42}$$

where the j index is an integer and it is related to the bulk coordinates. Radial and angular equations are

$$\frac{1}{r^n}\partial_r(r^n\Delta\partial_r R_\Lambda)+\left(\frac{K_{\omega m}^2}{\Delta}-\frac{j(j+n-1)a^2}{r^2}-E_\Lambda+2ma\omega+a^2\omega^2\right)R_\Lambda=0, \tag{2.43}$$

$$\frac{\partial_\theta(\sin\theta\cos^n\theta\partial_\theta S_\Lambda)}{\sin\theta\cos^n\theta}+\left(a^2\omega^2\cos^2\theta-\frac{m^2}{\sin^2\theta}-\frac{j(j+n-1)}{\cos^2\theta}+E_\Lambda\right)S_\Lambda=0. \tag{2.44}$$

The exact solution of these equations has been presented in [44] and it turns out that some parts of the calculation are similar to the 4-dimensional case.

Another interesting case of emission into the bulk is graviton emission. While one can derive a set of partial differential equations (PDEs) describing the gravitational perturbations of a higher-dimensional rotating black hole, these PDEs can not be decoupled into ordinary differential equations (ODEs) for all modes. The only mode that up to now could be decoupled to the ODEs is the tensor mode under some special assumptions regarding the MP background.

The numerical results [44] for the emission of scalars by a rotating higher dimensional black hole demonstrated that grey-body factors are enhanced with angular momentum of black hole compared to the non-rotating one. In contrast to the brane scalar emission, energy emission rate doesn't increase with angular momentum while it still increases with the value of n. This is because the enhancement in the grey-body factors cannot be compensated by the decrease in the black hole temperature with rotation parameter. Comparing the brane and bulk scalar emissions reveals that the bulk scalar emission is only a portion of the brane emission and becomes important for large values of extra dimensions moreover, it may be suppressed as the rotation parameter increases. This study confirmed that a rotating black hole, considering the scalar channel, emits a small fraction of its mass and angular momentum into the bulk. However to give the final answer to the energy balance between brane and the bulk one also needs to consider the detailed study of the bulk graviton emission from a rotating black hole.

Partial results [46] (tensor type gravitational perturbation) for graviton emis-

sion from a simply rotating black hole[1] shows that the gravitational tensorial grey-body factors decrease as the number of space-like dimensions increase while for the fixed dimension they will enhance as the angular momentum parameter increases. The energy emission rate has the same dependence on the angular momentum parameter and the value of n as the scalar emission into the bulk. Comparing the total emission power (mass loss rate) of the tensor type gravitons with scalars demonstrates that at small values of n gravitons have very small contribution to this rate but as n increase their contribution becomes dominant.

2.5 Micro black hole event generators

The potential creation of the micro black holes during high energy collisions arose this question that how might the possible signals from micro black hole decay look like in the detectors. These hadronic collisions may take place at the LHC or collision of high energy cosmic rays by the Earth's atmosphere which is subsequently followed by their evaporation through the emission of Hawking radiation. To answer this question all the process of production and evaporation of the micro black hole have been studied in detail and using the results of these studies black hole simulations have been created. Using these simulators one can estimate the relative background contributions from the real data samples that have been recorded in different experiments. In recent years several micro black hole event generators have been developed for simulating the formation and decay of micro black holes formed in high energy collisions. Among them, CHARYBDIS2 [50] and BlackMax [51] are the most recent ones, and they include all the grey body factors which are known up to now as well as the effect of rotation has been taken into account in these two generators. The effect of rotation is very important as most of the black holes that might form at LHC might form at non-head on collisions, thus they would be highly rotating. The decay of this highly rotating black hole can be simulated by the black hole event generator and elementary particles are the output of these generators.

[1] A higher dimensional rotating black hole with a single angular-momentum component along the brane under the assumption that space-time metric is the warped product of two sub-manifolds [46].

The heavy particles (top quarks, Higgs and EW bosons, etc.) emitted by micro black hole evaporation decay quickly, i.e. before entering the detectors, and the partons and charged leptons emitted both by micro black hole evaporation and by these decays are further subject to parton and photon shower emissions, degrading their energy down to a scale where perturbative QCD can not be applied anymore, and hadronization takes place, followed by hadron decays. Non-perturbative effects in this context are described by means of phenomenological models. This same chain of processes also occurs in p-p collisions in the framework of the SM and the corresponding physics and model parameters have been constrained over the years by results obtained at accelerators. In particular, shower Monte Carlo (SMC) programs like PYTHIA [52], HERWIG [53] are commonly used to describe these processes. Thus for simulation of the following hadronization process micro black hole event generators can be interfaced to PYTHIA or HERWIG Monte Carlo event generators.

2.5.1 BlackMax phenomenology

A black hole is allowed to form if

$$b < b_{\max} \equiv 2r_h^n(E_{\rm cm}, b_{\max}E_{\rm cm}/2) \tag{2.45}$$

where b is the impact factor of two partons collision and is the function of the total center of mass energy of the parton-parton collision as well as the horizon radius. The horizon radius itself is again function of $E_{\rm cm}$, the fundamental Planck scale, and number of extra space like dimensions n. The momenta and location of these colliding partons can be obtained by knowing their energies and types. The most likely types in the proton-proton collision are the valence quarks u and d with electric charges $2/3$ and $-1/3$ respectively. Thus the formed black hole which is highly rotating also initially carries gauge and electric charges. This black hole before emitting any kind of Hawking radiation first loses some fraction of its energy, mass and angular momentum. These parameters evolves in the next step of the evaporation after their initial values reduces using the mass f_E, momentum f_p and angular momentum f_L loss factors. These three factors are input parameters in BlackMax with values in the range $[0, 1]$. As the result of

the initial angular momentum loss the black hole angular momentum will change its direction, the new direction can be reset using an introduced tilt θ in angular momentum. Then an angle ϕ will be randomly chosen and the angular momentum axis will be reset to (θ, ϕ).
At the next stage one can start to consider the Hawking radiation by including the available grey body factors for the all degrees of freedom. These factors have been calculated for different quantum numbers and different number of extra space-like dimensions and saved in different data files that can be used by BlackMax as input spectra, though it is necessary to transform them to the laboratory frame. Taking into account the degrees of freedom of SM particles the expected radiated flux for each type of particles can be calculated. The probability of emission of each particle type i with assigned energy, $\hbar\omega_i$, can be determined using the former spectra. BlackMax lets this particle be emitted in one generator time step, Δt, if for a random number, N_r, in the interval $[0, 1]$

$$L_{Fi} N_i \Delta t > N_r, \tag{2.46}$$

where L_{Fi} is the total number flux of particles of type i which can be obtained from the power spectrum and N_i is the number of degrees of freedom of that particle type. The next step is to choose the angular momentum quantum numbers (ℓ, m) of the emitted particle by calculating the emission probability of that particle using again the emission spectrum. Then using these quantum numbers the direction of emission according to the corresponding spheroidal wave functions can be calculated. Moreover if the particle carries SU(3) color, a 3-dimensional vector representing color will be randomly assigned to that particle. To prevent the black hole to gain a large electric or color charge two suppression factors as functions of two suppression parameters related to each charges have been introduced. The suppression parameters have approximately same orders as the electromagnetic and strong coupling constants. These suppression factors then will be compared to N_r and the particle can be emitted only if they are smaller than this value. In this sense the chance of emission will be given to the particles which reduces the electric or color charge of the black hole.
Effects of rotation in BlackMax can be switch on or off. If one decides to take the rotation into account then BlackMax may also need an angular momentum

suppression factor. Different suppression factors have been included in BlackMax and one can choose each of them when setting the input parameters. The same comparison with N_r takes place here as well and if the suppression factor is greater than the value of N_r, the emission of particles will be aborted.
For the final stage of the black hole evaporation, where the black hole mass is close to the fundamental Planck scale, BlackMax assumes that evaporation is a burst of particles which conserves energy, momentum, and all the other quantum gauge numbers.

2.5.1.1 Primary analysis from BlackMax

In this section we investigate the behavior of the event generators at LHC energies as well as at higher energies such as those reachable in the interactions of ultra high energy cosmic rays with the Earth's atmosphere, leading to extended air showers (EAS). In particular, we work with the last version of BlackMax (2.02.0), both in the standalone mode, and interfaced to the PYTHIA SMC code. We perform simulations of the formation of both rotating and non-rotating micro black holes in p-p collisions in the $E_{CM} = 14$ TeV, for the fundamental Planck scale $M_D = 3.5$ TeV, a micro black hole minimum mass is constrained to be $M_{\min} = 4.5$ TeV. In the simulation of micro black hole evolution, the mass, linear and angular momentum loss fractions were assumed to be equal to 0.1, whereas angular momentum and charge suppression factors were assumed to be equal to 1 and 20 for the case of color suppression factor, moreover baryon and lepton numbers, as well as their difference, conserved. With these settings we investigated the kinematical properties of particles emitted during the micro black hole evolution as computed by BlackMax and also after the Parton Shower + Hadronization + Hadron decay chain, as computed by the interface of BlackMax with PYTHIA. The micro black hole signals may appear in the detectors as high multiplicity of particles with high transverse momentum. Thus it is interesting to study the multiplicity of the different degrees of freedom in different transverse momentum regions. Examples of our selected results are presented in the figures (2.4), (2.5), (2.6) and (2.7). In figure (2.4) one can see that the number of produced gravitons intensively increases with number of extra dimensions.

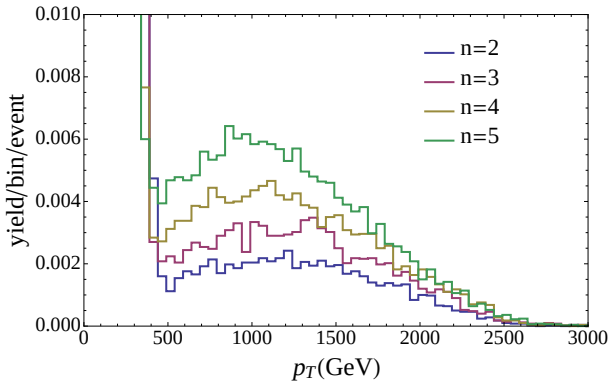

Figure 2.4: Transverse momentum distribution of gravitons expressed in terms of yield (number of particles)/bin/event for different number of spatial extra dimensions for non-rotating micro black hole

However if one compares this multiplicity with multiplicities of other produced particles which are shown in the figures (2.5b), (2.5d), (2.5f), (2.6b) and (2.6d) one can see that graviton multiplicity doesn't have long p_T tail and in general even in low p_T range, with a peak as $p_T \to 0$, graviton multiplicity is much lower than the other SM particles. This may imply that the number of particles carrying missing energy and not contributing to the visible signals is not large. In figures (2.5), (2.6) and (2.7) this dependence is presented for different particles taking into account their electric charges as well as the effect of rotation. From these figures it is evident that for the non-rotating micro black holes the multiplicity increases by number of spatial extra dimensions however this increase is not drastic if one compares it with the same case for the rotating-black hole.

In figure (2.6e) and (2.6f) the multiplicity versus p_T is presented for different particle species regarding their electric charge only for the case $n = 2$ extra dimensions for both rotating and non-rotating micro black holes. In both plots the higher multiplicity belongs to the particles with positive charges compared with negatively charged particles and emission of quarks and gluons is preferred over all other types of particles.

This effect is also shown in figure (2.7) with a comparison of the multiplicity of *up* quarks in different energies with all the other particles. It is evident that the number of emitted quarks has a large rate compared with all the other particles.

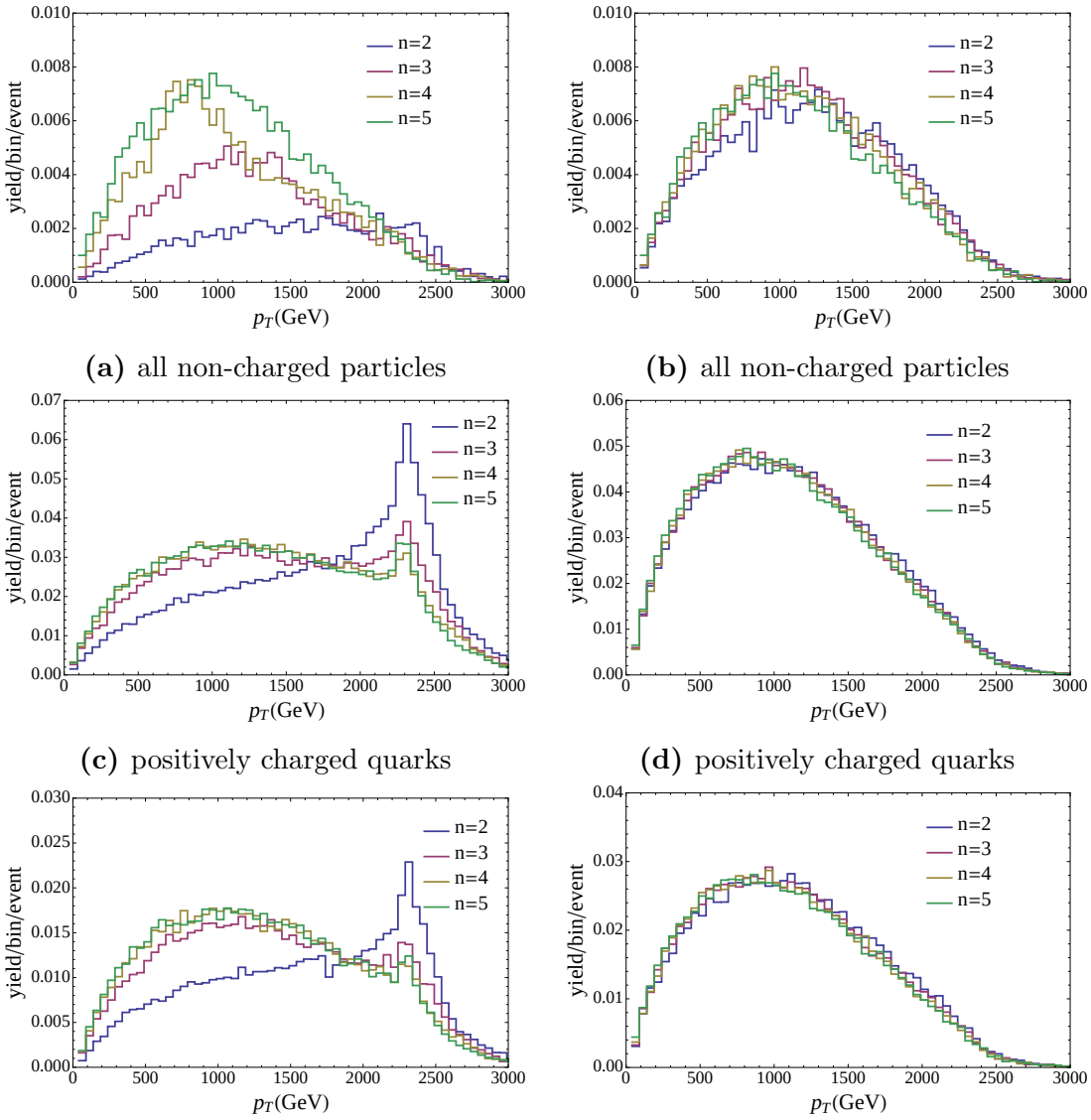

(a) all non-charged particles

(b) all non-charged particles

(c) positively charged quarks

(d) positively charged quarks

(e) negatively charged quarks

(f) negatively charged quarks

Figure 2.5: Transverse momentum distribution of all the non-charged particles, quarks with positive charges and negative charges expressed in terms of number of particles/bin/event for different number of spatial extra dimensions receptively for the rotating micro black hole at (a),(c) and (e) and for non-rotating micro black hole at (b), (d) and (f).

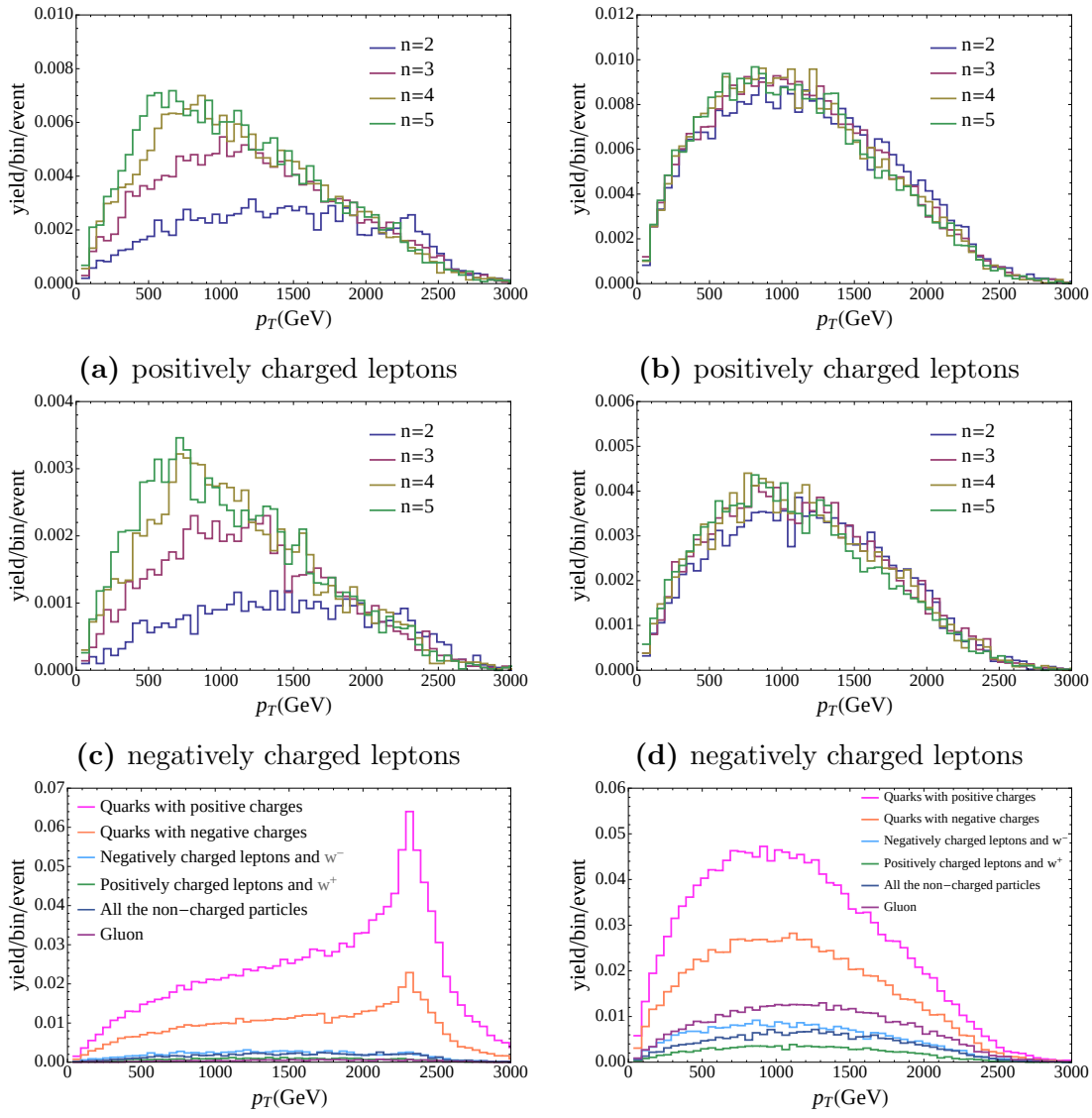

(a) positively charged leptons

(b) positively charged leptons

(c) negatively charged leptons

(d) negatively charged leptons

(e) all particle species for $n = 2$

(f) all particle species for $n = 2$

Figure 2.6: Transverse momentum distribution of leptons with positive and negative charges expressed in terms of the number of particles/bin/event for different number of spatial extra dimensions and the same distribution for different particle species for $n = 2$, for rotating micro black hole at (a),(c) and (e) and non-rotating micro black hole at (b), (d) and (f).

This is because the micro black hole is created from the collision of two protons

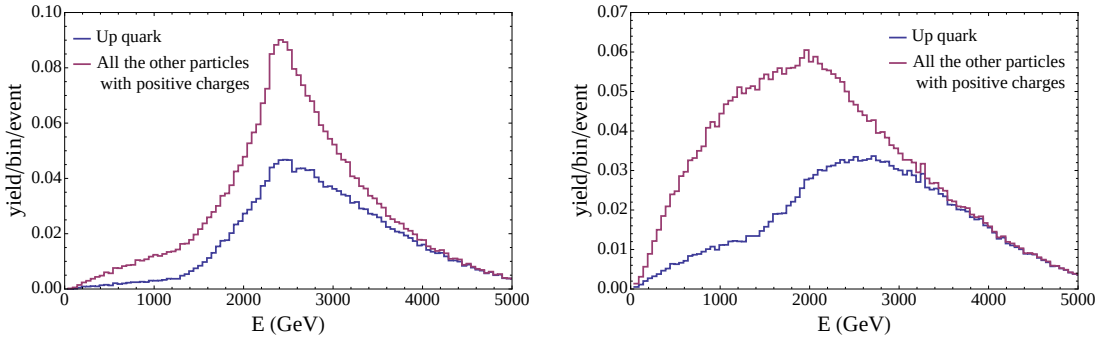

(a) rotating black hole **(b)** non-rotating black hole

Figure 2.7: Energy distribution of *up* quark and all the other positively charged particles expressed in terms of number of particles/bin/event for number of spatial extra dimensions $n = 2$ for rotating micro black hole at (a) and non-rotating micro black hole at (b).

and each proton has two *up* and one *down* valence quarks, so one may expect to see more *up* quarks in the decay products. Moreover the *up* quark has a positive electric charge and one can say that the formed micro black hole right after creation is positively charged, thus it prefers to emit particles that carry positive charges. One should note that quarks and gluons also carry the color charge and they have more degrees of freedom in comparison with other particles and that is another reason to see higher multiplicity of quarks and gluons. The other interesting feature of the emission of quarks and gluon is appeared in the plot for rotating black hole for which they have a peak at high p_T. This means that micro black holes signals are likely to appear as an enhancement in the number of quarks and gluons at high p_Ts.

2.5.1.2 Behavior in higher energies than LHC reach

Searches for micro black holes have been conducted by the CMS and ATLAS collaborations at LHC in the framework of the more general "searches for exotica". The analyses conducted so far have not lead to any evidence for micro black hole formation in p-p collisions at $E_{CM} = 7$ TeV. However, these analyses have been criticized, since quantum gravity effects, expected to be important at

LHC energies, have been neglected or treated too naively in the event generators used. The situation is globally still controversial, and the exclusion at the present LHC energy certainly does not limit the possible formation of micro black holes at higher energies.

We performed simulations of the formation of non-rotating micro black holes in p-p collisions in the $E_{CM} = 100$ and 50 TeV, at two different values for the fundamental gravity mass scale, i.e. $M_D = 4$ and 15 TeV, a micro black hole mass constrained in the range $2\ M_D < M_{MBH} < E_{CM}$, and $n = 2$ spatial extra dimensions without fermion splitting [54]. Like before in the simulation, the mass, linear and angular momentum loss fractions were assumed to be equal to 0.3, whereas angular momentum, charge and color suppression factors were assumed to be equal to 0.2, and baryon and lepton numbers, as well as their difference, conserved. With these settings we performed the simulation using BlackMax and also we interfaced the BlackMax output with PYTHIA. Examples of selected results are presented in figurs: (2.8), (2.9), (2.10) and (2.11). In figure (2.8a) and (2.8b)

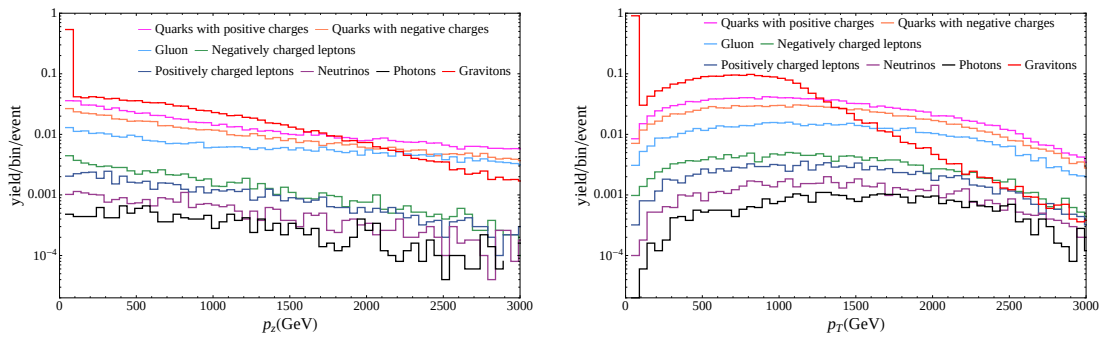

(a) **(b)**

Figure 2.8: Parallel (a) and transverse (b) momentum distributions for different SM degrees of freedom as computed by BlackMax for a micro black hole formed at a center of mass p-p collision energy $E_{CM} = 50$ TeV for $M_D = 4$ TeV.

the longitudinal and transverse momentum distributions (expressed in terms of number of particles/bin/event) are shown for different SM particle species for the case of micro black hole production at $E_{CM} = 50$ TeV. After evaporation of the micro black hole the (anti-)quarks give rise to the largest contributions followed by gluons, (anti-)leptons and photons. Contributions from particles with opposite

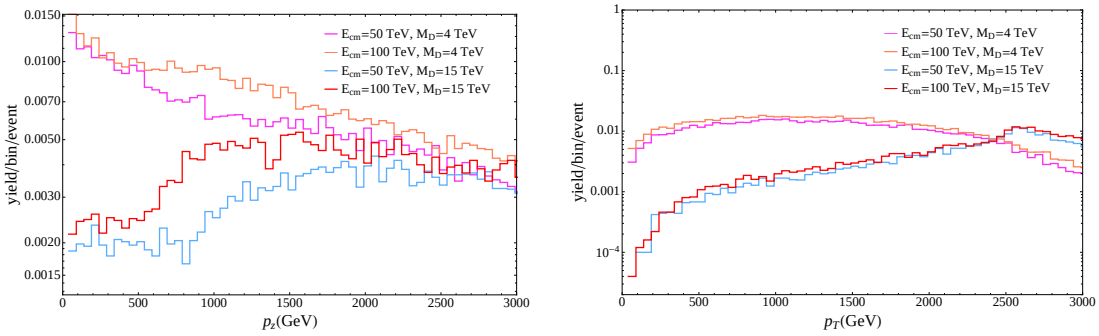

(a) **(b)**

Figure 2.9: Gluon parallel and transverse momentum distributions as computed by BlackMax for a micro black hole formed at two different center of mass p-p collision energies (E_{CM} = 50, 100 TeV) for M_D = 4 TeV and M_D = 15 TeV.

charges are shown separately: for any given flavor the contribution of positively charged particles is larger than that coming from negatively charged particles, due to the fact that during the final burst in the micro black hole evolution, positive charged particles are predominantly emitted, because the majority of micro black holes are positively charged.

The p_z distributions are almost monotonically decreasing with similar slopes for all SM particles, whereas the p_T distributions show some broad peaks, located at different p_T values according to the particle species. (Anti-)leptons are emitted in pairs, i.e. as $\ell\nu_\ell$, $\ell^+\ell^-$ or $\nu_\ell\bar{\nu}_\ell$, due to imposed lepton number conservation. Graviton distributions are also shown, and display a high p_T profile with a slope that decreases more rapidly than do those for SM particles, leading to a suppression of gravitons with respect to SM degrees of freedom at high p_T. In figure (2.9a) and figure (2.9b), the p_z and p_T distributions of a specific particle species, i.e. the gluon in this example, are shown as a function of the p-p collision E_{CM}, for different values of M_D. It is evident that, for a fixed value of M_D, the shape of the distributions at different E_{CM}'s is preserved with the total number of gluons increasing with E_{CM}. This is as expected because the cross-section for μBH formation increases with E_{CM}. On the other hand, changing the value of M_D leads to distributions with different shapes in addition to a changing value of the total cross-section. In particular, the position of the p_T maximum for gluon emission

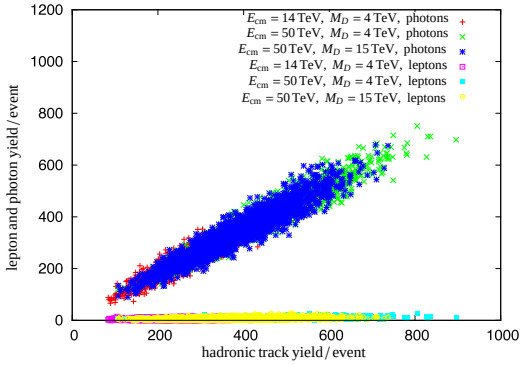

Figure 2.10: Photon (upper part) and all lepton (lower part) yields as a function of the yield of all hadronic tracks after BlackMax + PYTHIA. Each point correspond to a different simulated event. Regions with different colors correspond to different E_{CM} and M_D parameters adopted in the μBH simulation.

increases with M_D, ranging from $p_T \sim 1.1$ TeV for $M_D = 4$ TeV to $p_T \sim 4.3$ TeV for $M_D = 15$ TeV.

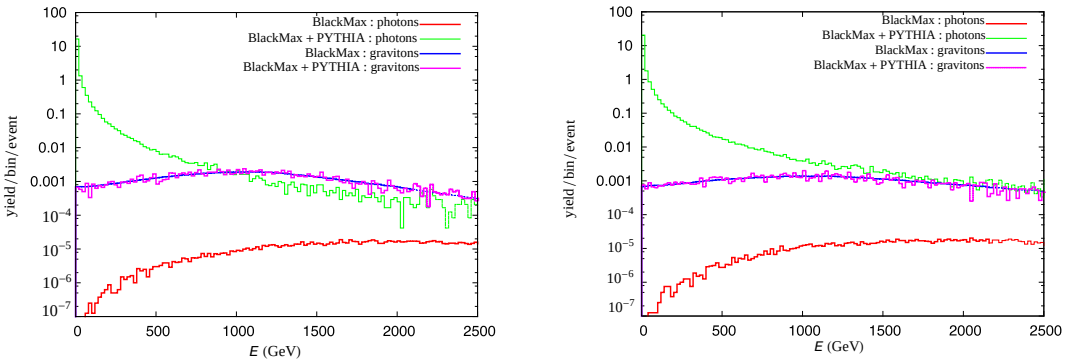

(a) E_{CM}=50 TeV M_D= 4 TeV **(b)** E_{CM}=100 TeV M_D= 4 TeV

Figure 2.11: Energy distributions of photons and gravitons emitted by a micro black hole at a CM p-p collision energy $E_{CM} = 50$ TeV (a) and $E_{CM} = 100$ TeV (b), for $M_D = 4$ TeV. Results after both BlackMax and BlackMax + PYTHIA are presented in each panel for comparison.

The SM yields from micro black hole evaporation are in general modified after parton and photon shower + hadronization + hadron decay, as simulated

by SMC codes, such as PYTHIA, which leads to hundreds of hadrons and photons. In particular, the number of emitted photons in each event turns out to be correlated to the number of emitted hadronic tracks, with a constant slope at increasing E_{CM}, as shown in figure (2.10). This slope is also independent of M_D, at a fixed E_{CM}. On the other hand, the total yield of emitted leptons turns out to be small (a few tens of particles) and does not show evident correlations with the number of hadronic tracks. This points towards the conclusion that the large number of photons is probably due light hadron (in particular π^0) decays, whereas electromagnetic shower effects are suppressed. It is also interesting to compare the shapes of particle spectra at different stages of the evolution of the entire system. In particular this can be carried out for distributions of particles that are not subject to hadronization, such as leptons, photons and gravitons. In figure (2.11a) and (2.11b) the energy distributions of photons and gravitons at the parton level after micro black hole evaporation and at the hadron level after PYTHIA are shown, for two different E_{CM} energies. It is evident that the contributions of the parton shower, the hadronization and hadron decay lead to a complete distortion of the original photon spectrum, disproportionately populating the region of low energies with photons emitted in these last processes. The photon distributions at the evaporation level are very similar for both $E_{CM} = 50$ and 100 TeV, whereas, at the hadron level, the photon distribution at $E_{CM} = 100$ TeV is clearly much more populated than the corresponding one for $E_{CM} = 50$ TeV due to the stronger SMC effects. On the other hand, the graviton distributions are completely unaffected by shower effects, and in the case of $E_{CM} = 100$ TeV display a flatter profile in comparison to that at $E_{CM} = 50$ TeV.
To investigate the spectra of the emitted particles from rotating black hole at different energies we performed the simulation using CHARYBDIS2, considering the same initial parameters as BlackMax, and we interfaced it to HERWIG for SMC, see figure (2.12). In contrary with non-rotating case we see that for higher center of mass energies we have less produced particles, while the spectrum of emitted particles is harder in higher energies figure (2.12b).

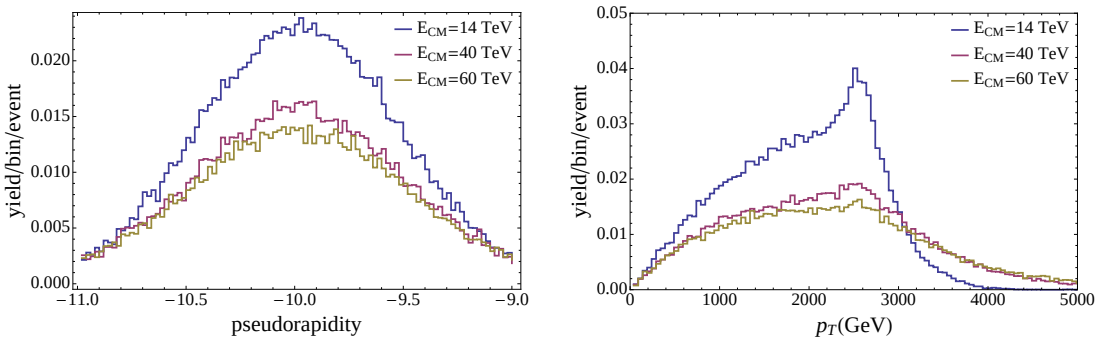

(a) pseudorapidity **(b)** transverse momentum

Figure 2.12: Multiplicity of the positively charged quarks at (a) different pseudorapidity and (b) different transverse momentum and for 3 different center of mass energies $E_{cm} = 14,\ 40$ and 60 TeV

2.5.1.3 A test in BlackMax

It is important to know about the sensitivity of the micro black hole event generators to the exact form of the grey body factors. To test this sensitivity we changed grey body factors by 15% in the BlackMax codes [55]. Then we investigated the final output of the BlackMax before and after this change of the grey body factors for spinor and gauge particles. Results of this study are shown in figures (2.13) and (2.14). Figures (2.13a) and (2.14a) represent the implemented change in the grey body factors for gauge bosons and spinor fields and figures (2.13b), (2.14b) and (2.14c) show the multiplicity of the gauge bosons, quarks and charged leptons before and after the change in grey body factors. As is clear, the multiplicity of the gauge bosons has not changed and the change of the quark and charged lepton multiplicities is negligible, indicating that BlackMax has low sensitivity to the exact form of grey body factors. In this sense, in the absence of the grey body factors for graviton emission from a rotating micro black hole one may introduce an approximate profile for graviton emission and possibly study the final products of the micro black hole decay. This may help one to see, in particular, if the graviton emission increases with rotation and possibly competes with emission of the SM particles.

For the case of non-rotating micro black holes we used CHARYBDIS2 to investigate the effect of grey-body factors. We switched off the grey body factors at

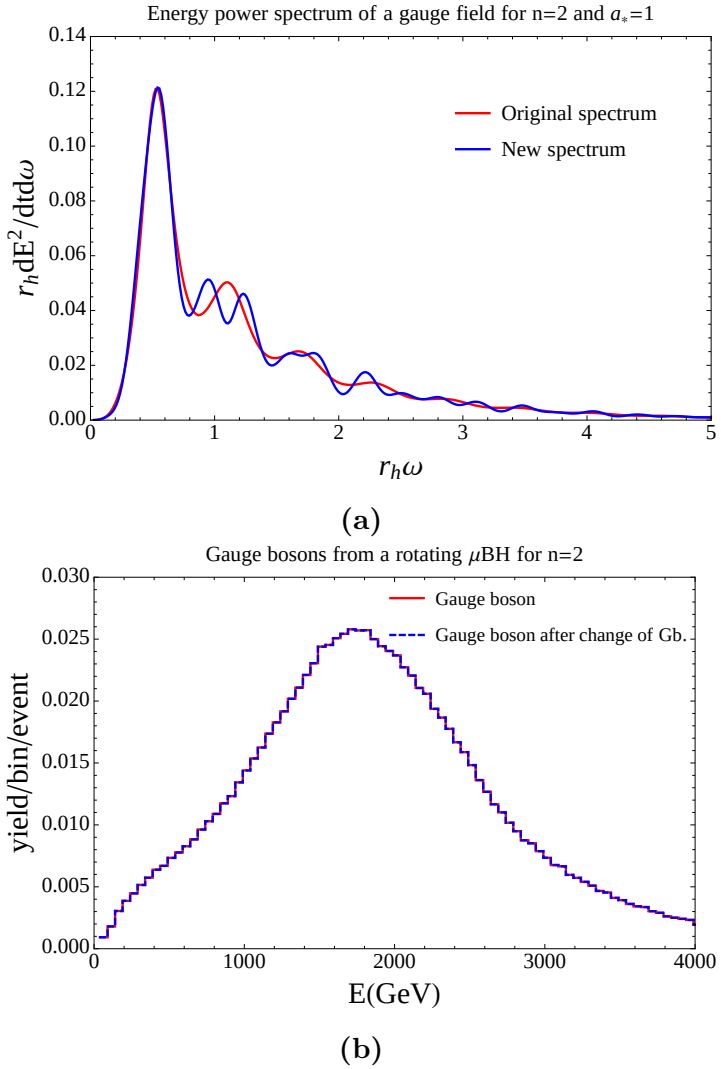

Figure 2.13: (a) Energy power spectrum from a gauge field and (b) gauge boson multiplicity

two different energies, $E_{\rm cm} = 14$ and 100 TeV, in CHARYBDIS2 and we compared the multiplicity of the positively charged quarks and gravitons with the time that this switch was on figure (2.15). One can see that even in the case of non-rotating micro black holes final product is not changing drastically with or without including grey body factors. It is evident in figure (2.15b) that for higher energies the effect of grey-body factor is more weak suggesting that the spectrum is more like the black body spectrum.

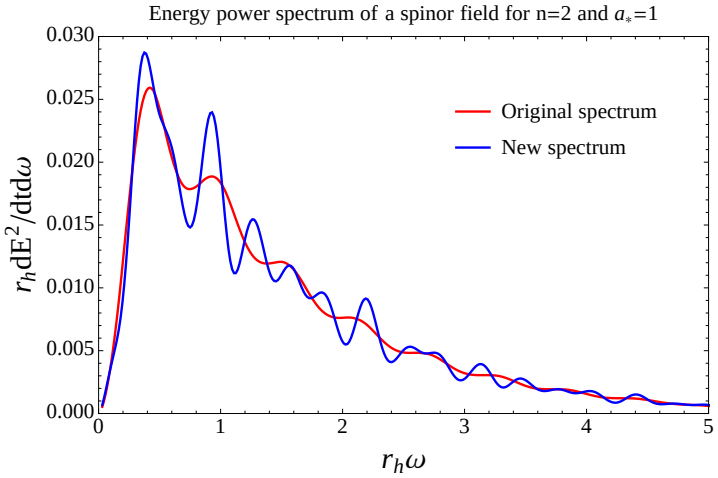

(a)

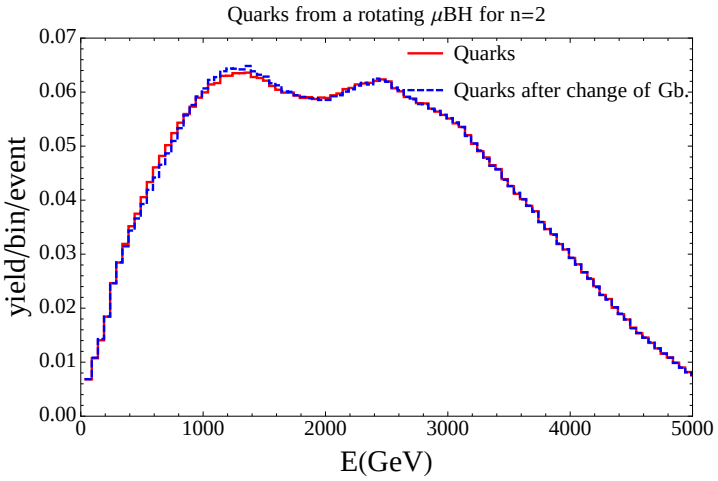

(b)

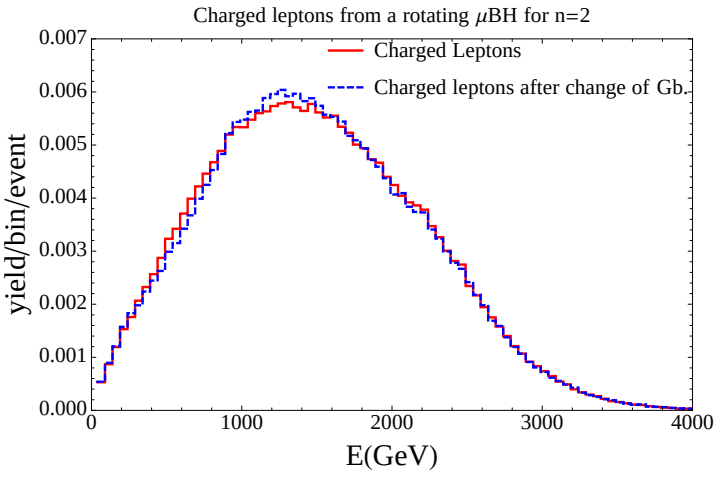

(c)

Figure 2.14: (a) Energy power spectrum from a spinor field, (b) and (c) quark and charged lepton multiplicities

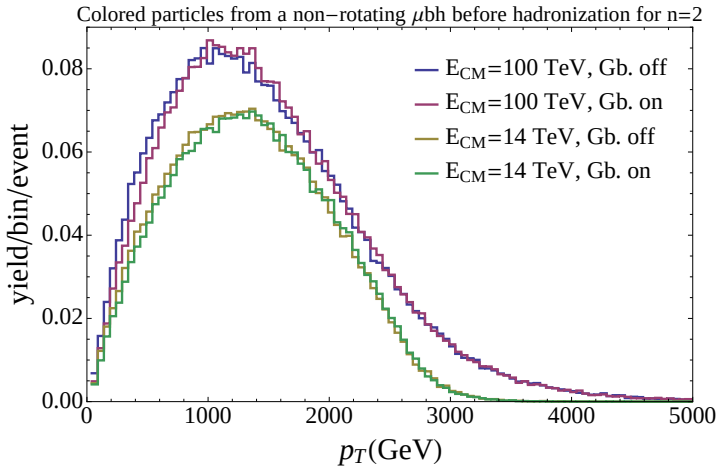

(a)

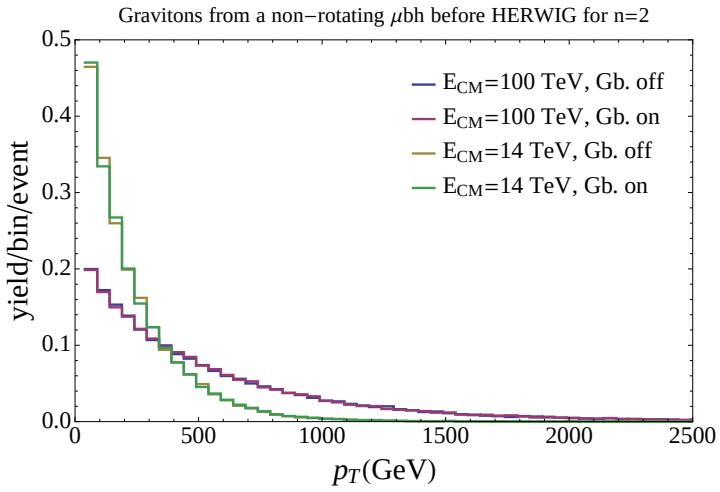

(b)

Figure 2.15: (a) Quarks, gluons and (b) graviton multiplicity with grey body factor switch on and off.

3

Quasi-Normal Modes

One way to study the properties of a black hole is to investigate how the black hole interacts with its environment. One can carry out this investigation by perturbing the black hole space-time and then studying how the black hole responds to this perturbation. The black hole space-time can be perturbed by scattering of the wave packets on the black hole [56], letting a test particle fall into the black hole or passing close by black hole [57, 58, 59], etc.
The first study regarding scattering of radiation by a black hole was carried out by Vishveshwara [56]. He found that black holes leave their fingerprints on the scattered waves and using these fingerprints one can obtain useful information about the black hole and the related space-time.

3.1 Quasi-normal modes

It is known that when we excite objects they respond to the excitation with a very specific sound that is like their fingerprint. The same thing holds also for black holes. It should be noted that response to the perturbation of the black hole space-time, either by oscillation of fields in its vicinity or oscillation of the space-time itself, is part of the evolution of the gravitational waves emission in time. In general this evolution can be divided into three stages: first an initial wave burst in a relatively short time by the source of perturbation, then a long period of exponentially damped "ringing" or oscillations that are dominated by frequencies that do not depend on the source of the perturbation, the so called

"quasi-normal modes", and finally a power law tail suppression of QNMs at very large time, see figure (3.1). The frequencies associated to the QNMs are called "quasi-normal frequencies".

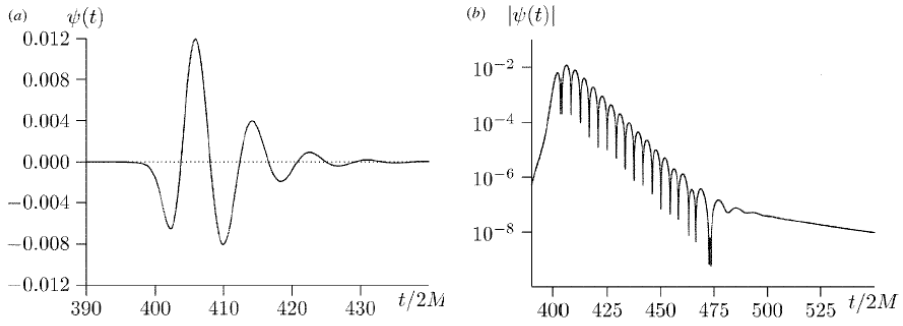

Figure 3.1: Left: response of the Schwarzschild black hole to the perturbation by a gaussian wave packet. Right: Evolution of gaussian wave packet in vicinity of a Schwarzschild black hole in log-scale.

3.1.1 Quasi-normal modes vs. normal modes

Lets consider some familiar objects around us like a bell, a guitar or a pendulum. If we excite these systems their response to the excitation is by set of natural real frequencies, the normal frequencies, that is given as a superposition of stationary modes, the normal modes. If one neglects the dissipation the preferred time dependent harmonic states [60] of motion are

$$\chi_n(t,x) = e^{i\omega_n t}\chi_n(x), \qquad n = 1, 2, 3, ..., \tag{3.1}$$

where ω_n's are real and we can assume that χ is some complex valued field and the general solution can be expressed as a superposition of normal modes

$$\chi(t,x) = \sum_{n=1}^{\infty} a_n e^{i\omega_n t}\chi_n(x). \tag{3.2}$$

Normal modes are stationary states, namely if a system oscillates in a purely normal mode, it will never stop oscillating. Clearly, when we assume that there is no damping this means that these modes form a complete set. However in a

more realistic case, with considering an energy loss mechanism, modes (QNMs) will not form a complete set and it is not possible to write a stationary normal mode expansion because these modes appear only over a limited time interval. The latter situation is relevant for black holes; when their space-time oscillations generate gravitational waves that carry energy to infinity. So dissipation here cannot be neglected and that's why their characteristic sounds are expressed by quasi-normal modes not normal modes. Here "quasi" means that the system is open and it loses energy through gravitational wave radiation. [3]

3.1.2 Quasi-normal modes importance

Black hole parameters The importance of the study of quasi normal modes is very much related to the crucial role that black holes play in general relativity. Black holes can be described by their intrinsic parameters: mass, angular momentum and charge and they may be counted as the hydrogen atom of quantum mechanics. So any tool that leads us to an estimation of these parameters is valuable and one way to identify these parameters is using quasi normal frequencies.

Gravitational wave detection Another motivation for studying quasi normal modes comes from gravitational wave detection. In general these signals are so weak that in order to be able to detect them one needs strong source of gravitational wave emission such as black hole collisions or stellar collapse [61]. There are various experiments that have been designed to detect gravitational waves and between them experiments like LISA [62], VIRGO [63] and LIGO [64] are to detect gravitational wave signals from black holes. The dominant signal that may be detected will be the signals from fundamental modes: quasi normal mode with the lowest frequency or lowest imaginary part.

Thermalization time-scales in the AdS/CFT On one hand we know that QCD is based on the gauge group SU(3) and at low energies QCD becomes strongly coupled and very difficult to study. This is because one cannot use perturbative methods to study processes involving energies of the order of

$\Lambda_{\rm QCD}$ or lower. At these energies one can use conformal field theory that includes SU(N) Yang-Mills theory in the limit $N \to \infty$ and study the fields using perturbative methods.

On the other hand one has string theory that contains a particle with zero mass and spin two, namely graviton. The correspondence between these theories at very large N limit (inverse string coupling constant in string theory) is called the AdS/CFT correspondence [65]. According to the AdS/CFT correspondence (gauge-gravity duality), a black hole in AdS space-time corresponds to an approximately thermal state of a strongly coupled system in the CFT. The AdS/CFT offers an approach to deal with non-perturbative nature of QCD. For example it is possible to perform the expansion of the correlators on the supergravity part and using them obtain correlation functions in a gauge theory at strong coupling.

Quasi normal modes as the response to the black hole perturbation in AdS space-time are the same as the response to the perturbation of a thermal system. It is very complicated to calculate these modes in the strongly coupled systems in CFT but one can calculate these modes using black hole perturbation. Finally one can compute the thermalization time-scale in the strongly coupled CFT from the quasi normal frequencies [66] that have been computed in AdS.

Black hole area quantization The Ehrenfest principle [67] states that any classical adiabatic invariant corresponds to a quantum entity with discrete spectrum. Using this principle Bekenstein conjectured that the horizon area of a non-extremal quantum black hole that behaves like an adiabatic invariant should have a discrete eigenvalue spectrum [68]. In [69] Bekenstein suggests that when a black hole captures a neutral particle, its horizon area will change. This area is minimized when the particle center of mass is at a turning point of a proper distance that cannot be smaller than $\hbar/\mu$, $\sim$ its Compton wavelength, where μ is the rest mass of the particle. Using this assumption he set a lower bound on the increase of the black hole surface area. Later Hod [70] set the lower bound on the area increase for the situation that the black hole captures a charged particle. Although the

physical mechanisms where different for two cases of charged and neutral particles the latter lower bound was at the same order of magnitude as the neutral case. After finding this universality Hod suggested that the black hole surface area has the following form

$$A_n = \gamma n l_p^2, \qquad n = 1, 2, 3, ..., \tag{3.3}$$

where γ is a dimensionless constant that can be determined using the black hole quasi normal modes, and l_p is the Planck length. At the next step Hod investigated the black hole perturbation equations and quasi-normal modes as the solutions to these equations. He considered the asymptotic limit of quasi normal modes in which the mode number $n \to \infty$. This limit was considered because his analysis was based on "Bohr's correspondence principle" which naively says "quantum transitions should not take time" [70]. When $n \to \infty$ the black hole oscillations are highly damped which means they have very big imaginary part and consequently a very small relaxation time ($\tau = \omega_I^{-1}$). These modes for the Schwarzschild black hole [71] are given by

$$M\omega_n = 0.0437123 - \frac{i}{4}\left(n + \frac{1}{2}\right) + O\left[(n+1)^{-1/2}\right]. \tag{3.4}$$

Hod argued that the numerical value of the real part of (3.4), ω_R, agrees with the expression $(\ln 3)/(8\pi)$. He justified this by using the relations $A = 16\pi M^2$ and $dM = E = \hbar\omega$. He found that $\Delta A = 4l_p^2 \ln 3$ and consequently $\gamma = 4\ln 3$. Finally he conclude that the area spectrum for the quantum Schwarzschild black hole is given by

$$A_n = 4\ n\ l_p^2 \ln 3, \qquad n = 1, 2, 3, ... \tag{3.5}$$

Hod established these results just according to the numerical coincidence however later on Motl [72] and Motl and Neitzke [32] obtained the same results using analytical techniques. We should mention that this result does not depend much on the details of black hole geometry.

3.1.3 Quasi-normal modes and black hole parameters

Black hole quasi normal modes may provide help to identify the black hole parameters. If one considers the Schwarzschild, Reissner-Nordstrom or Kerr black holes, the fundamental parameters are mass, charge and angular momentum accordingly. One should note that depending on the type of black hole under consideration we may be able to extract some helpful information from quasi-normal mode about other parameters like cosmological constant, extra dimensions, external magnetic field. The dependence of these parameters on the quasi normal modes for the case of three former types is described in below.

Black hole mass It is possible to investigate the dependence of quasi-normal modes on the mass of a black hole using two different assumptions. We may either assume that the mass is not changing by considering a stationary background like Schwarzschild or we may consider the black hole mass as a function of time in the case of evaporating black holes in a time dependent background like Vaidya background [73, 74].

For instance the fundamental quasi normal frequency for the quadrupole mode ($l = 2$) in Schwarzschild background in geometrical units is given by [3]

$$\omega M = 0.37367 - 0.08896i \tag{3.6}$$

To convert (3.6) into kHz, one can multiply ωM by $2\pi(5.14kHz)M_{\odot}/M$ then the oscillation frequency is

$$\nu = \nu_R + i\nu_I = (12.074 - 2.875i)\frac{M_{\odot}}{M}kHz \tag{3.7}$$

The real part of ν is the frequency and $\frac{1}{\nu_I}$ represents the damping timescale. It is worthwhile to mention that the band width of a ground based gravitational interferometer like Virgo and LIGO is about 10 - $40Hz$ up to few kHz and this can detect the signal from black holes with mass range

$$10M_{\odot} \lesssim M \lesssim 10^3 M_{\odot} \tag{3.8}$$

The same dependence ($\omega \sim M^{-1}$) holds for the case of time-dependent black hole background. It should be noted that the black hole mass changes with

time in realistic cases. A Schwarzschild black hole gaining or losing mass via absorption or evaporation is a good example. In [75] the evolution of the massless scalar field in the time-dependent Schwarzschild black hole background have been studied numerically. It has been shown that in contrary with the stationary black hole case the decay and oscillation timescale change with the evolution of time. In the absorption process that black hole gains mass, both the real and imaginary parts of the quasi-normal frequencies decrease with the increase of time. While when the black hole loses mass, both the real and imaginary parts of the quasi-normal frequencies increase with the increase of time.
We will discuss about this kind of space-time in more detail in chapter (6).

Black hole electric charge The relation between the quasi normal modes and black hole electric charge, Q, has been investigated with study of the Reissner-Nordstrom black hole in [76, 77]. To study the perturbation equations in this charged background one might consider both axial and polar modes, however quasi normal modes for both of these perturbations are identical as the two effective potentials carry the same physical information. For small electric charge both the oscillation frequency and damping rate increase with increase of Q. If one considers electromagnetic perturbations in this background, because of electric charges there will be interactions between these two fields. This effect may increase the electric charge and oscillation frequency while the damping rate decreases.

Black hole angular momentum To understand the relation between the black hole rotation parameter and black hole quasi normal modes one can calculate the quasi normal modes of the Kerr black hole [78]. In the Kerr geometry quasi normal modes are distinguished by their azimuthal and longitudinal indices m and l and also by their overtone number n. Quasi normal modes of Kerr black hole are functions of the rotation parameter a and total black hole mass M. Depending on different l and m the behavior of the real and imaginary parts of the quasi normal modes may change. For any kinds of perturbation the damping rate depends on whether $m > 0$ or $m < 0$. For increasing a, with $m > 0$ the damping rate decreases, also for

$m < 0$ damping rate decreases but more quickly while oscillation frequency increases with increase of m. For all kinds of perturbations in the high damping limit the behavior is universal. In the high damping limit, the real part of all modes with $m > 0$ typically shows a minimum as a function of the rotation parameter a, and then approaches the limit $\omega_R = m$ for $a \to M$ [79].

Detailed study of quasi-normal modes of rotating black holes is always of interest because it will give information about the stability of the black hole. We will discuss this issue in details in this chapter.

3.1.4 Quasi-normal tail

At the beginning of this chapter we discussed about three different stages of the response of a black hole to the perturbation. The last stage of this respond is a power law falloff of the field. This phenomenon is known as quasi normal tail. It was first shown by Price [80] that for the Schwarzschild geometry at late times of the formation a black hole in any multipoles with $l \geq s$ of a field perturbation with spin, s, slowly dies with a power-law tail,

$$\psi \sim t^{-(2l+p+1)}. \tag{3.9}$$

Where p depends on the presence of a static l-pole field. For the field outside the star prior to the onset of the collapse $p = 1$. If developing the l-pole perturbation takes place during collapse process $p = 2$. He argued that this tail is because of backscattering of the potential at very large spacial distances. This behavior was confirmed by numerical studies in linearized perturbation as well as in a non-linear evolution [81, 82] . What we mean by tail is the decay of the wave as the tail of the perturbation at late times is not a sharp cut off of the wave. This behavior is the same for stars and black holes because it is independent of the initial data and it only depends on the asymptotic far region. These power law tails form even when no horizon is present in the background.

3.1.4.1 Green's function approach

Beside explaining this phenomena by considering it as the result of the gravitational wave scattering from the effective potential, it can be also explained by considering it as the branch cut in the associated Green's function [2, 3]. Using the Klein-Gordon equation (2.7) (without implying $\Psi \sim e^{-i\omega t}$), the time evolution of the field $\Psi(r_*, t)$ can be written as

$$\Psi(r_*, t) = \int dr'_* G(r_*, r'_*; t)\partial_t \Psi(r'_*, 0) + \int dr'_* \partial_t G(r_*, r'_*; t)\Psi(r'_*, 0), \tag{3.10}$$

using (2.7) one can define two operators D and $\bar{D}(\omega)$ which act on Green's function as

$$DG(r_*, r'_*; t) = \delta(t)\delta(r_* - r'_*), \qquad \bar{D}(\omega)\bar{G}(r_*, r'_*; \omega) = \delta(r_* - r'_*) \tag{3.11}$$

We can consider that the potential is zero at left and right boundaries. The boundary condition at infinity is purely outgoing for both black holes and stars while for the left boundary depending on the object that we may consider it can be

$$\text{Boundary condition} = \begin{cases} \textit{Black holes} & \bar{\Psi}(r_*, 0) \propto e^{-i\omega t}, \quad r_* \to -\infty \\ \textit{Stars} & \bar{\Psi}(r_*, 0) \to 0, \quad r_* \to 0 \end{cases} \tag{3.12}$$

Taking two functions $f(\omega, r_*)$ and $g(\omega, r_*)$ that satisfy the left and right boundary conditions respectively as the solution of the equation

$$\bar{D}(\omega)f(\omega, r_*) = \bar{D}(\omega)g(\omega, r_*) = 0 \tag{3.13}$$

one can write

$$\bar{G}(r_*, r'_*; \omega) = \begin{cases} f(\omega, r_*)g(\omega, r'_*)/W(\omega) & , \quad r_* < r'_* \\ f(\omega, r'_*)g(\omega, r_*)/W(\omega) & , \quad r_* > r'_* \end{cases} \tag{3.14}$$

where $W(\omega)$ is the Wronskian of g and f functions. If one considers the inverse transformation

$$\bar{G}(r_*, r'_*; \omega) = \int_0^\infty dt \;\; G(r_*, r'_*; t) \;\; e^{i\omega t}, \tag{3.15}$$

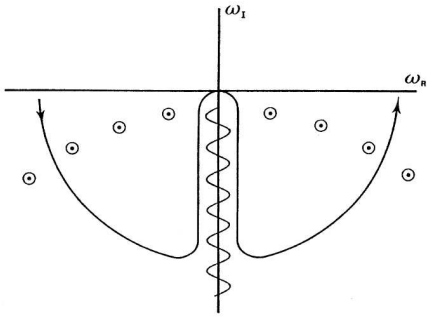

Figure 3.2: Singularity structure of $\bar{G}(r_*, r'_*; \omega)$ in the lower half of ω plane [2]

one may close the counter on the complex $\omega-$plane by a semicircle with radius C in the lower half plane where it will led to take the limit $C \to \infty$, see figure (3.2). Then one has to consider the the negative imaginary part of the $\omega-$plane because of the singularities of the Green's function. Apart from the shape of potential the function $g(\omega, r_*)$ that was to satisfy the boundary condition in spatial infinity has form of the branch cut on $Im\omega < 0$ and this contribution is called tail contribution.

It should be noted that the decay tail for massive and massless fields is not the same. If one considers the massive fields the late time tail is more oscillating than decaying [83]. In fact quasi normal oscillations decay with an oscillatory inverse power tail profile. In this case a late time tail will appear in the Minkowski space time, this space time is dispersive for the massive field and this may cause a different decay behavior. For instance for a massive scalar field in the Minkowski space time the late time tail has the form [3]

$$|\Psi_{flat}| \sim t^{-\ell-\frac{3}{2}} \sin \mu t, \tag{3.16}$$

where μ is the inverse Compton wavelength.

The late time behavior for D-dimensional ($D > 4$) backgrounds also have a different form depending on whether D is even or odd. The reason is that the Green's function has completely different structure for odd and even dimensions [61]. In odd dimensional background tail is due to the contribution of flat background Green's function

$$|\Psi_{odd}| \sim t^{-(2\ell+D-2)}, \tag{3.17}$$

however for even D-dimensional background there is not such a contribution and all the contribution to the tail is from black hole itself

$$|\Psi_{even}| \sim t^{-(2\ell+3D-8)}. \tag{3.18}$$

As it is clear for the even D-dimensional background the power-law decay takes place more rapidly than the odd D-dimensional one.

3.2 Quasi-normal modes: derivation

To calculate quasi-normal modes one needs to perturb the related wave equation in the assumed background. The type of the quasi-normal modes will depend on the type of ordinary differential equations that one solves. One may consider perturbations to the scalar field, electromagnetic field for scalar and electromagnetic quasi-normal modes or the linearized perturbation to the Einstein's equations itself to obtain gravitational quasi-normal modes. The methods for studying all of these three kinds are not different regarding each case, but in general there are various methods to calculate quasi-normal modes and we will explain some of them in the following. The most important thing to derive quasi normal modes is defining the proper boundary conditions.

3.2.1 Boundary conditions

To determine the quasi-normal modes of any kind one has to solve the wave equations that we discussed earlier. Solutions to these equations should satisfy specific boundary conditions both at the black hole horizon and at null infinity. If we consider the case of the Schwarzschild black hole an asymptotically flat space-time, quasi-normal modes will be defined by the condition that there are only pure ingoing waves at the event horizon and a purely outgoing wave at null infinity.

For instance, if $\Psi_{event\ \ horizon} \sim e^{-i\omega r_*}$ and $\Psi_{null\ \ infinity} \sim e^{i\omega r_*}$ are two independent solutions at the event horizon and null infinity for vanishing potential at these points, it is easy to see that the required boundary conditions has been

satisfied

$$\Psi_{event\ \ horizon} \sim pure\ \ ingoing\ \ wave \sim e^{-i\omega r_*}, \qquad r_* \to -\infty \tag{3.19}$$

and far from horizon in null infinity

$$\Psi_{null\ \ infinity} \sim pure\ \ outgoing\ \ wave \sim e^{i\omega r_*}, \qquad r_* \to +\infty \tag{3.20}$$

At event horizon we have a purely in-going wave because this solution has not seen the potential yet while solution to the wave equation far from horizon can have both ingoing and outgoing parts due to the effective potential that out to get through it. This potential falls off asymptotically both at the event horizon and null infinity. In this case boundary condition has to be imposed in such a way that the in-going part of the solution at infinity cannot survive. Then one only remains with purely out-going wave at infinity.

3.2.2 Analytical methods and numerical integration of perturbations equations

Because of the importance of the quasi normal modes in gravitational wave detection and determining the black hole parameters various analytical, semi-analytical and numerical methods have been developed during the recent years. We will give a short explanation of some of them in the following section. Details of these methods have been presented in [3].

The numerical method for integration of the wave equation has been presented in various literature. The method that mostly has been used is originally introduced by Gundlach, Price and Pullin in [81]. According to this integration technique one should rewrite the wave equation in the light cone coordinates. Thus we rewrite the wave equation like (2.7) in the new light cone coordinates (u, v)

$$\left(4\frac{\partial^2}{\partial u \partial v} + V(u,v)\right)\Psi(u,v) = 0, \tag{3.21}$$

to integrate (3.21) numerically, we act the time evolution operator

$$\exp\left(h\frac{\partial}{\partial t}\right) = \exp\left(h\frac{\partial}{\partial u} + h\frac{\partial}{\partial v}\right) \tag{3.22}$$

on $\Psi(u, v)$ and we use (3.21) to obtain

$$\Psi_N = \Psi_E + \Psi_W - \Psi_S - V_\ell \frac{h^2}{8}(\Psi_E + \Psi_W) + O(h^4) \tag{3.23}$$

where the points $N = (u+h, v+h)$, $S = (u, v)$, $E = (u, v+h)$, and $W = (u+h, v)$ form a null rhombus, figure (3.3), and h is the grid scale factor. We can calculate the values of the Ψ function inside the rhombus that is build on two null surfaces $u = u_0$ and $v = v_0$ starting from initial data specified on them. In this way one can find out the time-domain profile of the perturbation. Then using other methods like Prony method [3] one can extract the quasi normal frequencies from the time-domain profile of the perturbation.

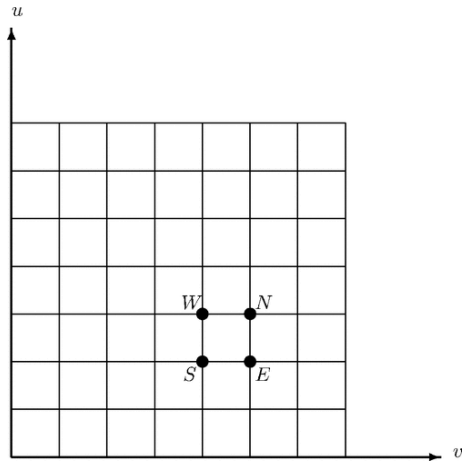

Figure 3.3: The integration grid. Each cell of the grid represents an integration step. The points illustrate the choice of (S, W, E, and N) for the particular step of the integration. The initial data are specified on the left and bottom sides of the rhombus. [3].

3.2.2.1 WKB method

This method is a semi-analytic technique that is based on an analogy between perturbative equations in the Schwarzschild background and the Schrödinger equation of a particle encountering a potential barrier. For instance, consider a Schrödinger like wave equation

$$\frac{d^2\psi}{dr^2} + R(r)\psi = 0 \tag{3.24}$$

where $R(r)$ has the form

$$R(r) = \frac{1}{f(r)^2}(\omega^2 - V(r)) \tag{3.25}$$

where ω is a complex frequency, $V(r)$ is the potential and $f(r)$ is the black hole metric function. The two complex and linearly independent solutions to the wave equation (3.24) are

$$\begin{cases} \Psi_1^t(r) = & Q^{-1/2}(r)\exp\left(+i\int_t^r Q(r')dr'\right) \\ \Psi_2^t(r) = & Q^{-1/2}(r)\exp\left(-i\int_t^r Q(r')dr'\right) \end{cases} \tag{3.26}$$

where $Q^2 = R$. Having the asymptotic WKB solution of the wave equation at both event horizon and spatial infinity, one needs to match these solutions near the top of the potential barrier.

This method is applicable for the equations that include the effective potential that approaches a constant value at the event horizon and at spatial infinity. Using this method one can derive a formula that gives the real and imaginary part of the quasi normal frequency in terms of the black hole parameters.

For instance in the large multipole limits the quasi normal modes of the Schwarzschild black holes for the Pochl-Teller potential [84] were calculated [85]

$$\omega = \frac{1}{3\sqrt{3}M}\left(\ell + \frac{1}{2} - (k + \frac{1}{2})i\right) + O(\frac{1}{\ell}), \tag{3.27}$$

where k is the overtone number and ℓ is multipole number. This formula is valid for scalar, Dirac and electromagnetic fields.

The WKB method is a powerful method in the case of wave propagation in stationary background, however for the cases that mass or charge are function of time this method is less accurate [74].

3.2.2.2 Continued fraction

The continued fraction method is an accurate method for calculating the quasi normal modes. This method was first applied by Leaver [86]. According to this method if one lets $\Psi(t, r, \theta, \phi)$ be a component of a perturbation to a massless spin s field, the wave equation is

$$r(r-1)\Psi_{\ell,rr} + \Psi_{\ell,r} - \left[\frac{\rho^2 r^3}{r-1} + \ell(\ell+1) - \frac{\epsilon}{r}\right]\Psi_\ell = 0, \tag{3.28}$$

where $\rho = -i\omega$ is a new frequency variable and $\epsilon = -1, 0, +3$ stands for scalar, electromagnetic or gravitational field respectively. Applying the boundry conditions at the event horizon $r = 1$ and spatial infinity $r = +\infty$, the solution can be written as

$$\Psi_\ell = (r-1)^\rho r^{-2\rho} e^{-\rho(r-1)} \sum_{n=0}^{\infty} a_n (\frac{r-1}{r})^n \tag{3.29}$$

The boundary conditions will be satisfied for those values of $\omega = \omega_n$, quasi normal modes, that makes (3.29) convergent. The expansion coefficient a_n can be determined by the following recurrence relation that starts with $a_0 = 1$

$$\alpha_0 a_1 + \beta_0 a_0 = 0, \tag{3.30}$$

$$\alpha_n a_{n+1} + \beta_n a_n + \gamma_n a_{n-1} = 0, \qquad n = 1, 2... \tag{3.31}$$

where α_n, β_n and γ_n are simple functions of n, ρ and other parameters of differential equation. This recurrence relation gives us the condition under which the series in (3.29) is convergent. For this purpose, if one looks at the $n \to \infty$ behavior of the a_n coefficients, one can find that the a_ns form a solution sequence to the recurrence relation (5.4) and the ratio of successive a_n can be written in the form of a continued fraction

$$\frac{a_{n+1}}{a_n} = \frac{-\gamma_{n+1}}{\beta_{n+1}-} \frac{\alpha_{n+1}\gamma_{n+2}}{\beta_{n+2}-} \frac{\alpha_{n+2}\gamma_{n+3}}{\beta_{n+3}-} ..., \tag{3.32}$$

this equation is like an $n = \infty$ boundary condition on the sequence a_n. Thus from (3.32) at $n = 0$ and using (3.30) at $n = 0$ as boundary condition on the ratio $\frac{a_1}{a_0}$ we will get two expressions such that if we equate them we will have

$$0 = \beta_0 - \frac{-\gamma_1}{\beta_1-} \frac{\alpha_1\gamma_2}{\beta_2-} \frac{\alpha_2\gamma_3}{\beta_3-} ... \tag{3.33}$$

as α_n, β_n and γ_n are functions of the frequency ρ, and the determination of quasi normal frequency can be carried out by finding the roots of (3.33) numerically. It turns out that the convergence of the continued fraction is slow when the imaginary part of the quasi-normal frequency increases in comparison with its real part. This problem is investigated by Nollert at [71].

3.3 (In)stability

Knowing whether a black hole solution or in general a compact object is stable against perturbations or not is a very important issue in physical studies. The 4-dimensional solutions of Einstein's field equations are guaranteed to exist by the uniqueness theorem, however higher dimensional solutions require some other methods to approve their existence since uniqueness theorem is not applicable for these solutions.

One way to verify the existence of higher dimensional solutions is by proving that the assumed solution is stable under small perturbations. There are different ways to investigate the stability of a solution against perturbations. To investigate the stability of a wave equation one should consider all the three types of perturbations, namely, scalar (in $D = 4$ polar), vector (in $D = 4$ axial) and tensor perturbations. Studies of 4-dimensional solutions have shown that they are usually stable against perturbations but for higher dimensional black holes the scenario is different because different types of instabilities will emerge when one studies them.Types of instabilities for the case of non-rotating and rotating black holes are also different.

The instabilities of higher-dimensional rotating black holes, like the Myers-Perry solution, have received much attention in recent years. Though the full analysis of this case is not available as the perturbation equations are not separable, the numerical study for some special case of this solution shows the existence of instabilities for large angular momentum [87].

3.3.1 What do the quasi-normal modes tell us about (in)stabilities?

One method to find out about in(stability) of a solution is by studying the quasi normal modes. If one investigates these modes either numerically or analytically and finds out that all of them decay in the time domain, it means that the solution is stable but if even one of the modes is growing this tells us that the solution is unstable.

We mentioned earlier in this chapter that the quasi normal frequencies have

complex forms and the imaginary part of this frequency shows how damped the oscillation on that frequency is, taking into account that damping means that the imaginary part has to be negative. Hence modes that have positive imaginary parts can be considered as the growing modes and existence of these modes implies the existence of an instability. If one can show that there are no growing modes in the quasi-normal frequency spectrum of a black hole, this can be a proof of the stability of a black hole. In other words, modes with positive imaginary parts, unstable modes, are purely imaginary, namely, they have zero real parts. This means that these modes are non-oscillatory [88]. Beside the non-oscillatory property of unstable modes, one can distinguish them from the evolution of the time domain profile. For instance consider figure (3.4).

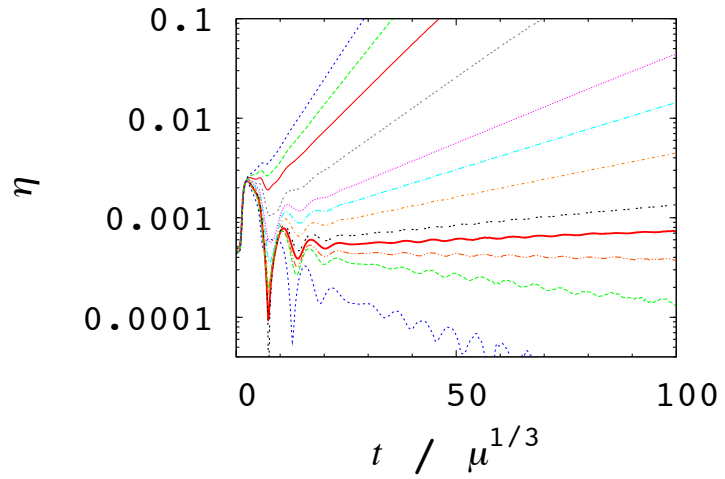

Figure 3.4: Evolution of deformation parameter η for 6-dimensional Myers-Perry black hole of single spin parameter for different initial spin parameters between 1.039 to 0.674 from upper to lower curves and for initial perturbation amplitude equal to 0.005 [4].

As is clear from an initial spin parameter (red thick solid curve) to higher initial spin parameters, the deformation parameter increases exponentially with time which shows an instability, otherwise, an exponential damping is seen for the curves below the red thick solid curve and the growth and damping rates of η are quite small, showing an stability [4]. For the curves that indicate instability, the

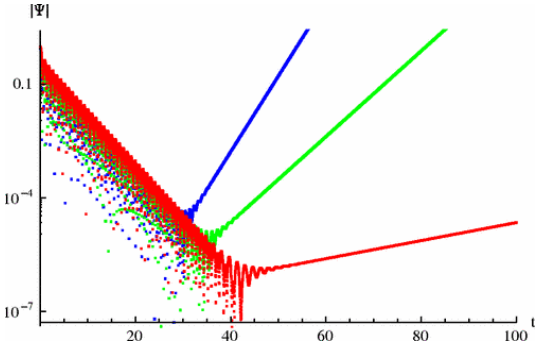

Figure 3.5: The picture of instability, developing at large multipole numbers: $D = 6$, $\ell = 8$ (red), $\ell = 12$ (green), $\ell = 16$ (blue), $\alpha = 1.3$. Tensor type of gravitational perturbations [5].

time domain of the instability starts immediately after the initial outburst. There is also another possibility that the time domain of evolution develops after a long period of damped quasi-normal oscillations. An example is from the black holes in the Einstein-Gauss-Bonnet theory. One can see in figure (3.5) that as the multipole number increases the instability starts earlier in the time-domain evolution [5].

4

Large-D limit method

We all know that Einstein's equations even in the simplest case of symmetric vacuum solutions are not easy to solve. One way that helps to deal with the difficulties is by using numerical relativity but even in this case one may encounter some numbers that are not easy to explain. Thus having an analytical solution is always preferable. One can learn from $SU(N)$ Yang-Mills and Chern-Simons gauge theories that while number of colors N is large one can use a very small parameter, $1/N$, to simplify these theories and extract more physics out of them. This method was introduced by 't Hooft in [89] and is a very powerful non-perturbative method to investigate non-linear gauge theories. The successful application of the method of the large N limit to study the structure of gauge theories like Yang-Mills and Chern-Simons theories was a motivation to search for a very small parameter in general relativity as well.

The natural parameter in general relativity is the number of space-like dimensions D. If one takes this parameter to be very large then one may find very small parameter $1/D$ and expansion using this small parameter enables one to perform perturbative calculations and understand different aspects of general relativity. One should notice that taking the number of space-like dimensions to be large doesn't mean that there are infinite number of dimensions, however this can be a tool to help us to highlight some aspects of the theory that are hard to study by the other means. As the gauge group of gravity is the local Lorentz group $SO(D-1,1)$, it is possible to extract a lot of information by study of the $\frac{1}{D}$ expansion using the large D method. Of course there are analogies between

the large D limit and the large N limit techniques but one should not forget that D is the dimensionally of space-time which may impose more difficulties in calculations compared to the large N limit calculations of $SU(N)$ gauge theories. Thus one should note that it is not clear if this works in the quantum gravity level or not but what confidently have been confirmed is the application of this method in the context of classical general relativity. This is because classical general relativity is very well defined in any number of dimensions. One can say that general relativity is the theory of black holes and using the large-D method [90] is an alternative method for studying this theory and its fundamental objects, black holes. You will see in the following section that in this limit black holes will behave like non interacting particles and one can consider them as a system of dust particles. Using this method general relativity may simplify drastically. This simplification is the result of the appearance of two scales in the theory; one very small $1/D$ and one very large r_0, the horizon radius. The hierarchy between these two scales defines two different regions in black hole space time while each of these regions contains different physics.
Although the idea of the large D limit has been already discussed in [91, 92, 93], it was just recently that was shown that black holes can be considered as non interacting particles that they do not attract each other and their collision cross sections vanishes [90] and in this chapter we follow the logic of this recent study.

4.1 Vacuum solution in large D limit

For a start we consider the Schwarzschild-Tangherlini solution, a solution that generalizes the four-dimensional Schwarzschild solution, in $D = 3+n$ dimensions with a horizon r_0

$$ds^2 = -f(r)dt^2 + \frac{dr^2}{f(r)} + r^2 d\Omega_{n+1}^2, \qquad f(r) = 1 - \left(\frac{r_0}{r}\right)^n, \tag{4.1}$$

where $d\Omega_{n+1}^2$ is the line element of the (n+1)-sphere. When $D \to \infty$ this area will decrease in the radial direction rapidly as the number of dimension grows. This also implies a vanishing cross section for colliding black holes. In general

one can say that the large D black hole is very small. For instance consider the length scale which is related to the surface gravity at the horizon r_0 by

$$\ell_\kappa = \kappa^{-1} \sim \frac{r_0}{D}, \tag{4.2}$$

it is clear that in the limit where $D \to \infty$ this length scale is much smaller than the horizon radius r_0.

Note that if one considers D as a large parameter, it is appropriate to keep r_0 fixed. In this regard because of very strong localization of the gravitational field in this limit the length scale $\frac{r_0}{D}$ appears to be very small. This is like a measure for the extension of a near horizon region, where all the non-trivial physics happens, and this scale for large D is very small as well.

The potential develops a very large gradient near the horizon, $\sim D/r_0$. This means that the geometry at distance scales of r_0 from the horizon is flat. Moreover, because of lack of any gravitational field outside the horizon the horizon acts like a surface of infinite curvature. This implies that there is no interaction between black holes.

By introducing a new coordinate $R = (r/r_0)^n$ and considering that at large n near the horizon the limit is defined by $\ln R \ll n$, the metric (4.1) will turn to [94]

$$ds^2 = -\frac{R-1}{R}dt^2 + \frac{r_0^2}{n^2}\frac{dR^2}{R(R-1)} + r_0 d\Omega_{n+1}^2 \tag{4.3}$$

for the near horizon region.

4.1.1 Different regions in large D limit

One of the important features of the large D limit is scale hierarchy. There is a hierarchy between the parameter $1/D$ compared to the radius of the horizon r_0

$$\frac{r_0}{D} \ll r_0 \tag{4.4}$$

This hierarchy has some implications that results in the classification of the different regions in the black hole space-time. One can define a far region where $|r - r_0| \gg r_0/D$ and a near region where $|r - r_0| \ll r_0$. The far region has the trivial geometry of flat space-time. The near region, influenced by the dynamics

of the black hole itself, has the non-trivial but well known geometry of the two dimensional string black hole [94]. There is also an overlap region in which the far and near regions interact, $r_0/D \ll |r - r_0| \ll r_0$. For a better understanding of this geometry one can consider a sphere of influence. If r_0 is the horizon radius at the $D \to \infty$ the gravitational field will effectively vanish for all $r > r_0$ however for large but finite D there is a very small area around the horizon, $r - r_0 \lesssim r_0/D + O(D^{-2})$, where the black hole still exerts some gravitational influence and it will vanish exponentially fast outside this region.

This means that if a particle falls into the black hole, it takes some times to reach the singularity at $r = 0$. It is possible to calculate the proper time of this particle between the moment that it crosses the radius $r = R$ until it reaches $r = 0$. This time is

$$t = \int dr \left(\frac{r}{r_0}\right)^{(D-3)/2} = \frac{2r_0}{D-1}\left(\frac{R}{r_0}\right)^{\frac{D-1}{2}}, \tag{4.5}$$

in the large D limit this particle takes a time that diverges exponentially with D to get to the region of the sphere of influence from any finite distance outside this sphere but the time that it takes to get from the moment that it enters this region until it reaches the singularity is very short; from (4.5) starting from $r = r_0$ one can find

$$t \simeq \frac{2r_0}{D} + O(D^{-2}). \tag{4.6}$$

This particle spends most of this time in the sphere of influence that includes the region $r_0 - r \lesssim r_0/D$ but after passing this region again it reaches the singularity exponentially fast in D. This tells us that this interior is very small.

One may think that the existence of these regions is the result of taking the long wavelength limit of the field that is propagating in the black hole background however this is not the case here as having this structure in different regions is a property of the geometry itself.

Although here we are speaking about the Schwarzschild-Tangherlini solution this classification of different regions is valid for all black holes for which the horizon length scale as well as their gravitational field remains finite at large D.

4.1.2 Myers-Perry black hole

The Myers-Perry (MP) solution of Einstein's equations describes the space-time of a higher dimensional rotating black hole. For the odd space-time dimension $D = 2N + 3$[1] with equal angular momenta, $a_i = a$, the metric is cohomogeneity-1 (only depends on the radial coordinate) and has the form [95]

$$ds^2 = -\frac{g(r)}{h(r)}dt^2 + \frac{1}{g(r)}dr^2 + r^2 h(r)(d\psi - \Omega(r)dt + A_a dx^a)^2 + r^2 \hat{g}_{ab}dx^a dx^b, \quad (4.7)$$

where

$$g(r) = 1 - \left(\frac{r_0}{r}\right)^{2N}\left(1 - \frac{a^2}{r^2}\right), \quad (4.8)$$

$$h(r) = 1 + \frac{a^2}{r^2}\left(\frac{r_0}{r}\right)^{2N}, \quad (4.9)$$

$$\Omega(r) = \frac{a}{r^2 h(r)}\left(\frac{r_0}{r}\right)^{2N}, \quad (4.10)$$

and A_a is Kahler potential and $\hat{g}_{ab}$ is the Fubini-Study metric on $\mathbb{CP}^N$[2]. One may consider this form of MP solution because of the symmetries of $\mathbb{CP}^N$ that will help to decouple the perturbation equations when it is needed. However finally using the relation between $\mathbb{CP}^N$ harmonics and spherical harmonic of S^{2N+1} one can get the desired results. The solution (4.7) is asymptotically flat and the event horizon is located at $r = r_+$, the largest positive root of $g(r)$ where r_+ can be defined as the size of the $\mathbb{CP}^N$ factor of the horizon. At large N, r_+ becomes [96]

$$r_+ \simeq r_0\left(1 - \frac{a^2}{r_0^2}\right)^{1/2N}, \quad (4.11)$$

and at any $r > r_+$ the space time is flat when $N \to \infty$. If one takes the large N limit in (4.11) one gets

$$r_+ = r_0(1 + O(N^{-1})) \quad (4.12)$$

[1] MP solution is parametrized by a mass radius parameter, r_0, and $\lfloor (D-1)/2 \rfloor$ angular momenta, so when D is odd one get $N + 1$ independent angular momenta which enhance the symmetry.

[2] See Appendix (B) for more details

Then one can set $r_0 = 1$ for the rest of the calculations. One should note that here a and r_0 are kept fixed in such a way that the metric remains finite and in general one can take $a < r_0$ in large N to be away from extremal limit of angular momentum.

To get the form of the metric in the near zone region, one can change the coordinate in (4.7) as follows

$$R = r^{2N}\left(1 - \frac{a^2}{r^2}\right)^{-1}, \tag{4.13}$$

and setting $a = \tanh\alpha$ gives

$$\begin{aligned} ds^2 = &\frac{1}{4N^2}\frac{dR^2}{R(R-1)} - (1 - \frac{\cosh^2\alpha}{R})dt^2 + (1 + \frac{\sinh^2\alpha}{R})(d\psi + A_a dx^a)^2 \\ &- \frac{2\sinh\alpha\cosh\alpha}{R}dt(d\psi + A_a dx^a) + \hat{g}_{ab}dx^a dx^b. \end{aligned} \tag{4.14}$$

If one takes $\alpha = 0$, the limit where there is no rotation, the Schwarzschild metric in the near zone region can be recovered. Alternatively, there is possibility to implement the following frame transformations to get to the (4.14) again as it has been shown in [96].

$$dt \to dt\cosh\alpha - (d\psi + A_a dx^a)\sinh\alpha, \tag{4.15}$$

$$d\psi + A_a dx^a \to (d\psi + A_a dx^a)\cosh\alpha - dt\sinh\alpha. \tag{4.16}$$

Thus one can say that the near zone metric (4.14) is just a local boost of the near zone Schwarzschild metric. This is very important concept for the large D analysis of a higher dimensional rotating black hole. The reason is that when one considers the gravitational perturbations in the MP background which may classify into scalar, vector and tensor type modes, the resulting equations for each of these modes normally are coupled to each other and this makes them analytically hopeless to solve. However, in the large D limit and using the former boost relation, it will be less difficult to decouple the equations. This is a very big achievement for this method as one can use the decoupled equations to investigate the stability of the MP black hole, or one can use them to calculate the different types of graviton emission into bulk from this rotating black hole, something that up to now has been done only for some special class of MP solutions and only for the tensor mode emission, not scalar and vector emissions.

4.2 Quasi normal modes in the large D limit

We have reviewed the quasi-normal mode physics in chapter (3). It is still interesting to see how it would be possible to calculate these modes using the large D limit method. In the large D limit quasi-normal modes, like other quantities in this limit can be controlled by the scale r_0/D. In [6] it has been shown that in the large D limit a large class of black holes (non-extremal, static and asymptotically flat ones) have a universal set of quasi normal mode with frequency that depends only on the horizon radius

$$\omega_{(\ell,k)} r_0 = \frac{D}{2} + \ell - \left(\frac{e^{i\pi}}{2} \left(\frac{D}{2} + \ell \right) \right)^{1/3} a_k, \tag{4.17}$$

with a_k

$$a_k \simeq \left(\frac{3\pi}{8} (4k-1) \right)^{2/3}, \tag{4.18}$$

where k is the overtone number. Equation (4.17) is only valid for modes such that ℓ/D and overtone number are of order D^0. The damping ratio for these modes goes like $D^{-2/3}$ and their lifetime is very long in the r_0/D time scale, so they resonate almost like normal modes.

These modes can be classified into two different classes [97]. For the first class in which most of them reside, a class of non-decoupled modes that are the non-normalizable states of the near horizon geometry with frequencies of order D/r_0. The second type are the modes that can be decoupled from the asymptotic far region and their frequencies are of order $1/r_0$. These modes have very small amplitude and they cannot tunnel between the near and far regions so they will be strongly suppressed in the far region.

If one considers a potential barrier close to the horizon, then the only waves that can penetrate the potential are the ones with frequencies of order D because of the height of the potential. For instance, in the case of the Schwarzschild space-time

$$V_{max} \to D^2 \omega_c^2. \tag{4.19}$$

Where ω_c is a critical frequency of $O(1/D)$. It is clear that waves with frequencies $\omega = O(1/r_0) \ll D^2\omega_c^2$ will be trapped either outside or inside the barrier and

they don't have a chance of tunneling as $D \to \infty$. In figure (4.1) the effective potential for large D is shown. Quasi normal modes correspond to bound states in

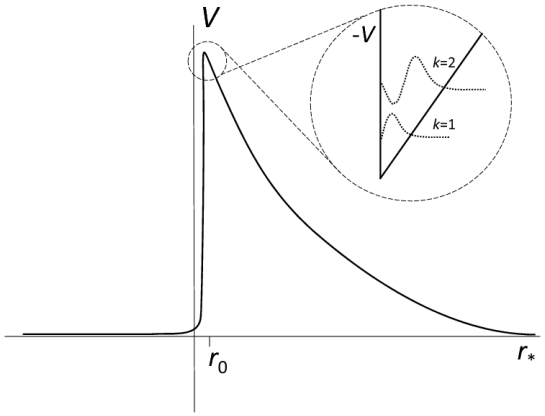

Figure 4.1: Effective potential at large D. The maximum of this potential is a sharp peak at large D and the inverted potential $-V$ that contains the least damped modes for two lowest overtone numbers [6].

the inverted potential $-V$. These modes are the least damped modes with small $|\text{Im}\omega|$ for small overtone numbers $k \ll D$, and they are only sensitive to the structure near the tip of the potential. One should note that this approximation breaks down when $k \sim D$. The right hand side of figure (4.1) represents the barrier to the flat space time. Waves with frequencies $\omega > D/2r_0$ will be perfectly absorbed by the black hole and waves with $\omega = O(D^0/r_0)$ will be perfectly reflected by this potential. The sharp peak at $r_* = r_0$ is the same for most of the background metrics in the large D limit and thus they share the same universal modes, however their potential may have a more complicated structure that is responsible for the other quasi normal modes that cannot be derived by this calculation.

4.2.1 MP quasi normal modes using large D

Quasi normal modes of MP black holes have been discussed in [96] using the large-D method to investigate the MP black hole instabilities. In this work they have considered the odd dimensional MP and they assumed that all the angular momenta are equal and non-zero. The quasi normal mode in this case can be

calculated by perturbing the metric (4.7) and solving the decoupled equations by implementing the proper boundary conditions, ingoing at the event horizon and outgoing in the asymptotic far region. We already mentioned that in the asymptotically far region the space-time is flat, so if one requires purely outgoing modes as a boundary condition at large space time dimension then it will result in, far field solution $= O(R^{-1})$. This can also be used to put constraints on the overlap zone that subsequently gives a condition on near zone modes. Implementing the ingoing boundary condition in the near region is more complicated as this near region has the form of (4.14). The next step is to implement the boundary condition at the event horizon in the near region. One can demand that the metric perturbation must be regular at the event horizon. So near $R = 1$, after expanding the perturbation at large N one will have

$$(R-1)^{-2i(\omega-m\Omega_H)/\kappa} = 1 - \frac{i(\omega-am)}{2\sqrt{1-a^2}N}\log(R-1) - \frac{(\omega-am)^2}{8(1-a^2)N^2}(\log(R-1))^2 + \frac{i\log(R-1)}{4(1-a^2)^{3/2}N^2}\left[-2a^2(\omega-am) - ((1-2a^2)\omega+am)\log(1-a^2)\right] + O(N^{-3}), \tag{4.20}$$

where κ is the surface gravity. The next-to-next-to-leading order frequencies of perturbations with the regular boundary conditions satisfy the following cubic equation

$$\begin{aligned} 0 = \frac{1}{\omega - a(m+2) + i(\ell-2)\sqrt{1-a^2}}[&\omega^3 + \omega^2\left(-3am + i(3\ell-4)\sqrt{1-a^2}\right) \\ &+ \omega\left(3a^2\ell^2 - 6iam\sqrt{1-a^2}(\ell-1) - 6a^2\ell + 3a^2m^2 - 3\ell^2 + 7\ell - 4\right) \\ &+ am(2 + (4a^2-5)\ell + 3(1-a^2)\ell^2 - a^2m^2) \\ &+ i\sqrt{1-a^2}(-(1-a^2)\ell^3 + (3-2a^2)\ell^2 + \ell(3a^2m^2-2) - 2a^2m^2)]. \end{aligned} \tag{4.21}$$

Roots of this equation give the frequencies of the three independent quasi normal modes. For instance, non-axisymmetric modes can be derived when $\ell = m$, then using (4.21) one can write

$$\omega^{(1)}_{m,m} = am - im\sqrt{1-a^2}, \tag{4.22}$$

$$\omega^{(2)}_{m,m} = a(m-1) - \sqrt{(m-1)(1-a^2)} - i\left[(m-1)\sqrt{1-a^2} + a\sqrt{m-1}\right], \quad (4.23)$$

$$\omega^{(3)}_{m,m} = a(m-1) + \sqrt{(m-1)(1-a^2)} - i\left[(m-1)\sqrt{1-a^2} - a\sqrt{m-1}\right]. \quad (4.24)$$

For axisymmetric modes when $m = 0$, one of the roots of (4.21) is purely imaginary and the other ones are related, $\mathrm{Re}\omega^{(+)} = -\mathrm{Re}\omega^{(-)}$ and $\mathrm{Im}\omega^{(+)} = \mathrm{Im}\omega^{(-)}$. For the lowest mode $\ell = 2$ one can find

$$\omega^{(0)}_{2,0}, \qquad \omega^{(\pm)}_{2,0} = \pm\sqrt{1+a^2} - i\sqrt{1-a^2}. \quad (4.25)$$

4.3 (In)stability of black holes in the large-D limit

(In)stability of black holes in general and more specifically stability of rotating black holes in the MP back ground has received considerable attention in recent years. We already mentioned in section (4.1.2) the difficulty of decoupling perturbation equations in the MP background, however, even in the simplest cases, such as the Schwarzschild black hole, it is not trivial to carry out the decoupling of the equations and determining the stability or instability directly from the equations of motion.

It should be noted that for higher dimensional rotating black hole one should expect two kinds of instabilities: axisymmetric and non-axisymmetric instabilities. These types of instabilities have been investigated in [4, 98, 99] numerically. In [98] the gravitational perturbation equations for equal spin odd dimensional MP black holes have been studied and it has been shown that these equation can be reduced to ODEs with only radial dependance, but still coupled. Hence it is not possible to solve them analytically. However, if one expands these equations in the large D limit [96] for zero rotation parameter, these equations can be decoupled. One can do this for $a = 0$ because of the boost symmetry that exists at leading order in the $1/D$ expansion when $D \to \infty$. This means that the

MP metric is the boosted Schwarzschild metric up to leading order and coupling effects appear for source terms only in the higher order equations in the $1/D$ expansion. It should be noted that these source terms don't have the boost symmetry. Fortunately even having the decoupled equation up to the leading term means that one can solve the equations analytically. The analytical solution of these equation shows that linearized gravitational perturbations become unstable whenever the rotation parameter is larger than some critical value

$$\frac{a_c}{r_*} = \sqrt{1 - \frac{1}{\ell}}, \tag{4.26}$$

For the smallest critical value one finds the non-axisymmetric instability for the dominant mode $\ell = m = 2$

$$\frac{a}{r_*} > \frac{1}{\sqrt{2}}. \tag{4.27}$$

The dominant modes have complex frequencies and all of them satisfy the superradiance condition. For $m = 0$ the first unstable axisymmetric mode with $\ell = 4$ gives

$$\frac{a}{r_*} > \frac{\sqrt{3}}{2}. \tag{4.28}$$

and these axisymmetric modes are purely imaginary. Comparing these results with the ones from the numerical calculation of [99] shows good agreement, which again confirms the validity of the large-D limit as a tool for simplifying general relativity.

5

Grey-body factors in large-D limit of general relativity

In [90] it has been shown that it is possible to use the large-D limit as a tool to calculate the absorption probability or in a simple word the grey-body factors. In that paper they have chosen to perturb a scalar field in a non-rotating background and solve the perturbation equations in the limit where the number of spatial space-like dimension is large. While the grey-body factors for this kind of perturbation and background are well known both analytically and numerically, using the large-D method, it has been shown that it is possible to obtain the same absorption probability as the ones that are already in the literature. This motivated us to apply this method to calculate the absorption probability considering gravitational perturbations of a non-rotating background and if we could obtain the same results as the ones in the literature we will apply it for more sophisticated case of rotating black hole. To this end one needs to consider the metric of the desired space-time in higher dimensions and write it in an appropriate coordinate to be more convenient when one takes the large-D limit. Then one can write the perturbation equations for any incident field using the former metric. The simplification in the large-D limit shows up when one tries to solve the perturbation equations.

For example, considering the case of a scalar perturbation in the higher dimensional Schwarzschild background, the solution to the wave equation can be characterized by using the reflection $R_l(\omega)$ and absorption $T_l(\omega)$ amplitudes at infinity

and at the horizon. Then the absorption probability is simply

$$\gamma_l(\omega) = |T_l(\omega)|^2. \tag{5.1}$$

In this chapter we will show that using this limit the expressions which will lead us to a great simplification in this absorption probability.

5.1 Gravitational grey-body factor

The flat space-time has the following line-element

$$ds^2 = -f(r)dt^2 + \frac{dr^2}{f(r)} + r^2 d\Omega^2_{2+n} \tag{5.2}$$

where

$$f(r) = 1 - \left(\frac{r_0}{r}\right)^n \tag{5.3}$$

The linearized gravitational perturbations of the metric (5.2) can be decomposed into tensor (T), vector (V) and scalar (S) perturbations. The grey-body factors can be found by solving the equation of motion using the classical scattering theory in this space-time. The radial part of all these three kinds satisfies the following equation

$$f\frac{d}{dr}\left(f\frac{d\Phi}{dr}\right) + (\omega^2 - V(r))\Phi = 0, \tag{5.4}$$

where V(r) is the radial potential and for the vector and tensor type[1] can be written as

$$V(r)_{T,V} = \frac{f(r)}{r^2}\left[\ell(\ell+n) + \frac{n^2-1}{4} - \frac{q(n+1)^2}{4}\left(\frac{1}{r}\right)^n\right], \tag{5.5}$$

where we set the $r_0 = 1$ and q will be equal to -1 and 3 for tensor and vector type perturbations respectively. At large n we can write (5.4) as

$$f\frac{d}{dr}\left(f\frac{d\Phi}{dr}\right) + n^2(\hat{\omega}^2 - \hat{V}(r))\Phi = 0, \tag{5.6}$$

[1]The potential for scalar type is very different from tensor and vector types. In this chapter we concentrate on tensor and vector type graviton emissions.

with the potential

$$\hat{V}_{T,V}(r) = \frac{1}{4r^2}[(1 + 4\hat{\ell} + 4\hat{\ell}^2) - (\frac{1}{r})^n(k + (1 + 2\hat{\ell})^2)], \tag{5.7}$$

where we scaled ω and ℓ as

$$\hat{\omega} = \frac{\omega}{n}, \quad \hat{\ell} = \frac{\ell}{n}, \tag{5.8}$$

moreover we have ignored the term with power $2n$, namely $O(1/2r)^{2n}$ term. The maximum of this potential happens at

$$r = r_{max} = 1 + \frac{1}{n}\log\frac{n}{2}\left(1 + \frac{k}{4\hat{\ell}^2}\right) + O\left(\frac{1}{n}\right)^2, \tag{5.9}$$

for $\hat{\ell} \gg 1$. The value of the potential at this maximum is

$$\hat{V}(r_{max}) = (\hat{\ell} + 1/2)^2 + O\left(\frac{1}{n}\right), \tag{5.10}$$

and the maximum of the potential $\hat{V}(r)$ occurs for the frequency $\hat{\omega} = \omega_c$, so

$$\omega_c = \hat{\ell} + \frac{1}{2} + O\left(\frac{1}{n}\right), \tag{5.11}$$

while the maximum of $V(r)$ is proportional to $n^2\omega_c^2$, this implies that only waves

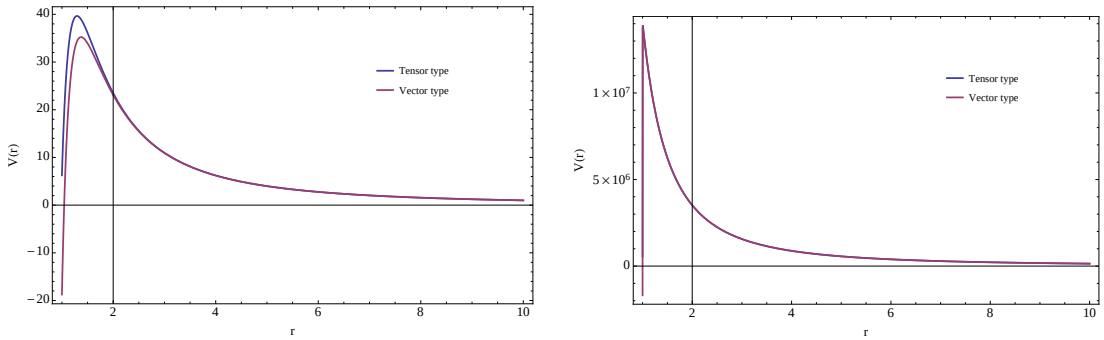

(a) **(b)**

Figure 5.1: (a) potential at $n = 4$ and $\ell = 2$ and (b) potential at $n = 1500$ and $\ell = 2$

with frequencies much larger than this frequency, $n\omega_c$, can penetrate into the

potential. Because in the limit where $n \to \infty$ the height of the potential becomes infinite, only waves with large frequencies compare to this height have the chance of tunneling through the potential. One should note that the maximum of this potential at large D is the same for both vector and tensor type perturbations figure (5.1).

5.1.1 The near-horizon solution

For the near horizon solution we should consider the radial distances close to the horizon $r \sim r_0$ and we already set the $r_0 = 1$. To solve the (5.6) we change the variable as $r \to f(r)$ and after taking large-D limit we obtain

$$(1-f)f\Phi''(f)+(1-2f)\Phi'(f)+\left(\frac{\hat{\omega}^2}{(1-f)f}-\frac{\hat{\ell}(\hat{\ell}+1)+\frac{1}{4}}{1-f}+\frac{q}{4}\right)\Phi(f)=0, \quad (5.12)$$

changing the function $\Phi(f) = f^{\alpha}(1-f)^{\beta}F(f)$ we will have

$$\begin{aligned} 0 =&(1-f)fF''(f)+\left(1+2\alpha-2f\left(\alpha+\beta+1\right)\right)F'(f) \\ &+\left(\frac{q-1}{4}+2\hat{\omega}^2-\alpha\left(2\beta+1\right)-\beta-\hat{\ell}(\hat{\ell}+1)\right)F(f), \end{aligned} \quad (5.13)$$

where

$$\alpha = -i\hat{\omega}, \quad \beta = -\sqrt{{\omega_c}^2-\hat{\omega}^2}, \quad (5.14)$$

equation (5.13) is a hypergeometric equation with the solution

$$\begin{aligned} F(f) =&A_1\,{}_2F_1(a,b,c;f) \\ &+A_2(-1)^{-2\alpha}f^{-2\alpha}\,{}_2F_1\left(1+a-c,1+b-c,2-c;f\right), \end{aligned} \quad (5.15)$$

where

$$a=\alpha+\beta+\frac{1}{2}-\frac{\sqrt{q+1}}{2}, \quad b=\alpha+\beta+\frac{1}{2}+\frac{\sqrt{q+1}}{2}, \quad c=1+2\alpha \quad (5.16)$$

and A_1 and A_2 are the integration constants. The boundary condition at event horizon demands that no outgoing wave should survive, thus we set $A_2 = 0$ and we use $\Phi(f) = f^{\alpha}(1-f)^{\beta}F(f)$ to obtain the near horizon zone solution

$$\Phi_{NH}(f) = A_1 f^{\alpha}(1-f)^{\beta}F(a,b,c;f), \quad (5.17)$$

taking $R = r^n$ (5.17) becomes

$$\Phi_{NH} = A_1 \left(1 - \frac{1}{R}\right)^{\alpha} \left(\frac{1}{R}\right)^{\beta} F(a, b, c; 1 - \frac{1}{R}), \tag{5.18}$$

using hypergeometric functions properties we can write (5.18) in the following form

$$\begin{aligned}\Phi_{NH} = A_1 \Gamma(c)(R-1)^{\alpha} R^{-(\alpha+\beta)} [&\frac{\Gamma(-2\beta)\, {}_2F_1(a, b; a+b-c+1; \frac{1}{R})}{\Gamma(c-a)\Gamma(c-b)} \\ &+ \frac{\Gamma(2\beta) R^{2\beta}\, {}_2F_1(c-a, c-b; c-a-b; \frac{1}{R})}{\Gamma(a)\Gamma(b)}].\end{aligned} \tag{5.19}$$

If we take the limit $1 \ll \log R \ll n$, which will give us the behavior of the wave at distances far from horizon, we will have

$$\Phi_{NH} = A_1 \Gamma(c) \left[\frac{\Gamma(-2\beta)}{\Gamma(c-a)\Gamma(c-b)} R^{-\beta} + \frac{\Gamma(2\beta)}{\Gamma(a)\Gamma(b)} R^{\beta}\right] \tag{5.20}$$

5.1.2 The far-field solution

Taking into account that in the far-field, where $r \to \infty$, we can set $f(r) \to 1$ and equation (5.4) will be

$$\Phi''(r) + n^2 \left(\hat{\omega}^2 - \frac{(\hat{\ell} + 1/2)^2 - 1/4n^2}{r^2}\right) \Phi(r) = 0. \tag{5.21}$$

Substituting $\Phi(r) = r^{\alpha}\psi(r)$ we obtain

$$\psi''(r) + \frac{2\alpha}{r}\psi'(r) + \left(\frac{\alpha(\alpha-1)}{r^2} + n^2 \left(\hat{\omega}^2 - \frac{(\hat{\ell} + 1/2)^2 - 1/4n^2}{r^2}\right)\right) \psi(r) = 0. \tag{5.22}$$

Then we change the radial coordinate to $r = \frac{z}{\omega}$ and we set $\alpha = 1/2$

$$\psi''(z) + \frac{1}{z}\psi'(z) + \left(1 - \frac{\nu^2}{z^2}\right) \psi(z) = 0, \tag{5.23}$$

where $\nu = n(\omega_c^2 - 1/4n^2)^{1/2}$ and at $n \to \infty$ it is equal to $n\omega_c$. The solution to (5.23) can be stated in terms of Bessel functions

$$\Phi_{FF} = \sqrt{r}(B_1 J_{n\omega_c}(nr\hat{\omega}) + B_2 Y_{n\omega_c}(nr\hat{\omega})) \tag{5.24}$$

5. GREY-BODY FACTORS IN LARGE-D LIMIT OF GENERAL RELATIVITY

If we take $R = r^n$ and we stretch the far field solution to smaller values of r, some intermediate region between the horizon and the asymptotic region, or equivalently using the following expression which is valid for frequencies smaller than critical frequency $\hat{\omega} < \omega_c$ [90]

$$\frac{\hat{\omega}}{\omega_c} r = \text{sech}\alpha \qquad \text{for} \qquad \hat{\omega} < \omega_c, \tag{5.25}$$

equation (5.24) will turn into

$$\Phi_{FF} = R^{1/2n}(B_1 J_{n\omega_c}(n\omega_c \,\text{sech}\,\alpha) + B_2 Y_{n\omega_c}(n\omega_c \,\text{sech}\,\alpha)) \tag{5.26}$$

Then in the limit that $\nu = n\omega_c \to \infty$ one can use Debye's expansion

$$\begin{aligned} J_\nu(\nu \,\text{sech}\,\alpha) &\sim \frac{e^{\nu(\tanh\alpha - \alpha)}}{\sqrt{2\pi\nu \tanh\alpha}} \\ Y_\nu(\nu \,\text{sech}\,\alpha) &\sim \frac{-2e^{\nu(\tanh\alpha - \alpha)}}{\sqrt{2\pi\nu \tanh\alpha}} \end{aligned} \tag{5.27}$$

to expand the Bessel functions in (5.26)

$$\Phi_{FF} = \frac{R^{1/2n}}{\sqrt{2\pi n\omega_c \tanh\alpha}}(B_1 e^{-n\omega_c(\alpha - \tanh\alpha)} - 2B_2 e^{n\omega_c(\alpha - \tanh\alpha)}), \tag{5.28}$$

in the limit where $1 \ll \log R \ll n$ we have

$$\alpha - \tanh\alpha = \alpha_0 - \tanh\alpha_0 - \tanh\alpha_0 \frac{\ln R}{n} + O(n^{-2}), \tag{5.29}$$

and using the above expansion (5.28) takes the form

$$\Phi_{FF} = \frac{1}{\sqrt{2\pi n\omega_c \tanh\alpha_0}} \left(B_1 K_{\hat{\omega}} R^{-\beta} - \frac{2B_2}{K_{\hat{\omega}}} R^{\beta} \right), \tag{5.30}$$

where

$$\beta = -\sqrt{{\omega_c}^2 - \hat{\omega}^2} = -\omega_c \tanh\alpha_0, \tag{5.31}$$

and

$$K_{\hat{\omega}} = e^{-n\omega_c(\alpha_0 - \tanh\alpha_0)} \quad \hat{\omega} < \omega_c. \tag{5.32}$$

If we expand the far field solution (5.24) for $r \to \infty$

$$\Phi_{FF_{r\to\infty}} = \frac{1}{\sqrt{2\pi\omega}} \left[(B_1 - iB_2) e^{i(r\omega - n\omega_c - \frac{\pi}{4})} + (B_1 + iB_2) e^{-i(r\omega - n\omega_c - \frac{\pi}{4})} \right], \tag{5.33}$$

this limit is equivalent to studying the wave for frequencies $\hat{\omega} > \omega_c$ and thus once more we define

$$\frac{\hat{\omega}}{\omega_c} r = \sec\gamma \qquad \text{for} \qquad \hat{\omega} > \omega_c. \tag{5.34}$$

Using (5.34) for the limit $\log R \ll n$ we obtain

$$\Phi_{FF} = \frac{1}{\sqrt{2\pi n \omega_c \tan\gamma_0}} \left((B_1 - i\, B_2) K_{\hat{\omega}} R^{-\beta} - \frac{(B_1 + i\, B_2)}{K_{\hat{\omega}}} R^{\beta} \right), \tag{5.35}$$

where

$$\beta = -\sqrt{{\omega_c}^2 - \hat{\omega}^2} = -i\,\omega_c \tan\gamma_0, \tag{5.36}$$

with

$$K_{\hat{\omega}} = e^{-n\omega_c(\gamma_0 - \tan\gamma_0) - i\,\pi/4} \quad \hat{\omega} > \omega_c. \tag{5.37}$$

5.1.3 Matching the solutions

To construct a valid solution for the whole radial regime we should connect the two solutions in the intermediate point. Using (5.20) and (5.30) we can derive the integration constants B_1 and B_2

$$\frac{B_1}{A_1} = \frac{\Gamma(c)\Gamma(-2\beta)\sqrt{-2n\pi\beta}}{K_{\hat{\omega}}\Gamma(c-a)\Gamma(c-b)}, \tag{5.38}$$

$$\frac{B_2}{A_1} = -\frac{K_{\hat{\omega}}\Gamma(c)\Gamma(2\beta)\sqrt{-2n\pi\beta}}{2\Gamma(a)\Gamma(b)}. \tag{5.39}$$

The reflection coefficient $\mathcal{R}_\ell$ can be defined as the ratio of the amplitude of the outgoing wave over the incoming wave

$$\mathcal{R}_\ell = \frac{B_1 - i\, B_2}{B_1 + i\, B_2}. \tag{5.40}$$

Thus the absorption probability can be written as

$$|\mathcal{A}_\ell|^2 = 1 - |\mathcal{R}_\ell|^2 = 1 - \left| \frac{B - i}{B + i} \right|^2 \tag{5.41}$$

where B is

$$B \equiv \frac{B_1}{B_2} = -\frac{2\Gamma(a)\Gamma(b)\Gamma(-2\beta)}{K_{\hat{\omega}}^2\Gamma(2\beta)\Gamma(c-a)\Gamma(c-b)}. \tag{5.42}$$

5.1.4 The absorption probability for low energy limit

In the low energy regime the absorption probability (5.41) can be written as follows

$$|\mathcal{A}_\ell|^2 = \frac{2i(B-B^*)}{BB^*}. \tag{5.43}$$

In (5.43) we only kept the dominant term in the denominator. The simplified analytical form of the grey-body factor for the tensor and vector parts is

$$|\mathcal{A}_\ell|^2 = \frac{K_{\hat{\omega}}^2 \sinh 2\pi\hat{\omega} \left|\Gamma(\frac{\sqrt{q+1}}{2} - \beta + i\hat{\omega} + \frac{1}{2})\right|^2 \left|\Gamma(-\frac{\sqrt{q+1}}{2} - \beta + i\hat{\omega} + \frac{1}{2})\right|^2}{2\pi\beta \left|\Gamma(-2\beta)\right|^2} \tag{5.44}$$

when $\hat{\omega} \ll \omega_c$, $K_{\hat{\omega}}^2$ turns to

$$K_{\hat{\omega}}^2 = \left(\frac{e\hat{\omega}}{2\omega_c}\right)^{(2n\omega_c)} \ll 1 \tag{5.45}$$

For these frequencies $\hat{\omega} \ll \omega_c$ we can rewrite (5.44) using (5.8) and (5.11) as

$$|\mathcal{A}_\ell|^2 \sim \left(\frac{e}{2\ell+n}\right)^{2\ell+n} \left(\frac{2}{2\ell+n}\right) \left(\frac{\omega^{2\ell+n+1} \left|\Gamma(\frac{\ell}{n}+1-G)\right|^2 \left|\Gamma(\frac{\ell}{n}+1+G)\right|^2}{\left|\Gamma(\frac{2\ell}{n}+1)\right|^2}\right), \tag{5.46}$$

where $G = -\frac{q+1}{2}$. Recalling that at the beginning of our calculations we assumed $\hat{\ell} \gg 1$, the first parenthesis in (5.46) can be written in terms of the Γ function

$$\left(\frac{e}{2\ell+n}\right)^{2\ell+n} \left(\frac{2}{2\ell+n}\right) = 4\pi \left(\frac{1}{2}\right)^{2\ell+n+1} \left|\Gamma(\frac{2\ell+n}{2}+1)\right|^{-2} \tag{5.47}$$

and substituting (5.47) in equation (5.46) we find

$$|\mathcal{A}_\ell|^2 \sim 4\pi \left(\frac{\omega}{2}\right)^{2\ell+n+1} \left(\frac{\left|\Gamma(\frac{\ell}{n}+1-G)\right|^2 \left|\Gamma(\frac{\ell}{n}+1+G)\right|^2}{\left|\Gamma(\frac{2\ell+n}{2}+1)\right|^2 \left|\Gamma(\frac{2\ell}{n}+1)\right|^2}\right). \tag{5.48}$$

The value of G is 0 for tensor gravitational perturbations; we compared the large-D limit results with grey body factors in [7] and we found good consistency with their results, see figure (5.2). While the expression (5.48) is equal to the absorption probability in [7][1] for tensor type gravitons, there is a difference between our results and [7] for vector type gravitons, figure (5.3). This difference arises

[1] $n_{\text{in this thesis}} = n_{\text{paper}} + 1$

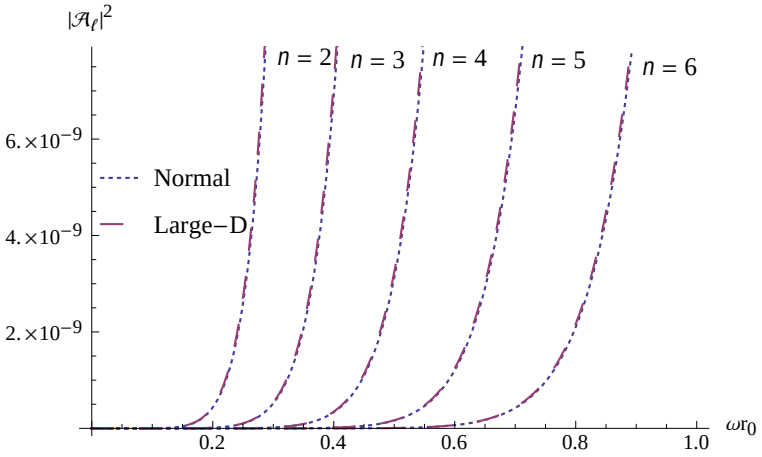

Figure 5.2: Absorption probability for $\ell = 2$, for tensor perturbation and $n = 2, 3, 4, 5, 6$ using large-D and without using large-D tool [7].

from the term G which in our case is equal to 1 for vector type and in the [7] is $G = 1 + \frac{1}{n}$. It should be mentioned that this difference is negligible for the $\ell > 4$ as you can see in the figure (5.4). In spite of having this agreement, one should note that the absorption probability for $\ell > 4$ cases is very small and the dominant probabilities belong to the lower values of angular momentum.

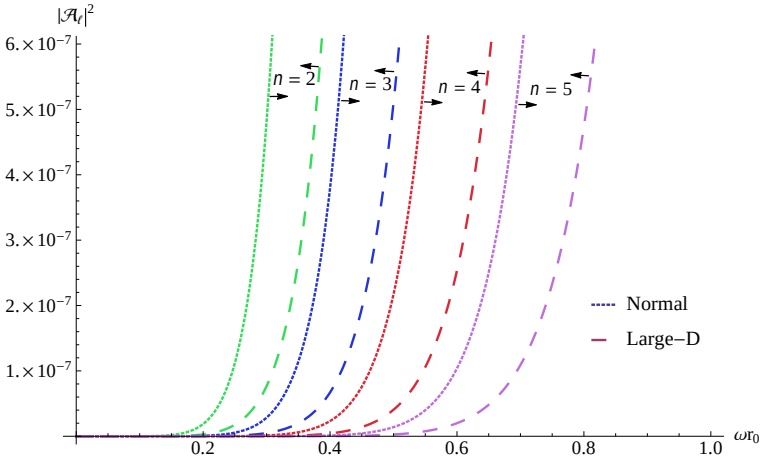

Figure 5.3: Absorption probability for $\ell = 2$, for vector perturbation and $n = 2, 3, 4, 5$ using large-D and without using large-D tool [7].

It is worthwhile to mention that we derived the analytic formula for absorption probability for small frequencies only because we wanted to compare our results

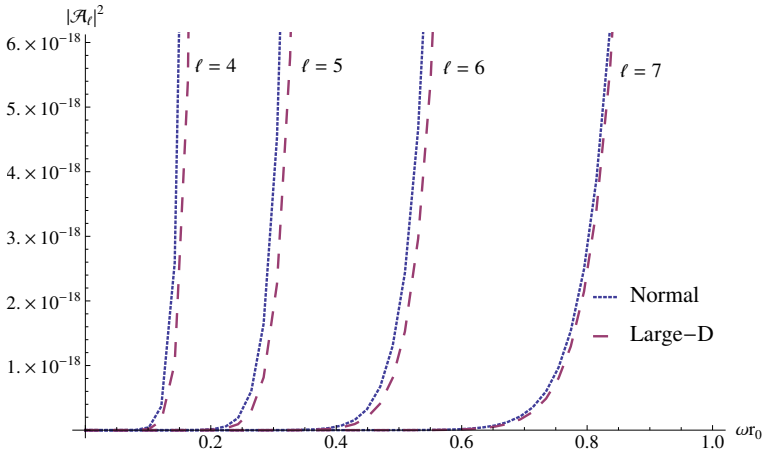

Figure 5.4: Absorption probability for $n = 2$, for vector perturbation and $\ell = 4, 5, 6, 7$ using large-D and without using large-D tool [7].

with the one in literature. However using the large-D method one can have the analytical solution for all the frequency ranges and the approach to obtain it is much simpler than the normal higher dimensional case.

6

Vaidya Metric Quasi-Normal Modes

6.1 Outgoing Vaidya space-time

The Vaidya metrics [100] are exact solutions of the Einstein equations. In the radiating coordinates (w, r, θ, ϕ) this metric has the form

$$ds^2 = -\left(1 - \frac{2m(w)}{r}\right) dw^2 + 2cdwdr + r^2 d\Omega^2, \tag{6.1}$$

where $c = 1, -1$ respectively corresponds to ingoing and outgoing radial flow and $m(w)$ is a monotonic mass function. In the presence of spherical symmetry this mass function can be the measure of the amount of energy within a sphere with real radius r and at a time t [101, 102]. For constant mass this solution reduces to the Schwarzschild solution in ingoing or outgoing Eddington-Finkelstein coordinate. One can also write this metric using null coordinates, $c = +1$, $w = v = t + r$ (advanced time) and, $c = -1$, $w = u = t - r$ (retarded time). Then the ingoing Vaidya metric can be written using advanced time and in this case the metric describes collapsing null dust [103]. The outgoing Vaidya space-time

$$ds^2 = -f(u, r)du^2 - 2dudr + r^2 d\Omega^2, \qquad f(u, r) = (1 - \frac{2m(u)}{r}) \tag{6.2}$$

describes the evolution of a radiating star or black hole, where $m(u)$ is the mass function of retarded time u that labels the outgoing radial null geodesics. In the

following we will restrict our analysis to the outgoing case as we are interested in the final stages of black hole evaporation. For (6.2) the only non-vanishing component of the Einstein tensor is

$$G_{uu} = -\left(\frac{2}{r^2}\right)\frac{dm(u)}{du} \tag{6.3}$$

The stress-energy tensor that leads to this solution is

$$T_{\alpha\beta} = -\frac{\frac{dm(u)}{du}}{4\pi r^2}(k_\alpha)(k_\beta) \tag{6.4}$$

where k_α is tangent to radial outgoing null geodesic, $k_\alpha k^\alpha = 0$. This stress-energy tensor describes a pressure less fluid with energy density $\rho = -\frac{dm(u)}{du}4\pi r^2$ moving with the four-velocity $\delta^u_a = k_\alpha$ (such a fluid is called "null dust"). To satisfy the null energy condition for which $\rho \geq 0$, the mass function $m(u)$ must be a decreasing function of increasing retarded time, namely $\frac{dm(u)}{du} < 0$, which means that the mass function decreases in response to the outflow of radiation and that is why this metric is appropriate for the study of the evolution of a radiating star or an evaporating black hole.

6.1.1 Vaidya symmetries

In addition to the obvious spherical symmetry of this space-time (6.2) when we consider also a linear mass function there is in addition a scaling symmetry. In fact this space-time possesses a conformal Killing vector K[104]

$$K_{\mu;\nu} + K_{\nu;\mu} = 2\rho g_{\nu\mu} \tag{6.5}$$

where ρ is a constant, indicating that this is actually a homothety symmetry. Homothety means that the metric with linear mass function scales upon a scaling of the coordinates by an overall factor

$$(u, r) \to (\zeta u, \zeta r) \qquad \Rightarrow \qquad ds^2 \to \zeta^2 ds^2, \tag{6.6}$$

for any real ζ. One consequence of this symmetry is that if $(u(\tau), r(\tau))$ is a solution to the geodesic equations then $(\zeta u(\tau), \zeta r(\tau))$ is also a solution.

6.1.2 Vaidya mass function

Mass in the Vaidya space-time is a function of time and depending upon considering whether one is the outgoing or ingoing Vaidya metric it may decrease or increase by time. The choice of mass function in the Vaidya metric is important because it can alter the space-time. In [105] a general mass function has been introduced that is an arbitrary function of (v, r)[1] and it has been shown that for different choices of this arbitrary function most of the known solutions of Einstein field equations with spherical symmetries can be found. For our analysis, we choose the linear mass function $m(u) = -\mu u$. This choice of mass function will let us to study very interesting phenomena at the end point of black hole evaporation and recover the Minkowski space-time after complete evaporation.
The linear mass function is the only mass function for which (6.5) is satisfied. Hence if we choose this mass function the space-time will enjoy homothety symmetry. Considering this symmetry we will show later that the perturbation equations in this space-time can be drastically simplified.

6.1.3 Vaidya horizons

In general, in the case of static black holes like the Schwarzschild black hole, the location of both apparent and event horizon is the same and it is marked by Schwarzschild radius $r_s = 2M$, where M is the mass of black hole and is constant. For Vaidya space-time which is a dynamic space-time the mass of the black hole changes, so the apparent and event horizons no longer coincide.
The apparent horizon for outgoing Vaidya space-time (6.2) can be derived by setting $f(u, r)$ to zero and then one can obtain the following hypersurface

$$r_{app} = 2m(u, r) \tag{6.7}$$

This hypersurface marks a past apparent horizon and the induced metric for this hypersurface is

$$ds^2 = -4m'(u)du^2 + (2m(u))^2 d\Omega^2. \tag{6.8}$$

[1]The same holds for (u, r)

Knowing that $m'(u) < 0$, (6.7) is a past apparent horizon and it is space-like. In contrary with the apparent horizon which is a local geometric notion the event horizon is a more global object and in general is more difficult to determine. To determine the location of the event horizon one needs to know the future behavior of the light ray and this requires that one knows the future evolution of the entire space time. We will return to this in (6.1.5) where we discuss the conformal structure of this space-time.

6.1.4 Vaidya singularities

Based on Geroch's [106] definition of a singularity, a "curvature singularity" can be defined if a scalar invariant is unbounded on an incomplete geodesic. Shell focusing singularity is one kind of curvature singularity that has been studied in [104] for ingoing Vaidya space-time. This type of singularity indicates a breakdown on the manifold and it occurs at the center of a spherically symmetric collapsing configuration of a perfect fluid or radiation shells. To study the singularities of outgoing Vaidya one can calculate a scalar invariant like the Kretschmann scalar

$$K_{\alpha\beta\gamma\delta}K^{\alpha\beta\gamma\delta} = K^2 = \frac{48\mu^2u^2}{r^6}. \tag{6.9}$$

From (6.9), it is clear that $r = 0$ is a curvature singularity. To see if this singularity is a shell focusing singularity or not one needs to look at the null geodesic equations.

Homothetic null geodesics can be defined by setting (6.2) to zero for linear mass function $m(u) = -u\mu$ while θ and ϕ are constant. Taking e^t as affine parameter [107], from null geodesic equations one can write

$$\frac{dr}{dt} = r + 2\mu u, \qquad \frac{du}{dt} = -2r, \tag{6.10}$$

writing this system of linear equations (6.10) in a matrix form one can calculate the eigenvalues

$$\eta_{1,2} = \frac{1 \pm \sqrt{1 - 16\mu}}{2}, \tag{6.11}$$

solving the null geodesic equation using this eigenvalues lead to

$$u = -\frac{1 \pm \sqrt{1 - 16\mu}}{4\mu} r. \tag{6.12}$$

From (6.12) in order to see where the $r = 0$ intersects with u, one needs to study three different possibilities for μ because choice of μ influences the description of space-time directly. If $\mu \leq \frac{1}{16}$, u will be zero only at $r = 0$ and the singularity at this point is shell focusing singularity and is naked. For $u < 0$ mass is not zero anymore and we will have a central singularity at $r = 0$. For $\mu > \frac{1}{16}$, there are no positive real roots for (6.12) and to study the nature of the singularity one may need more detailed investigation of the geodesic equations. In our studies we are interested in the limit where $\mu < \frac{1}{16}$ due to the special features of the space-time that emerges only for this range and we will explain it in this chapter.

6.1.5 Conformal diagram

In general the choice of mass function in Vaidya space-time determines its global and local structure and singularities. Here we will consider only the case of a linear mass function $m(u) = -\mu u$ for different values of μ [108]. For $\mu > 1/16$ the conformal diagram has been shown in figure (6.1). The red line shows the

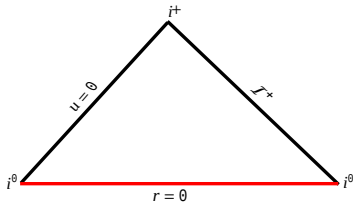

Figure 6.1: Conformal diagram for outgoing Vaidya with linear mass function for $\mu > 1/16$, red line represents $r = 0$ singularity.

singularity at $r = 0$ for $u < 0$. The next case is $\mu = 1/16$ which is represented in figure (6.2). In the last case in figure (6.3) the conformal diagram for $\mu < 1/16$ is shown. In this case the $u = 0$ boundary to the future of the endpoint of the $r = u = 0$ singularity is special in that the space-time there approaches that of Minkowski space. Indeed it has been shown in [109] that one can continuously attach the metric along this part of the $u = 0$ hypersurface to Minkowski space without introducing curvature singularities.

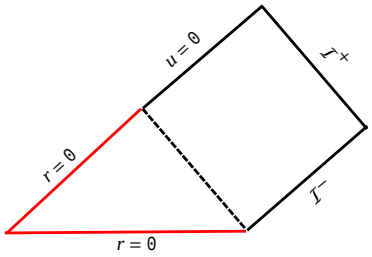

Figure 6.2: Conformal diagram for outgoing Vaidya with linear mass function for $\mu = 1/16$, red lines represent $r = 0$ singularities.

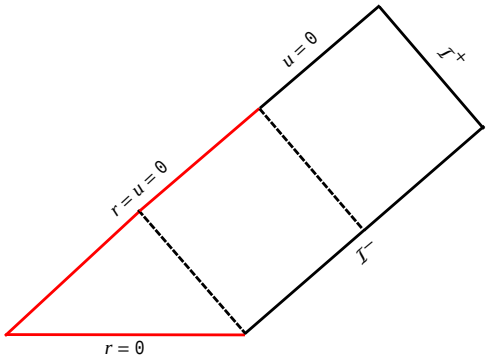

Figure 6.3: Conformal diagram for outgoing Vaidya with linear mass function for $\mu < 1/16$, red lines represent $r = 0$ singularities.

6.1.6 New model: disappearance of black hole at end of its evaporation

Considering the outgoing Vaidya metric with linear mass function, a new model for the final fate of black hole at the end of its evaporation has been has been suggested in [110]. As discussed in [108] for a linear mass function, different scenarios can be considered for different ranges of μ and this model suggests that for $0 < \mu < 1/16$ the space time contains a null singularity that vanishes at an interior point of the space-time. This space-time can be divided into three different regions characterised by a transition time u_t and illustrated in figure 4:

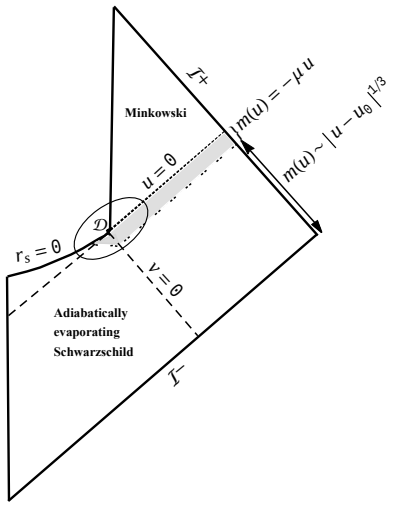

Figure 6.4: Conformal diagram for outgoing Vaidya with linear mass function

an adiabatic Schwarzschild region for all v with $u < u_t$ with $m(u) \sim |u - u_0|^{1/3}$ and also most of the region $v < 0$; a Vaidya region with linear mass function for $u_t < u < 0$, $v \geq 0$; a Minkowski space-time region for $u > 0$, $v > 0$. In this model the linear mass function is used when the mass of black hole becomes Planckian. This model suggests that black hole evaporation may result in the complete disappearance of the black hole and the singularity that it contains after which the space-time returns to Minkowski space-time [109]. An elaboration of this picture has been presented in [110] motivated by a detailed investigation of the future directed null geodesics for non-zero angular momentum together with a preliminary investigation of the wave equation for electromagnetic perturbations. There it is shown that the null singularity close to the vanishing point effectively becomes repulsive and thus is conjectured to be stable under effects of small perturbations.

6.1.7 Vaidya in double null coordinates

As our purpose is to find the quasi-normal modes of the outgoing Vaidya space-time, it is very useful to introduce the double null coordinate [108] for which both analytical and numerical calculations can be performed. In these coordinates

(u, θ, ϕ, v) the general form of the metric is

$$ds^2 = -2f(u,v)dudv + r^2(u,v)d\Omega^2 \tag{6.13}$$

For the outgoing metric, the energy momentum tensor has the form

$$T_{\mu\nu} = \frac{\mu}{4\pi r(u,v)^2}(\delta^u_\mu)(\delta^u_\nu) \tag{6.14}$$

Considering linear mass function with $\Delta = \sqrt{1-16\mu}$, $f(u,v)$ is

$$f(u,v) = \frac{1+\Delta}{2\Delta r(u,v)}(r(u,v) + u(1-\Delta)/4)^{2/(1+\Delta)}, \tag{6.15}$$

where $r(u,v)$ can be derived by solving this equation

$$\left(\frac{v}{|u|^{2\Delta/(1+\Delta)}}\right)^{1+\Delta} = \left(\frac{r(u,v)}{|u|} - \frac{1+\Delta}{4}\right)^{1+\Delta} / \left(\frac{r(u,v)}{|u|} - \frac{1-\Delta}{4}\right)^{1-\Delta}, \tag{6.16}$$

The values of $r(u,v)$ have been presented in [110] for specific values of Δ.

6.2 Vaidya potential

In order to study the quasi-normal modes of Vaidya space-time, we need to study the Klein-Gordon equation

$$\frac{\partial^2\psi}{\partial u \partial v} + W(u,v)f(u,v)\psi = 0 \tag{6.17}$$

where $W(u,v)$ is given by

$$W(u,v) = \frac{\ell(\ell+1)}{2r^2(u,v)} + \sigma\frac{m(u)}{r^3(u,v)} \tag{6.18}$$

where $\sigma = 1$ and $\sigma = 0$ correspond, respectively, to the scalar and to the electromagnetic perturbations. From here on, for calculational convenience, we extend the linear mass function $m(u) = -\mu u$ to all values of $u < 0$ and not just for the $u_t < u < 0$ as was shown in figure (6.4). Equation (6.17) describes wave propagation in the Vaidya background and $f(u,v)W(u,v)$ is the effective potential which describes how waves, electromagnetic and scalar fields are scattered by the geometry. It is clear that this potential depends on the black hole geometry and also on the spin of the perturbation under consideration.

6.2.1 Integrating the PDE

Following this goal, we insert the functions $f(u,v)$ and $V(u,v)$ into (6.17) for a linear mass function and we obtain,

$$\begin{aligned} &\frac{\partial^2\psi(u,v)}{\partial u\partial v} + \frac{1+\Delta}{4\Delta r(u,v)^4}\left(r(u,v) + \frac{(1-\Delta)}{4}u\right)^{2/(1+\Delta)} \\ &(\ell(\ell+1)r(u,v) - 2\sigma\mu u)\psi(u,v) = 0 \end{aligned} \tag{6.19}$$

One can then use the integration technique for derivation of quasi-normal modes proposed in (3.2.2) to solve this equation numerically. In the present context this equation was already studied for the special case of electromagnetic perturbations with $\ell = 1$ in [110] where it was observed that an initially ingoing gaussian wave-packet coming in from $\mathcal{I}_-$ with centre at small negative v appears to develop a quasi-normal like ringing as it evolves towards $u \to 0$.The numerical integration was carried out by sending in the direction of increasing u a Gaussian wave localized around $v_c < 0$.

In this thesis, in addition to the calculation for the electromagnetic field we also present the numerical integration to obtain the time profile of the perturbed outgoing Vaidya for both electromagnetic $\sigma = 0$ and scalar perturbations $\sigma = 1$ and for different angular momentum values. The results for the shape of the ingoing wave for $u \lesssim 0$ are presented in figure (6.5). In these figures the results of the integration with $\Delta = 1/2$[1] are displayed. Similar results can also be obtained for other values of Δ. The initial conditions were a gaussian wave form in v with centre at $v = v_c$ at $u = u_0 = -40$ and with varying widths. One can see that in particular there is a ringing of varying period reflecting the changing mass of the evaporating Vaidya metric, for $v \lesssim 0$. The ringing dies out rapidly and is not present for $v > 0$ in line with the fact that the "Planckian" black hole has vanished. The general form of these oscillations doesn't change for different values of the initial Gaussian, though their detailed structure does. This indicates that there are not true quasi-normal modes at particular discrete frequencies in contrast to what one finds for the Schwarzschild black hole. We believe that this is due to the time-dependent nature of the outgoing Vaidya metric.

[1] For the other values of Δ see the appendix (C)

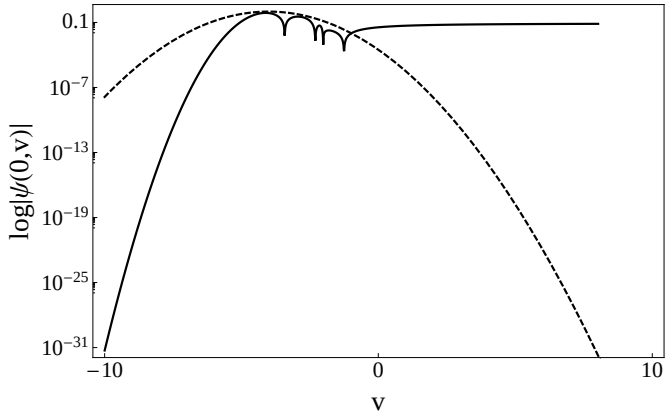

(a) $w = 1$, $v_c = -4$

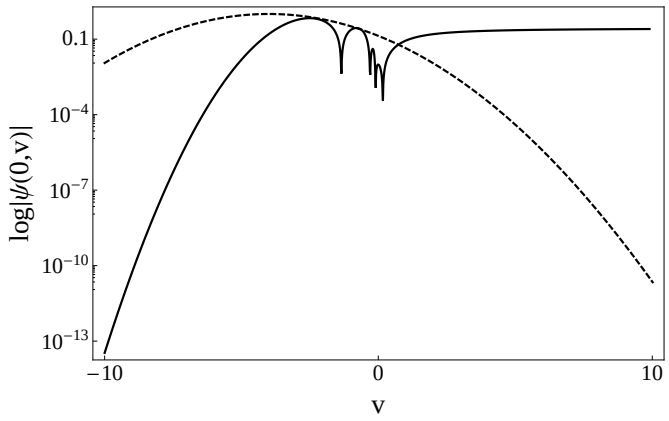

(b) $w = 2$, $v_c = -4$

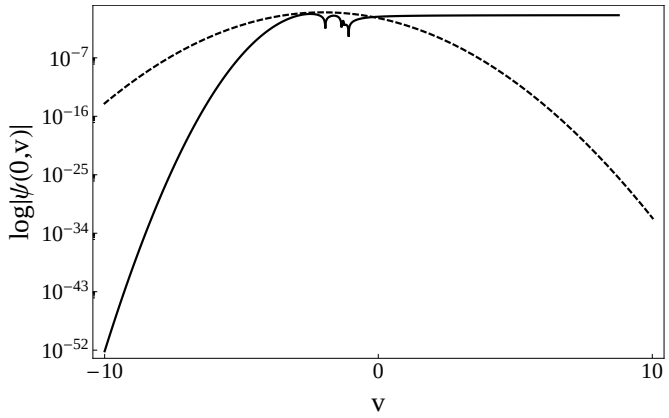

(c) $w = 1$, $v_c = -2$

Figure 6.5: Time profile of respond of outgoing Vaidya space-time to the electromagnetic perturbations for $\Delta = 1/2$ and $\ell = 1$ for different values of initial data. The dashed line indicate the Gaussian function that has been used as initial data which w is the width and v_c marks the center of the Gaussian.

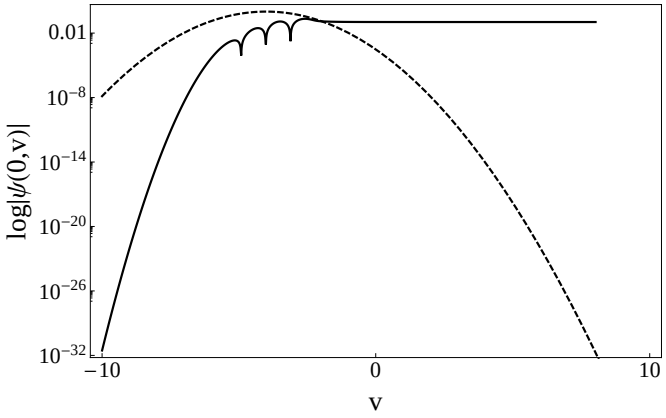

(a) $w = 1$, $v_c = -4$

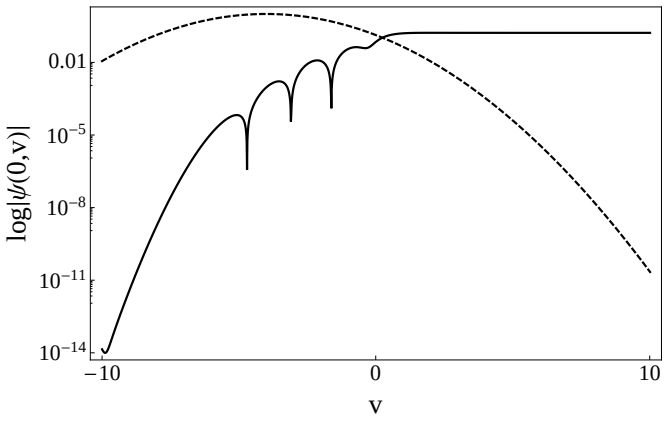

(b) $w = 2$, $v_c = -4$

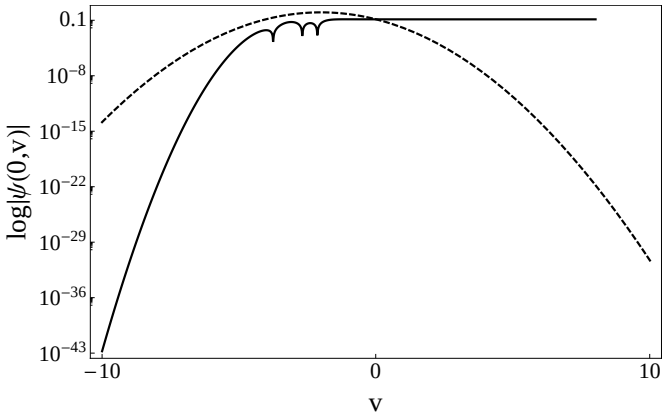

(c) $w = 1$, $v_c = -2$

Figure 6.6: Time profile of respond of outgoing Vaidya space-time to the scalar perturbations for $\Delta = 1/2$ and $\ell = 0$ for different values of initial data. The dashed line indicate the Gaussian function that has been used as initial data which w is the width and v_c marks the center of the Gaussian.

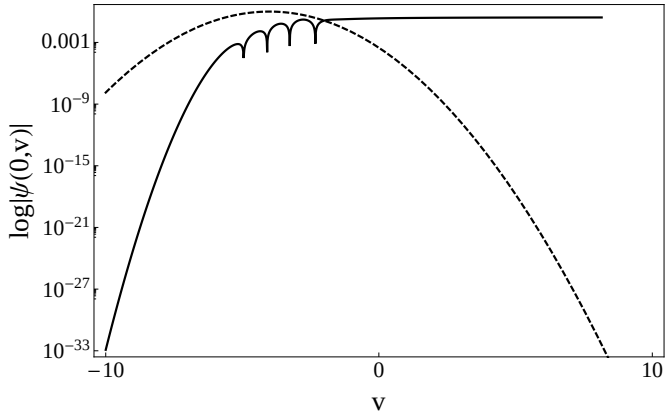

(a) $w = 1$, $v_c = -4$

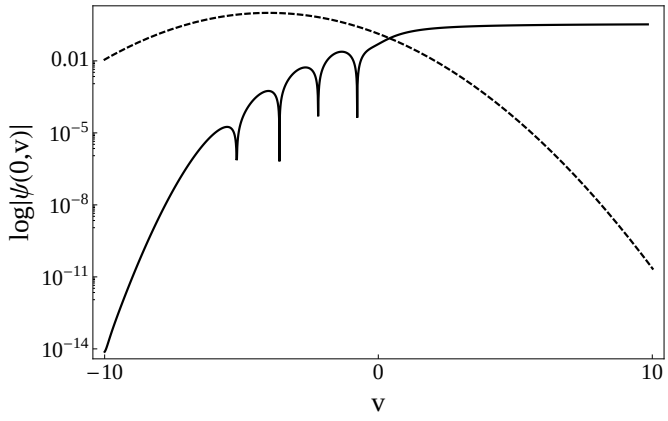

(b) $w = 2$, $v_c = -4$

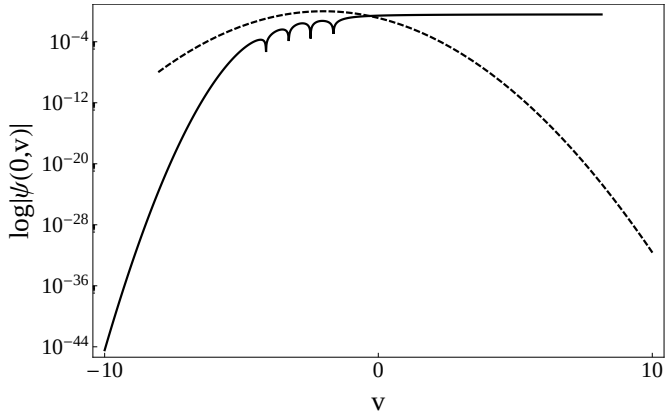

(c) $w = 1$, $v_c = -2$

Figure 6.7: Time profile of respond of outgoing Vaidya space-time to the scalar perturbations for $\Delta = 1/2$ and $\ell = 1$ for different values of initial data. The dashed line indicate the Gaussian function that has been used as initial data which w is the width and v_c marks the center of the Gaussian.

These results are in line with earlier studies of quasi-normal modes for dynamical backgrounds [111] where it has been pointed out that when the black hole mass decreases with time the oscillation period becomes shorter in contrast to the constant frequency quasi-normal modes of the Schwarzschild black hole.
These solutions show a constant tail after few oscillations for large values of $v > 0$, however we will see in the next section that as a consequence of the homothety of the metric, the $|\psi| \to$ const behavior at large positive v is most likely a consequence of numerical errors. In [112, 113] has been shown that there is a time window between the dominant period of quasi-normal ringing and the tail of these modes. In fact the tail behavior with a pure power law decay is only expected at infinitely late times. In practice the numerical integration is for a finite time interval and this causes an inherent error in the behavior of the tail.
In the next subsection we will show that, as a consequence of the scaling symmetry, the wave-equation can be separated, thus reducing the problem to that of an ordinary differential equation. We will also see from the separation ansatz that evolution is essentially a frequency dependent rescaling of the modes that are used to construct the initial Gaussian profile.

6.2.2 Reduction to an ODE

The main purpose of the current research was to present the wave-profiles that one can obtain from the numerical mesh integration method for different initial conditions and fields, as carried out in the previous section, and to then compare them with the individual mode solutions that we will obtain below via a more analytic method that takes advantage of the scaling symmetry of the space-time and equations. We will now look at individual modes of the wave-function that we obtain by using the homothety symmetry of the equations to carry out a separation of variables in the differential equation (6.19).
The homothety symmetry of this space-time suggests that we change the variable as follows

$$\bar{u} = -u = |u|, \qquad \bar{v} = v(-u)^{-2\Delta/(1+\Delta)}, \tag{6.20}$$

giving (from (6.16))

$$r = r(u, v) = |u| g(v/|u|^{2\Delta/(1+\Delta)}), \tag{6.21}$$

applying these changes to the equation (6.19) we find

$$\left(-\bar{u}\frac{\partial^2}{\partial\bar{u}\partial\bar{v}}+\frac{2\Delta}{(1+\Delta)}\frac{\partial}{\partial\bar{v}}+\frac{2\Delta}{(1+\Delta)}\bar{v}\frac{\partial^2}{\partial\bar{v}^2}\right)\psi(\bar{u},\bar{v})= \\ -\frac{1+\Delta}{4\Delta g(\bar{v})^4}\left(g(\bar{v})-\frac{(1-\Delta)}{4}\right)^{2/(1+\Delta)}(\ell(\ell+1)g(\bar{v})+2\sigma\mu)\psi(\bar{u},\bar{v}) \tag{6.22}$$

and with the ansatz

$$\psi(\bar{u},\bar{v})=\bar{u}^{\lambda}V(\bar{v}) \tag{6.23}$$

we obtain the following differential equation

$$\bar{v}\frac{\partial^2 V(\bar{v})}{\partial\bar{v}^2}+(1-\kappa)\frac{\partial V(\bar{v})}{\partial\bar{v}}+F(\bar{v})V(\bar{v})=0 \tag{6.24}$$

where $\kappa=\lambda/\alpha$ with $\alpha=\frac{2\Delta}{(1+\Delta)}$ and

$$F(\bar{v})=\frac{1}{2\alpha^2 g(\bar{v})^4}\left(g(\bar{v})-\frac{(1-\Delta)}{4}\right)^{2/(1+\Delta)}(\ell(\ell+1)g(\bar{v})+2\sigma\mu). \tag{6.25}$$

In the figure (6.8) we have shown the function $F(\bar{v})$ for $\Delta=1/2$. Notice that

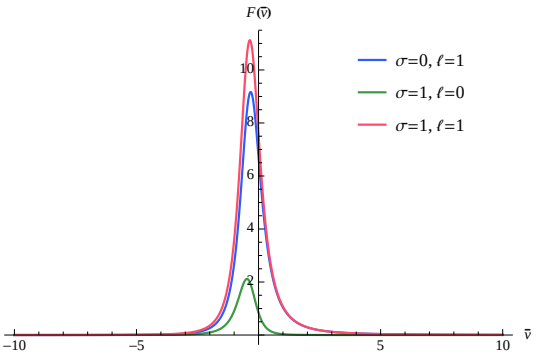

Figure 6.8: (a) $F(\bar{v})$ for $\Delta=1/2$ and $\sigma=0,1$, for 3 different values of angular momentum

this separation of variables leads to a very simple picture of the evolution of the wave function. In the following we will consider the setup where initial conditions for the wave-function profile are given at $\bar{u}\to\infty$ and then this profile is evolved towards $\bar{u}=0$. For given λ the wave-profile is then scaled by $\bar{u}^{\lambda}$ while its profile is simultaneously squashed in the v direction due to the $\bar{u}$ dependence in $\bar{v}$. Each

mode, corresponding to different allowed values of λ as evolves.
Writing (6.24) in the form of an ODE Schrödinger like equation leads to

$$\frac{\partial^2\phi(\bar{v})}{\partial\bar{v}^2} + \chi(\bar{v})\phi(\bar{v}) = 0 \tag{6.26}$$

where

$$\chi(\bar{v}) = \left(\frac{F(\bar{v})}{\bar{v}} - \frac{(\kappa^2-1)}{4\bar{v}^2}\right) \tag{6.27}$$

can be read as the potential. This potential falls off asymptotically as $\bar{v} \to \pm\infty$. This form of potential can lead us to a correct boundary condition by setting constrains on the value of κ. One should note that the value of the κ that appears as the power of advanced coordinate u in (6.23) can fix the necessary condition for having a non-flat geometry at $u \to -\infty$ while requiring regularity of $V(\bar{v})$ at $\bar{v} \to 0$, as we know that physically the solution has to be well behaved at this limit, can put restriction on value of κ.
To obtain some more information about the eigenvalue λ we will first consider the behaviour of the solutions to (6.24) around $\bar{v} = 0$. Expanding $V(\bar{v})$ around $\bar{v} \to 0$

$$V(\bar{v}) = \bar{v}^s \sum_{n=0}^{\infty} a_n \bar{v}^n \quad F(\bar{v}) = \sum_{n=0}^{\infty} b_n \bar{v}^n \tag{6.28}$$

with $b_0 \neq 0$. From (6.24) we obtain the indicial equation

$$s(s-\kappa) = 0, \tag{6.29}$$

which to leading order gives

$$V(\bar{v}) = \alpha + \beta\bar{v}^\kappa \tag{6.30}$$

and thus

$$\psi_\lambda = \alpha\bar{u}^{2\kappa/3} + \beta v^\kappa. \tag{6.31}$$

Decomposing $\kappa = -i\omega + \epsilon$ into real and imaginary parts, we see that well-behaved solutions around $v = 0$ require that $\epsilon \geq 0$. Note that this also means that around $v = 0$ the $\bar{u}$ dependent term is finite as $\bar{u} \to 0$, in agreement with the results of the numerical integration presented in the previous section. Obviously this implies a

divergence for large $\bar{u}$, but our physical setup does not include this region.
To obtain further information about the global structure of the solutions to the wave-equation we can expand around large positive $\bar{v}$. For large $\bar{v}$ approaching $\mathcal{I}_+$ we make the substitution $\bar{v} = e^{\bar{x}}$ and to leading order we also have $F(\bar{v}) \sim c\ \ell(\ell+1)/\bar{v}^{5/2}$, for some constant c. Together with the above substitution we obtain the equation

$$\ddot{V} - \kappa\dot{V} + c\ \ell(\ell+1)e^{-5\bar{x}/2} = 0. \tag{6.32}$$

The leading large $\bar{x}$ solution is

$$V(x) = \gamma + \delta e^{\kappa\bar{x}} \tag{6.33}$$

leading to (with $v = e^x$),

$$\psi_\lambda = \gamma\bar{u}^{2\kappa/3} + \delta e^{\kappa x} \tag{6.34}$$

and thus one has an outgoing wave of frequency ω for $\kappa = -i\omega$, requiring that $\epsilon = 0$. Note that the expansion around infinity has the same leading behavior as that around $v = 0$ due to the fact that the non-derivative term in the differential equation is subleading in both cases.
As in scattering problems for static space-times also here there will be a non-trivial relation between the coefficients α, β of the expansion around $v = 0$ and the coefficients γ, δ of the expansion around $v \to \infty$, and for outgoing waves at ∞ we require that $\gamma = 0$. The derivation of this transformation is beyond the scope of the current thesis as the numerical errors do not allow a complete and accurate integration from $\bar{v} = 0$ all the way to $\bar{v} \to \infty$.
As a consequence none of the solutions $\psi_\lambda(u, v)$ contain constant large v components.
We can now see from this more analytic approach and in particular the factorization of the wave-funtion for large $\bar{v}$ that the long constant tails that were obtained in the numerical integration of section 2. are numerical artifacts. An initial gaussian wave form in v at some $u = u_0$ will have a Fourier decomposition onto the basis of waves with outgoing modes. More precisely, the full solution for a given initial condition is

$$\Psi(\bar{u}, \bar{v}) = \int_0^\infty \omega a_\omega \bar{u}^{-i\omega}\psi_\omega(\bar{v}) \tag{6.35}$$

This clearly will remain unchanged due to the asymptotic form of the wavefuncion (6.34).

6.2.3 Numerical solution for $\Delta = 1/2$

To study the differential equation in double null coordinates we will proceed as in [110] and extract the $g(\bar{v})$ from (6.21) using the expression that already have presented for $r(u, v)$ and different values of Δ, $\Delta = 1/2$[1]

$$g(\bar{v})_{1/2} = \frac{1}{8}\left(3 + \frac{4}{3^{2/3}}\left(\sqrt[3]{9\bar{v}^3 - \sqrt{3}\sqrt{\bar{v}^6\,(27 - 64\bar{v}^3)}} + \sqrt[3]{9\bar{v}^3 + \sqrt{3}\sqrt{\bar{v}^6\,(27 - 64\bar{v}^3)}}\right)\right) \tag{6.36}$$

To proceed further one can rewrite the (6.25) using this $g(\bar{v})$ and solve the equation (6.24) numerically. We used the NDSolve package in mathematica to solve these perturbation equations. To use this package one needs proper initial conditions. Hence we first solve the perturbation equations analytically considering leading orders in the expansion of function $F(\bar{v})$ around zero. For instance the analytical solution for $\Delta = 1/2$ is

$$V(\bar{v}) \to \bar{v}^{\kappa/2}(c_1 J_{-\kappa}(\frac{8\sqrt[6]{2}\sqrt{\bar{v}}}{\sqrt{3}}) + c_2 J_{\kappa}(\frac{8\sqrt[6]{2}\sqrt{\bar{v}}}{\sqrt{3}})), \tag{6.37}$$

due to the possible presence of singularities in the numerical integration through $\bar{v} = 0$ we imposed initial conditions at two different $\bar{v} = -0.000001$ and $\bar{v} = 0.000001$ and integrated forwards and backwards in $\bar{v}$ to obtain the numerical solution. The results of numerical solution to these equations has been presented in the figures (6.9), (6.10) and (6.11). We show the solutions for $\epsilon = 0$ and also for $\epsilon = 1$. Note in particular that the $\epsilon = 0$ solutions show a ringing with variable frequency for $\bar{v} < 0$ together with no oscillations for $\bar{v} > 0$. This provides a confirmation of the ringing that was found in the previous section from the integration of the full wave equation for gaussian initial conditions.

6.2.4 Results and comments

It is worthwhile to mention several points about our results.

[1] For $\Delta = 1/3,$ and $1/5$, see the appendix (C).

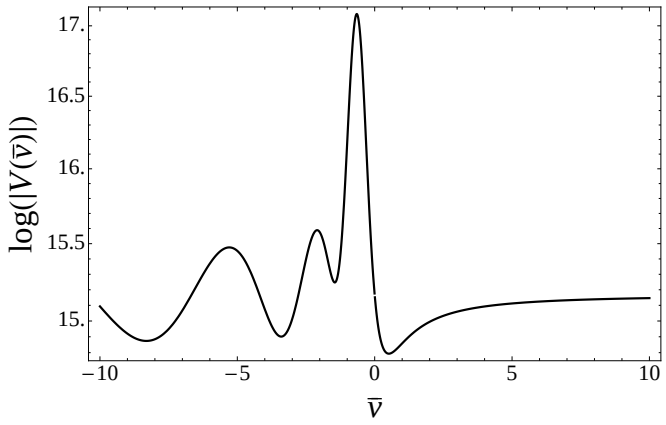

(a) $\sigma = 0$, $\ell = 1$ and $\kappa = 7i$

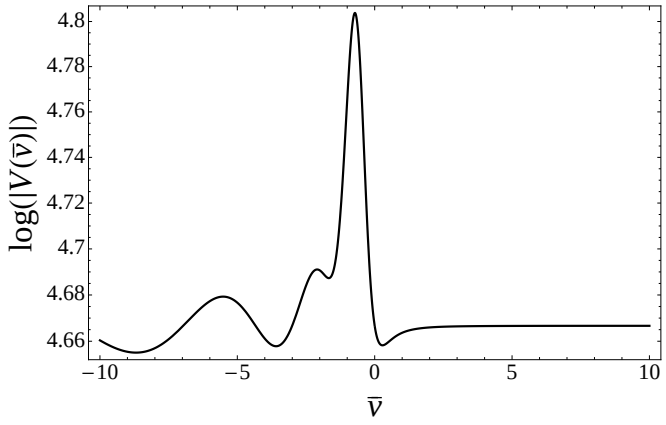

(b) $\sigma = 1$, $\ell = 0$ and $\kappa = 7i$

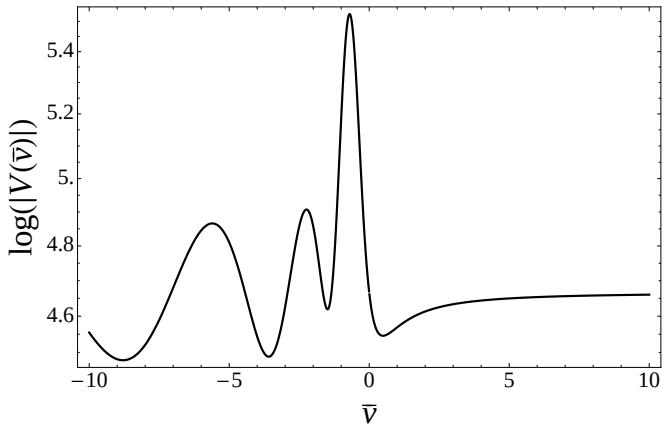

(c) $\sigma = 1$, $\ell = 1$ and $\kappa = 7i$

Figure 6.9: Time profile of electromagnetic, $\sigma = 0, 1$ for $\ell = 1$, and scalar perturbations, for $\ell = 0$ and 1, for $\Delta = 1/2$ and $\epsilon = 0$.

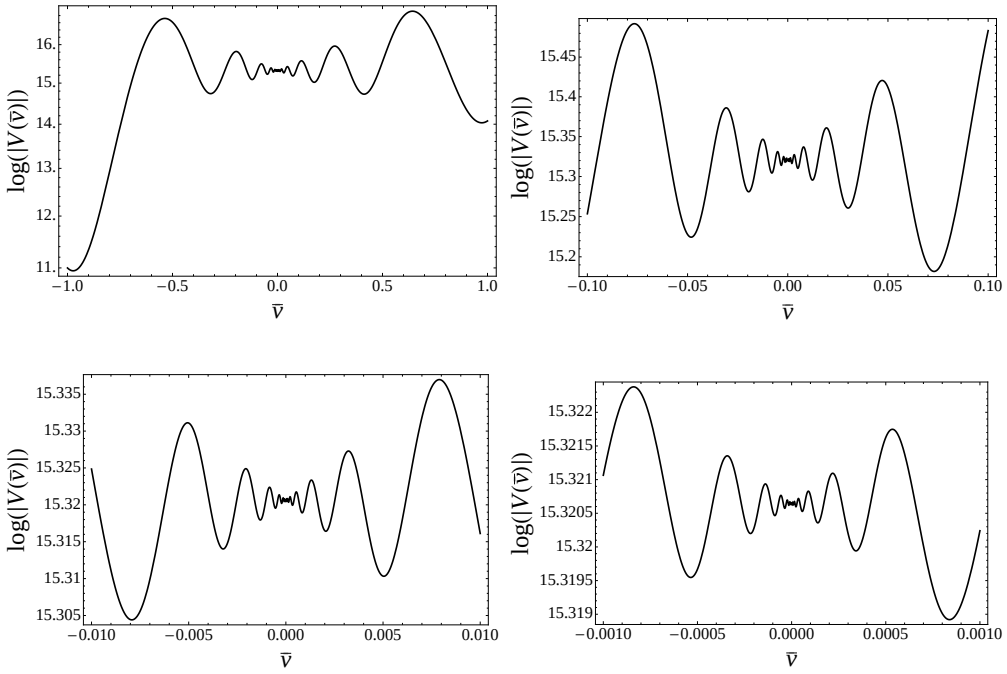

Figure 6.10: Time profile of electromagnetic perturbations, $\sigma = 0$, for $\ell = 1$, for $\Delta = 1/2$ with $\kappa = -7i + 1$.

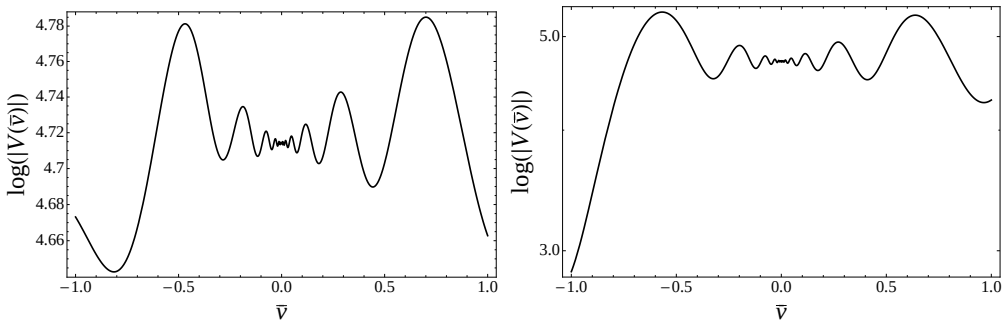

(a) $\ell = 0$ **(b)** $\ell = 1$

Figure 6.11: Time profile of scalar perturbation, $\sigma = 1$, for $\ell = 0$, 1, for $\Delta = 1/2$ with $\kappa = -7i + 1$.

Our analytical analysis shows that the constant tail that appears in the mesh calculation corresponds to constant part of the solution to the ODE wave equation, however the other part with $\kappa = -i\omega + \epsilon$ supports the decay of the oscillations at different values of $\bar{v}$.
Moreover for numerical solution to the ODE equations we used the initial condition that were coming from the leading term in potential, however for performing the integration we used the complete form of the potential and we found oscillations for both $\bar{v} > 0$ and $\bar{v} < 0$. If one compares the ODE solutions with the PDE ones, one can easily see that oscillations mostly are present for $v < 0$ and this can be because of the numerical error as it is pointed out in [112]. In this sense our ODE results confirm the existence of the quasi-normal type oscillations for the outgoing linear mass Vaidya metric with very high accuracy.
Up to now quasi normal modes for time dependent back grounds have been calculated for ingoing Vaidya and only using the double null coordinate technique while taking advantage of homothety symmetry of the background for the first time we were able to transform the equation to the ODE type and investigate the properties of the evaporating black hole at the end of its life in more details. The uncertainties in the numerical integration do not appear to allow us to find exactly these solutions, or there is a mixing between the ingoing wave (expansion around small $\bar{v}$) and the solutions for large $|\bar{v}|$. One may expect to see the exponential decay of the oscillations in mesh figures (6.5), (6.6) and (6.7) due to the exponential fall off of the Gaussian however one should note that, as we shown in this section, solution to the wave equation for small and large values of v has two parts; while one part has constant value . Hence the tail of the time profile may correspond to the constant part but it doesn't mean that the exponential fall off doesn't happen.
Having this result and knowing the special property of this sub-class of Vaidya can provide some evidence that the final stage of black hole evaporation may be modeled by linear mass Vaidya. In particular we see that although the linear mass Vaidya metric is not the same as Schwarzschild (in particular due to the null singularity), it does appear to display one well-known feature of the Schwarzschild black hole, quasi normal like oscillations as an ingoing wave approaches $u = 0$.

Indeed, one clearly sees that oscillations of increasing frequency appear just before reaching $v = 0$, indicating the approach to zero mass. Furthermore, as these oscillations appear with infinitesimally small wavelengths, this is also a clear indication of the breakdown of a semi-classical analysis around the final evaporation point.

Although they do not appear to play a clear role in the current analysis, the solutions to the ODE for $V_\lambda(\bar{v})$ contain solutions that have a scale invariant (fractal-like) oscillation around $\bar{v}$. These solutions occur for $\epsilon > 0$, and for finiteness at $\bar{v} \to \infty$ these solutions must have $\delta = 0$. This clearly introduces non-analytic behavior in the wave-function around $\bar{v} = 0$ and also some instability at infinity, nevertheless it is intriguing to speculate that upon entering the large back-reaction (Planckian) regime this feature remains. In such a case we would find a scaling close to the point of complete disappearance of the Vaidya-singularity analogous to the Choptuik scaling [114] that has been observed at the point of formation of black holes in numerical models that include the back-reaction between classical matter and the space-time metric.

The biggest obstacle to further progress is the difficulty in the numerical calculation of the Bogoliubov transformations required to obtain complete information about the modes V_λ. One possible approach to this question is the large-D limit. As there exists a Vaidya-metric in any dimension [115], one can take the large-D limit [90] and thus obtain a simplification of the potential $F(\bar{v})$. One may then use this to obtain a WKB matching of V_λ between the $\bar{v} = 0$ expansion and that at $\bar{v} \to \infty$, preliminary work is presented in appendix (D).

7

Discussion

One of the interesting and yet not well known part of the physics is study of the evolution of the black holes in general and micro black holes in particular. The study of the evaporation of the latter case is in our interest as any evidence of observing their signals in detectors would be a confirmation of the validity of theories which have been built by hypothesizing the existence of extra spatial dimensions. To this end, in this thesis, we have investigated different aspects of micro black hole evaporation.

7.1 Discussion of the results

In order to find out how micro black hole signals may look in the high energy experiments or ultra high energy cosmic rays observatories we performed a detailed analysis of the micro black hole event generator, BlackMax; the summary of our investigation is as follow

- We investigated the particle yield after hadronization in different transverse momentum ranges and for different numbers of extra spatial dimensions for both rotating and non-rotating micro black holes. For all particles we observed an enhancement in the particle yield as the number of extra dimensions increases. This enhancement is more drastic in the case of rotating micro black hole confirming the analysis in [50, 51].

- Moreover if the evaporating micro black hole is created from proton-proton collision as in LHC and also the most relevant process for the collision of UHECR's with the Earth's atmosphere then there is preferential emission of positively charged particles and also the emission of quarks and gluons in general is preferred over all other particles.

- Performing the analysis of the Monte Carlo data from a non-rotating micro black hole before and after hadronization we find out that effects of parton shower + hadronization + hadron decay may dramatically modify particle distributions after micro black hole evaporation, especially in the case of an SM quanta, such as photon. This is certainly a challenge that must be confronted when trying to distinguish the effects of different micro black hole models, potentially observable through micro black hole formation, evaporation and decay in high-energy and ultra-high-energy collisions, such as those explored at LHC and in cosmic ray experiments. Furthermore, from our preliminary investigations it appears that lepton distributions are less affected than photon ones and should thus be preferred for these micro black hole studies.

- The absence of proper simulation of graviton emission from a rotating black hole due to the lack of graviton grey-body factors in the micro black hole event generators lead us to check the sensitivity of the BlackMax to changes in the grey-body spectrum. After changing the grey-body factors we find out that the final products are either un-changed or the change is less than 5 percent. This can be a motivation for using the grey-body profile of other particles for gravitons just to check how the bulk emission of the graviton might change the emitted particles multiplicities and distributions on the brane.

- For the next step of our investigations regarding the graviton emission, we used large D method, a method in which the number of spatial extra dimensions can be arbitrarily large and this may give us an extra small parameter that can simplify the perturbation equations. We followed this

approach for graviton emission from a non-rotating black hole and we obtained an analytical expression at low frequencies for the tensor and vector type gravitational emission that is in complete agreement with the one which is already in the literature. This encourages us that one can use the large-D limit to also calculate the graviton emission from a rotating black hole and this work is still in progress.

- Finally in the last part of our research we studied the electromagnetic and scalar perturbation of out-going Vaidya space-time with linear mass function. We performed the detailed investigation of the relevant wave equations both numerically and analytically. First we solved these PDE equations numerically and we found that the time profiles contains oscillations that can be interpreted as quasi-normal modes. For further investigation we used the homothety symmetry of this space-time and we rescaled the fields which enabled us to write the equations in the form of ODE's. Having this simpler form of the perturbation equations enabled us to solve them analytically for different limits. Furthermore with detailed investigation of these solutions we could find the proper boundary conditions for solving the ODE's numerically. We were able to monitor how this space time respond to different types of perturbations, before it completely vanishes, by calculating the time profile of this respond. This time profile is similar to the ones that we obtained from the mesh calculations. Our results show that the out-going Vaidya space time with linear mass function has quasi-normal behavior close to the point where the singularity vanishes like the quasi normal behavior of the Schwarzschild black hole.

7.2 Future work

The most interesting application of this research is the possibility of confirming its validity in high energy experiments and observations.
First thing that we are concerned to do in the near future is to perform a more detailed analysis using black hole event generators. This work should be done to explain the peak that we observed in high p_T for colored particles out of rotating

black hole evaporation. The first step may be to investigate the invariant mass of hadronic jets before hadronization. We are motivated for this analysis also because of the bump that CMS and ATLAS observed in their data around 2 TeV at first run of the LHC. Although more analysis is required to find out if this bump is a statistical fluke or a new very heavy particle or maybe the micro black hole evaporation signal.

Our other task is to calculate the graviton grey-body factors of a rotating black hole at the large-D limit of general relativity. We already showed that using the large-D limit technique perturbation equations can be simplified drastically for the non-rotating case. Knowing that that the same simplification may hold also for the rotating case we are to start the graviton grey body calculation for this case. In the absence of graviton spectrum, this calculation (even if it won't be so exact) may help to improve the accuracy of the micro black hole event generators.

Appendices

Appendix A

Bogoliubov transformations

In order to calculate Hawking radiation spectra it is useful to introduce the Bogoliubov Transformation. Let's start with number operator for *in* and *out* modes which measures the number of *in* or *out* particles in a state

$$N_{\omega}^{in} = a_{\omega}^{+} a_{\omega}, \qquad N_{\omega}^{out} = b_{\omega}^{+} b_{\omega} \tag{A.1}$$

where $a_{\omega}^{+}, a_{\omega}$ and $b_{\omega}^{+}, b_{\omega}$ are creation and annihilation operators of two different vacuum states with following canonical communication relations

$$[a_{\omega'}, a_{\omega}^{+}] = \delta(\omega' - \omega), \qquad [a_{\omega}, a_{\omega'}] = [a_{\omega}^{+}, a_{\omega'}^{+}] = 0, \tag{A.2}$$

and the second vacuum state

$$[b_{\omega'}, b_{\omega}^{+}] = \delta(\omega' - \omega), \qquad [b_{\omega}, b_{\omega'}] = [b_{\omega}^{+}, b_{\omega'}^{+}] = 0. \tag{A.3}$$

Using the (A.1) one can say that the state $(a_{\omega})^n|0>_{in}$ contains n *in*-particles and state $(b_{\omega})^n|0>_{out}$ contains n *out*-particles. Now defining a linear transformation known as Bogoliubov transformation

$$\phi_{out_{\omega}} = \int d\omega' (\alpha_{\omega\omega'} \phi_{in_{\omega'}} + \beta_{\omega\omega'} \phi^{*}_{in_{\omega'}}) \tag{A.4}$$

$$\phi_{in_{\omega}} = \int d\omega' (\alpha^{*}_{\omega'\omega} \phi_{out_{\omega'}} - \beta_{\omega'\omega} \phi^{*}_{out_{\omega'}}) \tag{A.5}$$

one can express the number of *out*-particles in terms of the creation and annihilation operators of *in*-particles. Where $\alpha_{\omega'\omega}$ and $\beta_{\omega'\omega}$ are the Bogolubov coefficients and it can be expressed in terms of inner product of ϕ_{out_ω} and ϕ_{in_ω}

$$\alpha_{\omega\omega'} =< \phi_{out_\omega}, \phi_{in_{\omega'}} >, \qquad \beta_{\omega\omega'} = - < \phi_{out_\omega}, \phi^*_{in_{\omega'}} > \tag{A.6}$$

These coefficients satisfy

$$\int d\omega'(|\alpha_{\omega'\omega}|^2 - |\beta_{\omega'\omega}|^2) = \delta(\omega' - \omega) \tag{A.7}$$

Using (1.24), (1.27) and above-mentioned transformation the relation between *in* and *out* particles is

$$b_\omega = \int d\omega'(\alpha^*_{\omega'\omega} a_{\omega'} - \beta^*_{\omega\omega'} a^+_{\omega'}) \tag{A.8}$$

Finally we are able to produce the spectrum of the *out*-particles using vacuum state of the *in*-particles

$$_{in} < 0|N^{out}_\omega|0 >_{in} =_{in} < 0|b^+_\omega b_\omega|0 >_{in} = \int d\omega'|\beta_{\omega\omega'}|^2 \tag{A.9}$$

Appendix B

The geometry of the $\mathbb{CP}^N$

N-dimensional Complex projective space is a symmetric space and mathematically can be expressed by a complex manifold, $\mathbb{C}^{N+1}$, by complex coordinates Z^A for $A = (0, \alpha)$ where $1 < \alpha < N$. The point set $\mathbb{CP}^N$ is covered by the patches and coordinates of each patch can be defined by N inhomogenous coordinates [98] as follow

$$\zeta^\alpha = \frac{Z^\alpha}{Z^0}, \quad \text{for} \quad Z^0 \neq 0 \tag{B.1}$$

Using Z^A the flat metric has the form

$$ds^2_{2N+1} = dZ^A d\bar{Z}_A \tag{B.2}$$

Then if we introduce a new set of coordinates v^i with $0 < v^i < N - 1$ and we change the coordinates to R_N and ψ_N using following relations

$$Z_0 = e^{i\tau}|Z_0|, \quad Z^\alpha = Z^0, \quad \zeta^\alpha = R_N u^\alpha, \quad Z^A\bar{Z}_A = r^2, \quad f = 1 + \zeta^\alpha\bar{\zeta}^\alpha = 1 + R_N^2. \tag{B.3}$$

and also for v^i

$$u^N = e^{i\psi_N/2}|u^N|, \quad u^i = u^N v^i \quad \text{with} \quad u^\alpha\bar{u}^\alpha = 1. \tag{B.4}$$

The metric (B.2) will take the form

$$ds^2_{2N+2} = dr^2 + r^2 d\Omega^2_{2N+1} \tag{B.5}$$

whith

$$d\Omega^2_{2N+1} = (d\tau + A_{(N)})^2 + d\Sigma^2_{2N} \tag{B.6}$$

where $d\Sigma_{2N}^2$ is the unit $\mathbb{CP}^N$ metric and $A_(N)$ is the $\mathbb{CP}^N$ Kähler potential and they can be written in terms of coordinates (ψ_N, R_N).

$$\begin{aligned} d\Sigma_{2N}^2 =& \hat{g}_{ab} dx^a dx^b \\ =& \frac{dR_N^2}{(1+R_N^2)^2} + \frac{1}{4}\frac{R_N^2}{(1+R_N^2)^2}(d\psi_N + 2A_{(N-1)})^2 + \frac{dR_N^2}{1+R_N^2} d\Sigma_{N-1}^2 \end{aligned} \tag{B.7}$$

$\hat{g}_{ab}$ is the Fubini-Study metric and the Kähler potential is

$$A_N = \frac{1}{2}\frac{dR_N^2}{1+R_N^2}(d\psi_N + 2A_{(N-1)}) \tag{B.8}$$

The advantage of using this analysis is that one can start from the $\mathbb{CP}^1$ and iteratively construct the $\mathbb{CP}^N$ geometry as well as the complex coordinates Z^A that define how this geometry embedded in $\mathbb{C}^N$.

Appendix C

Vaidya calculations for different values of Δ

All the calculations that we performed in chapter (6) for $\Delta = 1/2$ can be carried out for different values of Δ. In this appendix we present the relevant calculations for $\Delta = 1/3$ and $1/5$. The solution to the electromagnetic and scalar perturbation equations in double null coordinate for $\Delta = 1/3$ and $1/5$ is shown in figures (C.1), (C.2), (C.3), (C.4), (C.5) and (C.6). In these figures the integration is carried out for different values of the initial data, namely, different forms of Gaussian waves. The general shape of these time profiles is similar to the ones for $\Delta = 1/2$.
For numerical integration we need the $g(\bar{v})$ which for $\Delta = 1/3$ is

$$g(\bar{v})_{1/3} = \frac{1}{2}\left(\bar{v}^2 + \bar{v}\sqrt{\bar{v}^2 + \frac{2}{3}} + \frac{2}{3}\right), \tag{C.1}$$

and for $\Delta = 1/5$

$$\begin{aligned} g(\bar{v})_{1/5} = \frac{1}{30}(9 + 10\bar{v}^3 + \sqrt[3]{5}\bar{v}(\sqrt[3]{27 + 200\bar{v}^6 + 180\bar{v}^3 - 3\sqrt{3}\sqrt{40\bar{v}^3 + 27}} \\ + \sqrt[3]{27 + 200\bar{v}^6 + 180\bar{v}^3 + 3\sqrt{3}\sqrt{40\bar{v}^3 + 27}})) \end{aligned} \tag{C.2}$$

using (C.1) and (C.2) one can calculate the $F(\bar{v})$ function that is presented in figure (C.7) for two values of Δ. The same argument as in chapter (6) is valid for the derivation of initial conditions in order to solve the perturbation equations numerically. As $\bar{v} \to 0$ the leading order solution for $\Delta = 1/3$ is

C. VAIDYA CALCULATIONS FOR DIFFERENT VALUES OF Δ

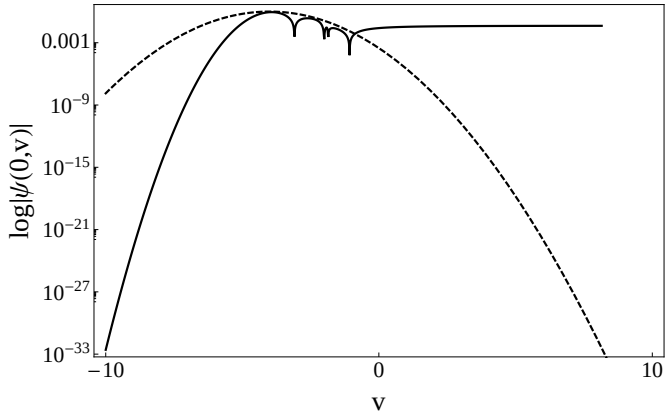

(a) $w = 1$, $v_c = -4$

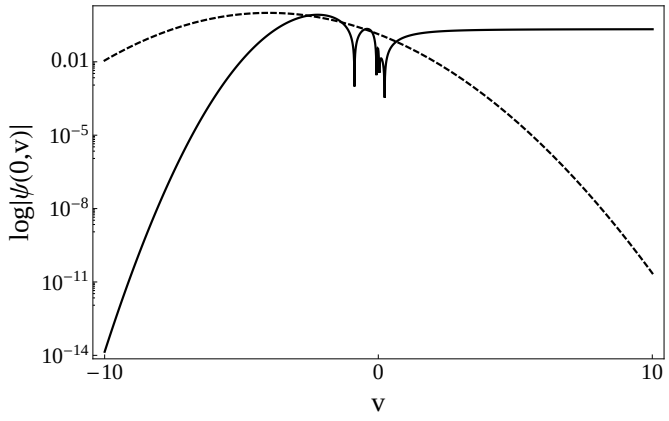

(b) $w = 2$, $v_c = -4$

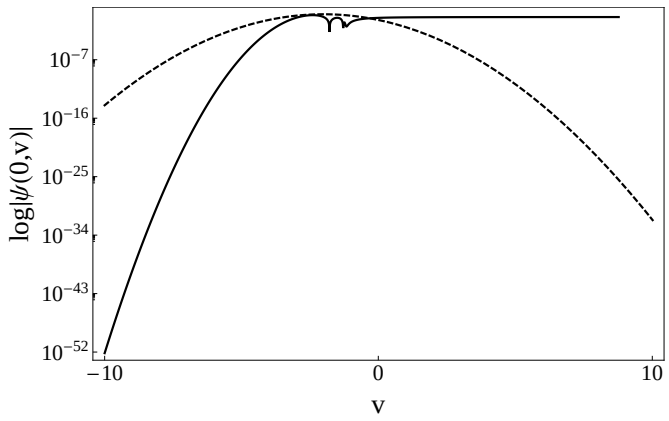

(c) $w = 1$, $v_c = -2$

Figure C.1: Time profile of respond of outgoing Vaidya space-time to the electromagnetic perturbations for $\Delta = 1/3$ and $\ell = 1$ for different values of initial data. The dashed line indicate the Gaussian function that has been used as initial data which w is the width and v_c marks the center of the Gaussian.

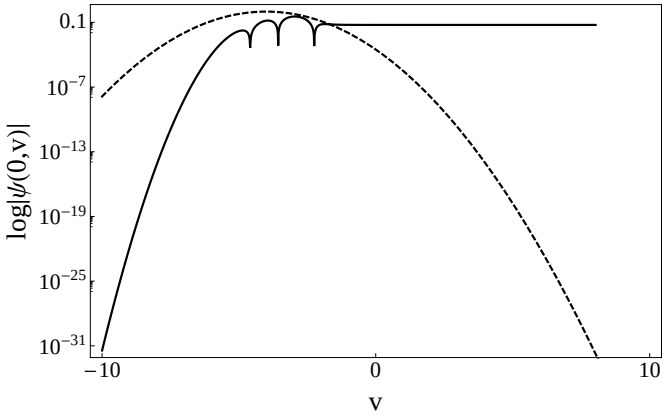

(a) $w = 1$, $v_c = -4$

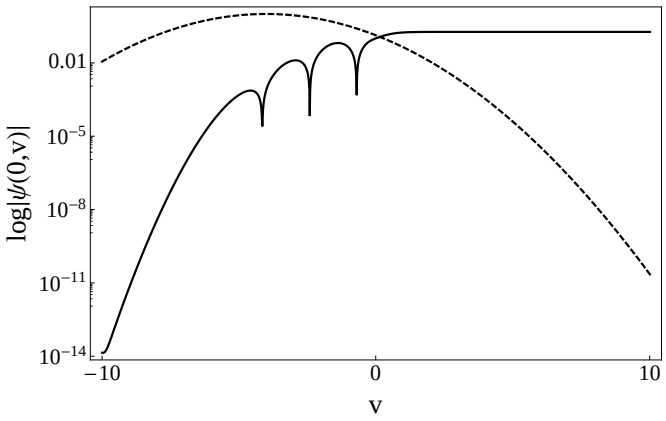

(b) $w = 2$, $v_c = -4$

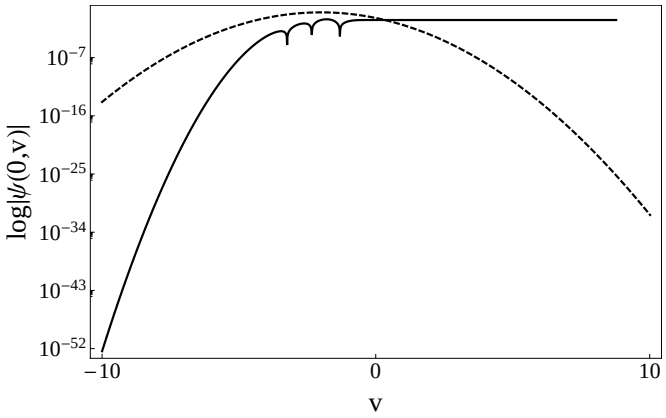

(c) $w = 1$, $v_c = -2$

Figure C.2: Time profile of respond of outgoing Vaidya space-time to the scalar perturbations for $\Delta = 1/3$ and $\ell = 0$ for different values of initial data. The dashed line indicate the Gaussian function that has been used as initial data which w is the width and v_c marks the center of the Gaussian.

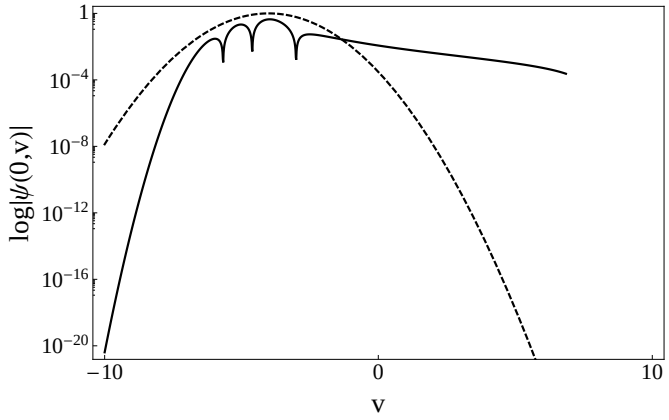

(a) $w = 1$, $v_c = -4$

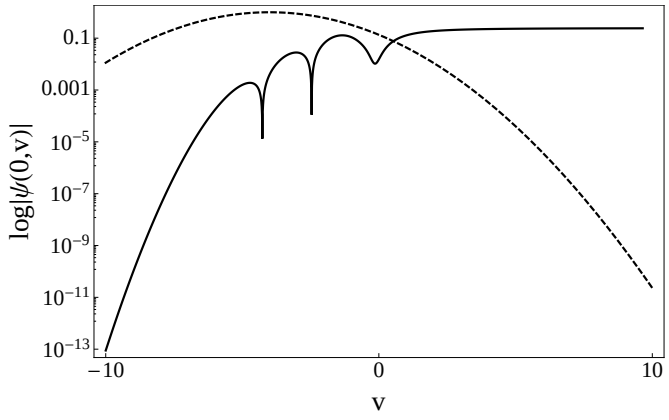

(b) $w = 2$, $v_c = -4$

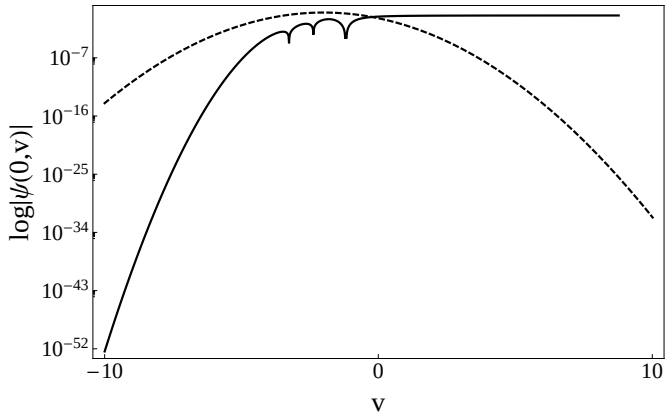

(c) $w = 1$, $v_c = -2$

Figure C.3: Time profile of respond of outgoing Vaidya space-time to the scalar perturbations for $\Delta = 1/3$ and $\ell = 1$ for different values of initial data. The dashed line indicate the Gaussian function that has been used as initial data which w is the width and v_c marks the center of the Gaussian.

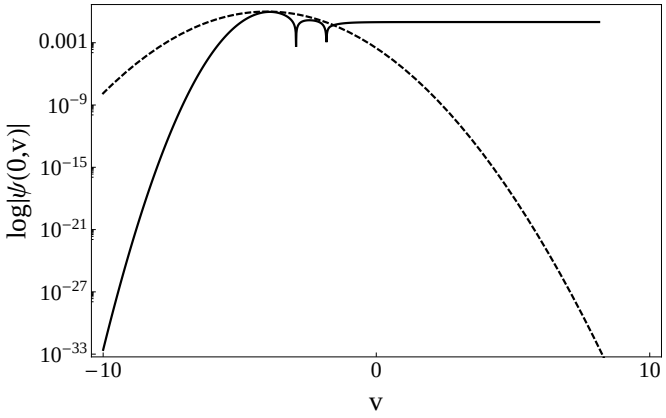

(a) $w = 1$, $v_c = -4$

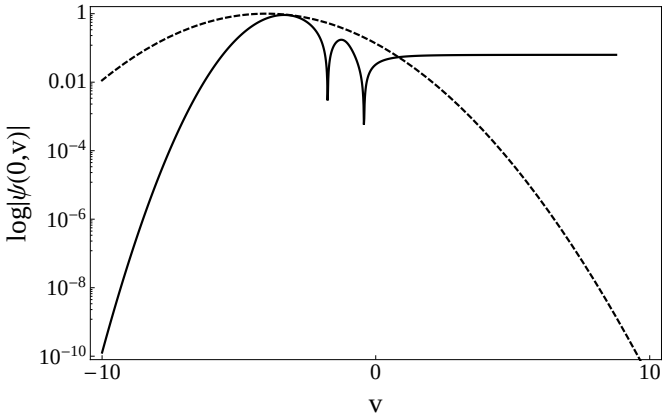

(b) $w = 2$, $v_c = -4$

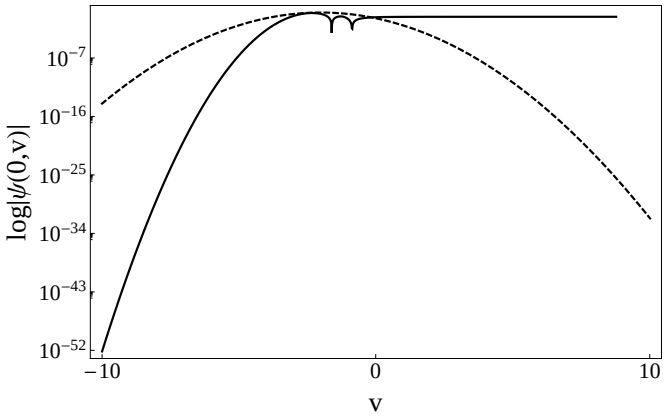

(c) $w = 1$, $v_c = -2$

Figure C.4: Time profile of respond of outgoing Vaidya space-time to the electromagnetic perturbations for $\Delta = 1/5$ and $\ell = 1$ for different values of initial data. The dashed line indicate the Gaussian function that has been used as initial data which w is the width and v_c marks the center of the Gaussian.

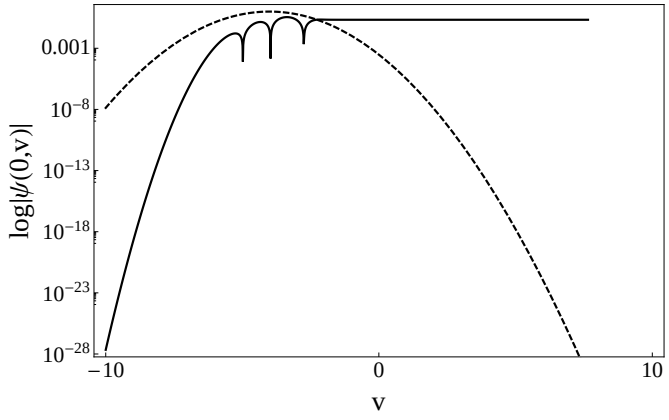

(a) $w = 1$, $v_c = -4$

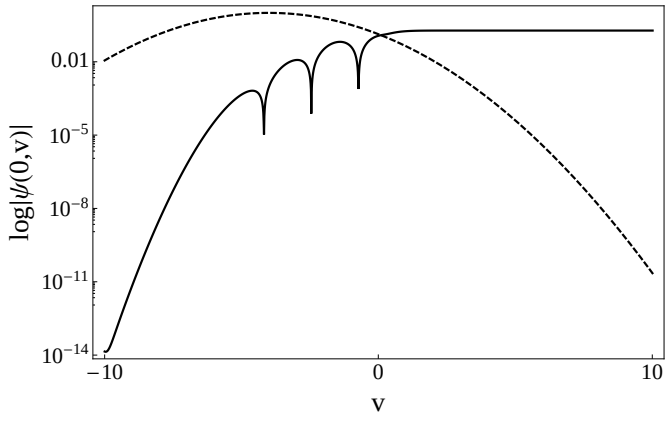

(b) $w = 2$, $v_c = -4$

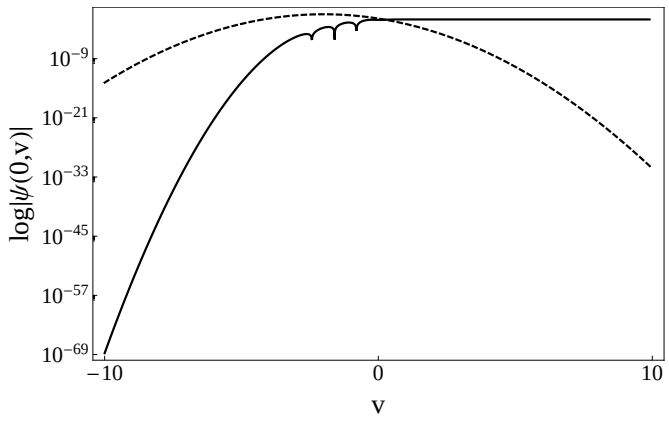

(c) $w = 1$, $v_c = -2$

Figure C.5: Time profile of respond of outgoing Vaidya space-time to the scalar perturbations for $\Delta = 1/5$ and $\ell = 0$ for different values of initial data. The dashed line indicate the Gaussian function that has been used as initial data which w is the width and v_c marks the center of the Gaussian.

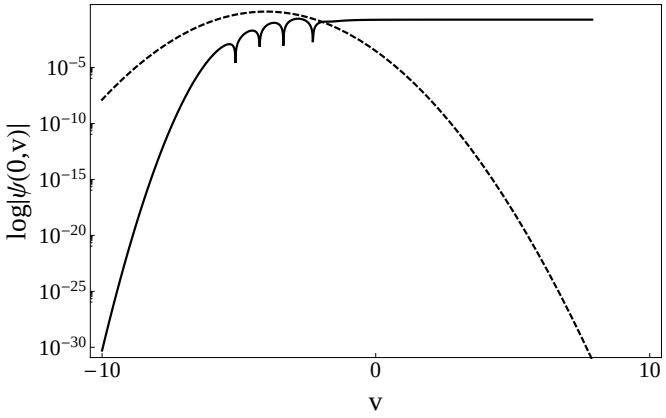

(a) $w = 1$, $v_c = -4$

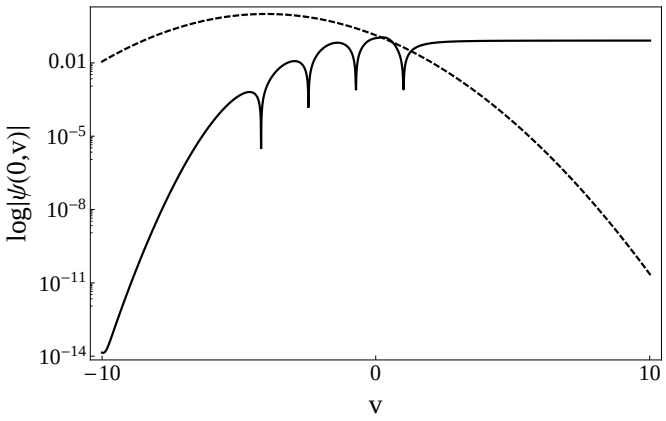

(b) $w = 2$, $v_c = -4$

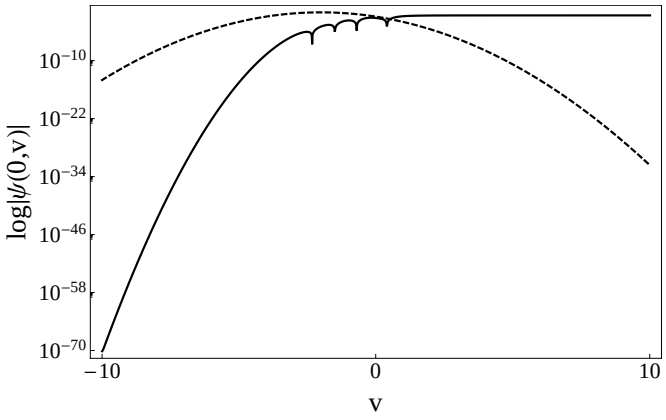

(c) $w = 1$, $v_c = -2$

Figure C.6: Time profile of respond of outgoing Vaidya space-time to the scalar perturbations for $\Delta = 1/5$ and $\ell = 1$ for different values of initial data. The dashed line indicate the Gaussian function that has been used as initial data which w is the width and v_c marks the center of the Gaussian.

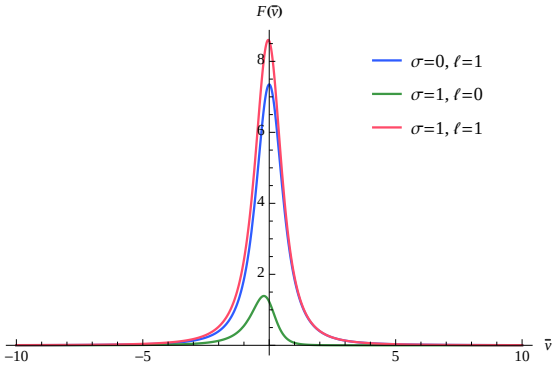

(a) $F(\bar{v})$ for $\Delta = 1/3$

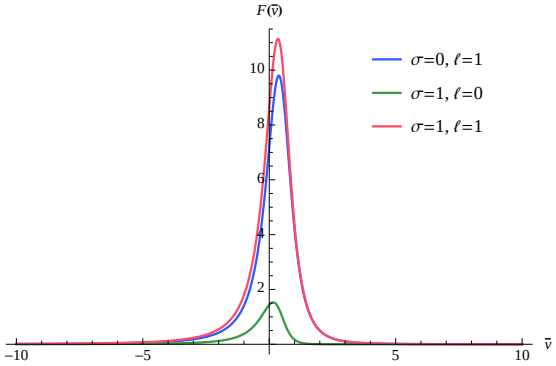

(b) $F(\bar{v})$ for $\Delta = 1/5$

Figure C.7: (a) $F(\bar{v})$ for $\Delta = 1/3$ and (b) $F(\bar{v})$ for $\Delta = 1/5$; for $\sigma = 0, 1$, for 3 different values of angular momentum

$$V(\bar{v}) \to \bar{v}^{\kappa/2}\left(c_1 J_{-\kappa}\left(2\sqrt[4]{2}3^{3/4}\sqrt{\bar{v}}\right) + c_2 J_{\kappa}\left(2\sqrt[4]{2}3^{3/4}\sqrt{\bar{v}}\right)\right) \tag{C.3}$$

and for $\Delta = 1/5$

$$V(\bar{v}) \to \bar{v}^{\kappa/2}\left(c_1 J_{-\kappa}\left(\frac{2\ 10^{2/3}\sqrt{\bar{v}}}{\sqrt{3}}\right) + c_2 J_{\kappa}\left(\frac{2\ 10^{2/3}\sqrt{\bar{v}}}{\sqrt{3}}\right)\right) \tag{C.4}$$

Using this solutions, for both cases, the initial conditions at two different points $\bar{v} = 0.000001$ and $\bar{v} = -0.000001$ were calculated for different values of $\kappa = -i\omega + \epsilon$. Results of numerical integration for $\epsilon = 0, 1$ is shown in figure (C.8) and (C.9) for $\Delta = 1/3$ and in figure (C.10) and (C.11) for $\Delta = 1/5$, respectively.

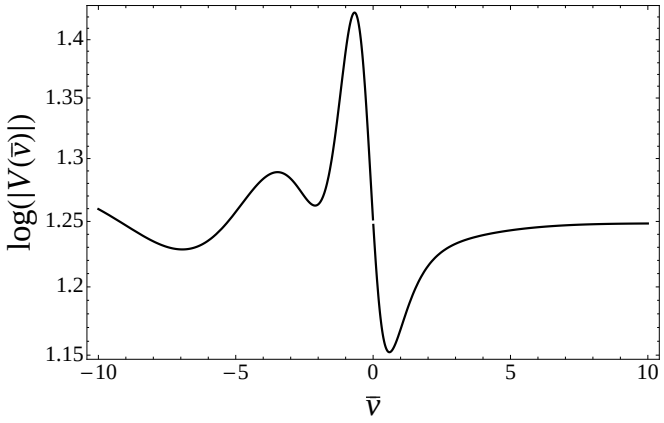

(a) $\sigma = 0$, $\ell = 1$

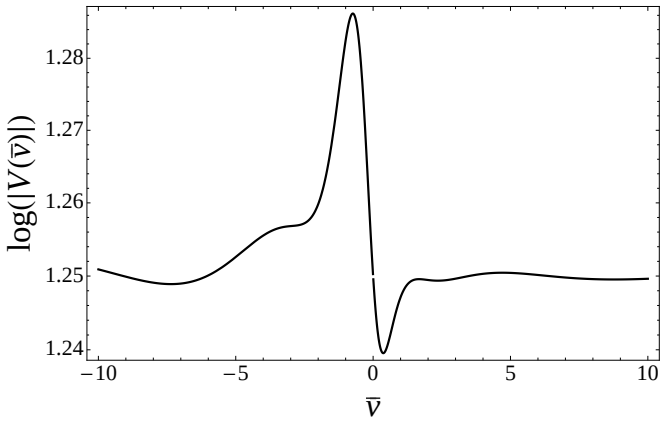

(b) $\sigma = 1$, $\ell = 0$

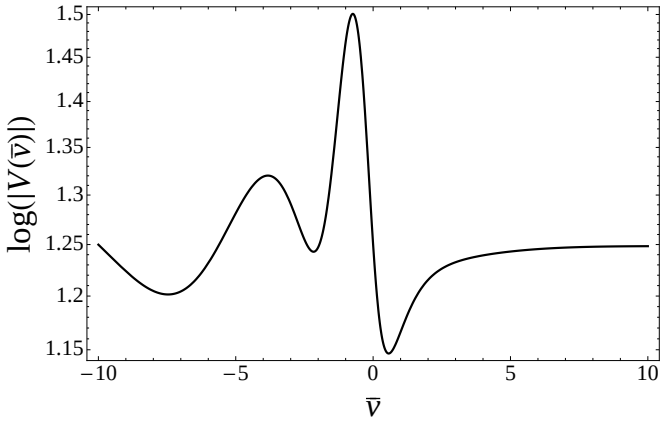

(c) $\sigma = 1$, $\ell = 1$

Figure C.8: Time profile of electromagnetic, $\sigma = 0, 1$ for $\ell = 1$, and scalar perturbations, $\sigma = 1, 1$, for $\ell = 0, 1$, for $\Delta = 1/3$ and $\kappa = -5i$

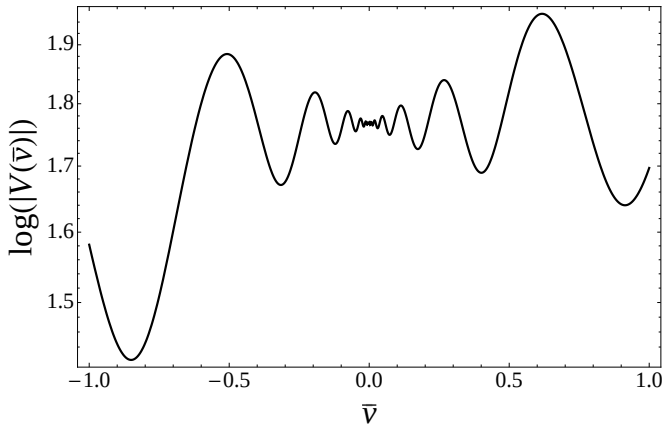

(a) $\sigma = 0$, $\ell = 1$

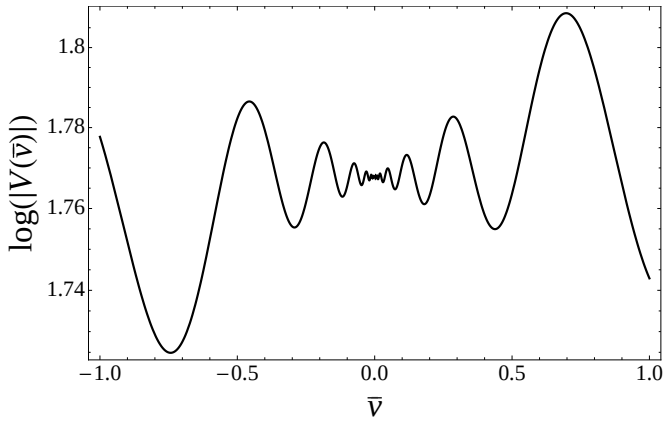

(b) $\sigma = 1$, $\ell = 0$

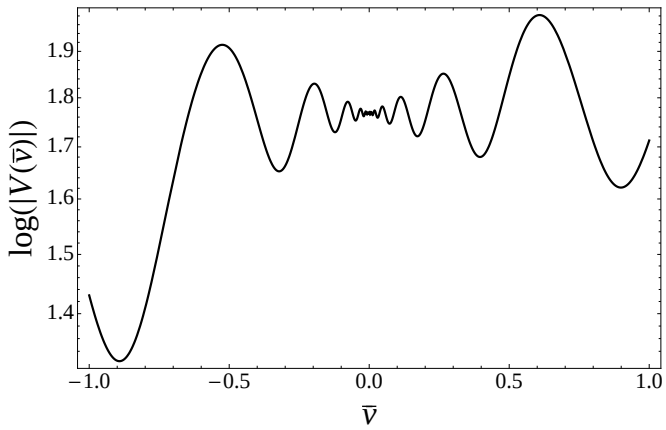

(c) $\sigma = 1$, $\ell = 1$

Figure C.9: Time profile of electromagnetic, $\sigma = 0, 1$ for $\ell = 1$, and scalar perturbations, $\sigma = 1$, 1, for $\ell = 0$, 1, for $\Delta = 1/3$ and $\kappa = -7i + 1$

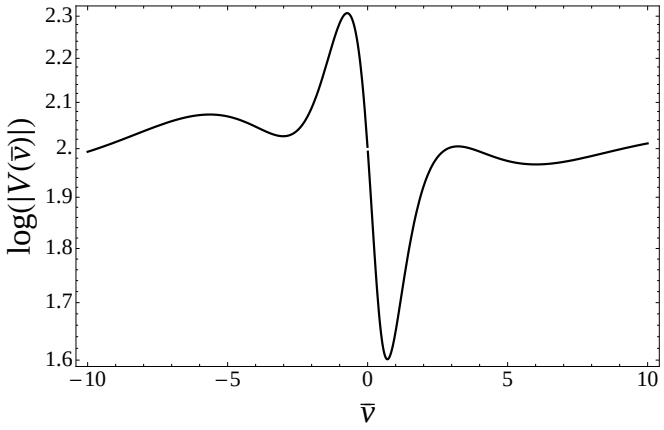

(a) $\sigma = 0$, $\ell = 1$

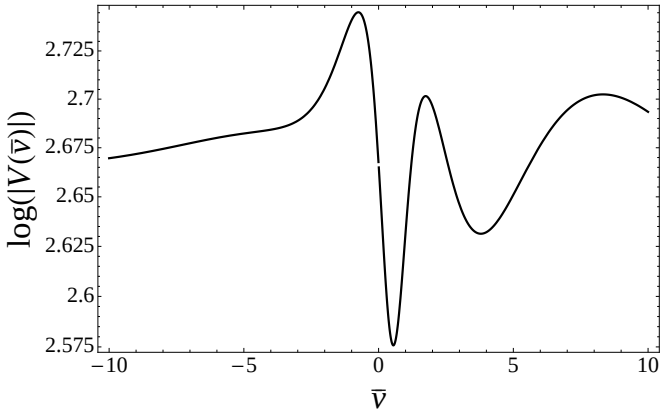

(b) $\sigma = 1$, $\ell = 0$

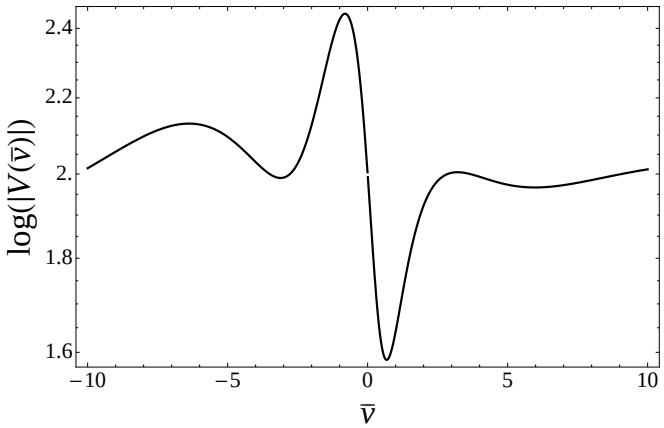

(c) $\sigma = 1$, $\ell = 1$

Figure C.10: Time profile of electromagnetic, $\sigma = 0, 1$ for $\ell = 1$, and scalar perturbations, $\sigma = 1$, 1, for $\ell = 0$, 1, for $\Delta = 1/5$ and $\kappa = -4i$

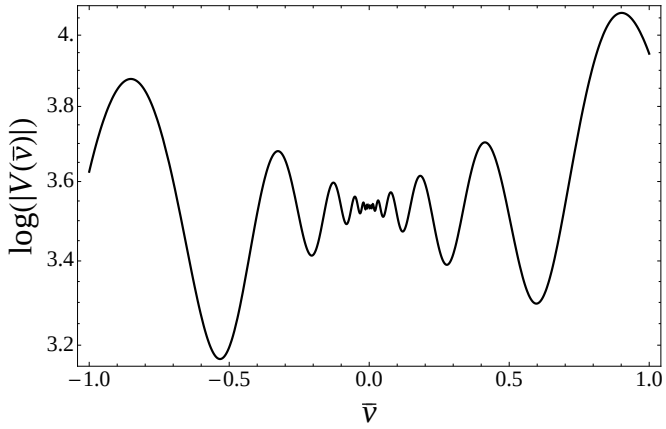

(a) $\sigma = 0$, $\ell = 1$

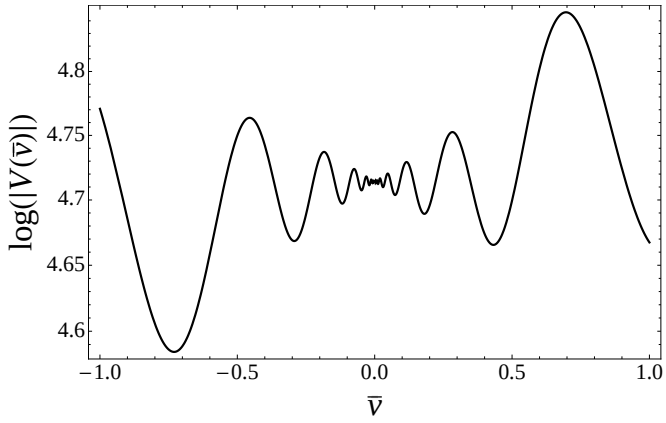

(b) $\sigma = 1$, $\ell = 0$

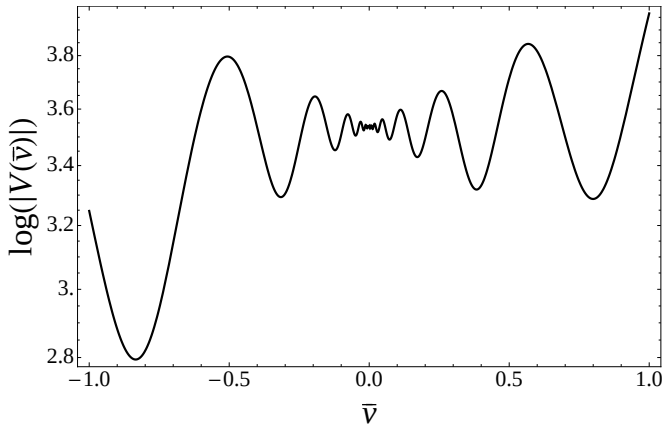

(c) $\sigma = 1$, $\ell = 1$

Figure C.11: Time profile of electromagnetic, $\sigma = 0, 1$ for $\ell = 1$, and scalar perturbations, $\sigma = 1$, 1, for $\ell = 0$, 1, for $\Delta = 1/5$ and $\kappa = -7i + 1$

Appendix D

Out-going Vaidya metric at large-D

We already discussed the large-D limit of general relativity in chapter (4) in which by taking the number of space-like dimensions to be large many interesting features of the model will let us simplify the black hole theory. In this section we will take the large-D limit of the higher dimensional out-going Vaidya space-time [115] in order to understand its properties more deeply. For the mass function

$$m(u) = \bar{\mu}(-u)^D \tag{D.1}$$

the higher dimensional out going Vaidya metric can be written

$$ds^2 = -\left(1 - \frac{2\bar{\mu}}{D}\left(\frac{-u}{2r}\right)^D\right)du^2 - 2dudr + r^2 d\Omega^2_{D+1} \tag{D.2}$$

where the mass parameter, $\bar{\mu}$, is restricted in the following interval [116]

$$0 < \bar{\mu} < \frac{1}{2}\left(\frac{D}{D+1}\right)^{D+1} \tag{D.3}$$

in order to let the metric to have the homothety symmetry. For mass function (D.1), metric (D.2) is a solution to the Einstein equation with the following stress-energy tensor

$$T_{uu} = \frac{\bar{\mu}(D+1)}{8\pi G u^2}\left(\frac{-u}{2r}\right)^{D+1} \tag{D.4}$$

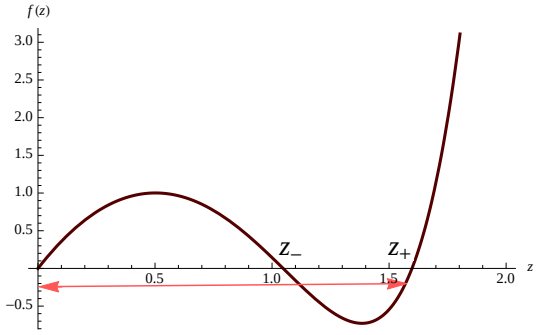

Figure D.1: $g_{\zeta\zeta}$ element of Vaidya metric for $D = 8$.

To make (D.2) mathematically simpler for the time that we want to take the large-D limit as well as for better understanding the geometry of this space-time we introduce the following new coordinate

$$z = \frac{-u}{2r}, \qquad u = -e^{\zeta} \tag{D.5}$$

using which (D.2) will change to

$$ds^2 = \frac{e^{2\zeta}}{4z^2}\left(f(z)d\zeta^2 - 4d\zeta dz + d\Omega^2_{D+1}\right), \tag{D.6}$$

where

$$f(z) = 4z(1 - z + \frac{2\bar{\mu}}{D}(z)^{D+1}). \tag{D.7}$$

It can easily be shown that $f(z)$ has only two non-zero real roots for any number of dimensions. This has been shown in figure (D.1) for $D = 8$. The structure of this space time is shown in figure (D.2). The null homothetic lines are the zeros of $g_{\zeta\zeta}$ of the (D.6) and, like the four dimensional case, for the limit (D.3) these zeros are the lines with constant values which emanate at null past infinity and they terminate at $u = 0$. We are particularly interested in the null line ($z = z_-$) which meets $u = 0$ at the point where the naked singularity vanishes as [110] suggests. The ($z = z_-$) corresponds to the smallest root of $f(z)$ and at large-D the perturbations around this root is desired $z = z_- - \frac{\tilde{z}}{D}$ and this perturbed region is located in the $0 < z < z_+$ that is marked by red arrow in figure (D.1). For this marked range z is an angular coordinate around ζ. Perturbation in this region is interesting because the evaporating Schwarzschild black hole at end stage of its

evaporation can be continuously attached to outgoing out-going Vaidya space-time and by perturbing this space-time around the vanishing point it is possible to investigate the structure of this space-time more carefully.
Perturbing metric (D.6) by scalar field and solving the perturbation equation which is equivalent to solve the Klein-Gordon equation in the former background we will get

$$\left(\frac{-f(z)}{2}\partial_z^2+(\frac{f(z)}{z}-\frac{f'(z)}{2}-2)\partial_z-2\partial_z\partial_\zeta+\frac{\partial_\zeta}{z}-2\ell(\ell+D)\right)\psi(\zeta,z)=0, \tag{D.8}$$

considering the homothety symmetry of the metric and implementing following separation

$$\psi(\zeta,z)=e^{\kappa\zeta}g(z), \tag{D.9}$$

we can write (D.8) in the form of ODE equation

$$g''(z)+A(z)g'(z)-B(z)g(z)=0, \tag{D.10}$$

where

$$A(z)=-\frac{2\left(-\frac{f'(z)}{2}+\frac{f(z)}{z}-2\kappa-2\right)}{f(z)},\quad \text{and}\quad B(z)=\frac{2\left(-2\ell(D+\ell)+\frac{\kappa}{z}\right)}{f(z)} \tag{D.11}$$

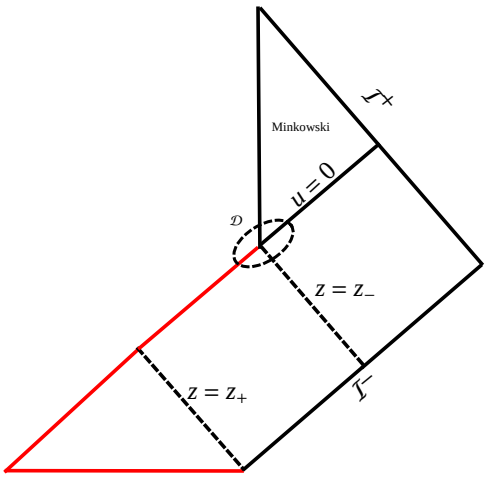

Figure D.2: Conformal diagram for outgoing Vaidya with linear mass function

writing (D.10) in the form of Schrodiner equation the potential will be

$$v(z) = -\frac{A'(z)}{2} - \frac{1}{4}A(z)^2 - B(z). \tag{D.12}$$

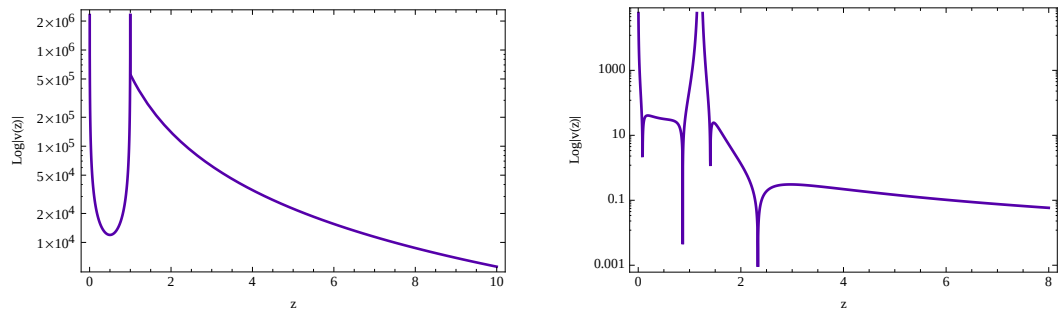

(a) **(b)**

Figure D.3: (a): potential $\log|v(z)|$ at $D = 1500$ for $\ell = 2$ at and $\kappa = 2$. (b): potential $\log|v(z)|$ at $D = 8$ for $\ell = 2$ and $\kappa = 2$

This potential is represented in figure (D.3a) and (D.3b) for $D = 1500$ and $D = 8$ respectively. One should note that the mass parameter, $\bar{\mu}$, for large-D is in the interval $[0, \frac{1}{2e}]$. It can be seen that at large-D the distance between two real positive roots of $f(z)$ is vanished implementing that at large-D the metric may have much simpler form.

Thus we find out that to take the large-D limit it is more appropriate to perform the following changes in the coordinates of metric (D.6)

$$z = y^{1/D+1}, \qquad \zeta = \frac{\tilde{\zeta}}{D+1} + \log(D+1), \tag{D.13}$$

then we will have

$$ds^2 = \frac{e^{2\tilde{\zeta}/(D+1)}}{y^{(D+2)/(D+1)}}\left((1 - y^{1/(D+1)} + \frac{2\bar{\mu}y}{D})d\tilde{\zeta}^2 - dyd\tilde{\zeta}\right) + \frac{e^{2\zeta}}{4y^{2/(D+1)}}d\Omega^2_{D+1} \tag{D.14}$$

looking at the (D.14) one finds that at large-D limit the $g_{\tilde{\zeta}\tilde{\zeta}}$ part of the metic will be zero. To be more close to the point where the null line z_- meets the vanishing point, once more we implement the following change

$$y = y_- - \tilde{y} \tag{D.15}$$

where y_- is equivalent to z_-. Thus at large-D one finds

$$ds^2 = \frac{1}{(y_- - \tilde{y})} d\tilde{y} d\tilde{\zeta} + r_0^2 e^{-4\Phi/(D+1)} d\Omega_{D+1}^2, \tag{D.16}$$

where

$$r_0 = \frac{1}{2y_-^{1/(D+1)}}, \qquad \text{and} \qquad \Phi = \frac{-1}{2}(\tilde{\zeta} + \frac{\tilde{y}}{y_-}) \tag{D.17}$$

It should be noted that $\frac{\tilde{y}}{y_-}$ is a very small value compareing with y_- and we used this approximation to get the Φ. Furthermore we only kept the first term when we were rescaling the ζ using (D.13). Metric (D.16) is the standard dilaton vacuum solution to $2D$ string theory [94]. One can find this by comparing (D.16) with

$$ds^2 = g_{\mu\nu} dx^\mu dx^\nu + r_0^2 e^{-4\Phi/(D+1)} d\Omega_{D+1}^2. \tag{D.18}$$

where $g_{\mu\nu}$ is a $2D$ metric and Φ is a scalar field. Moreover the D-dimensional action of this metric at large D

$$I = \frac{\Omega_{D+1} r_0^{D+1}}{16\pi G_2} \int dx^2 \sqrt{-g} e^{-2\Phi} \left(R + \frac{4D}{D+1} (\nabla\Phi)^2 + \frac{D(D+1)}{r_0^2} e^{4\Phi/(D+1)} \right), \tag{D.19}$$

reduces to the 2D string action

$$I = \frac{1}{16\pi G_2} \int dx^2 \sqrt{-g} e^{-2\Phi} (R + 4(\nabla\Phi)^2 + 4\lambda^2), \tag{D.20}$$

where $\lambda = (D+1)/2r_0$ and

$$G_2 = \lim_{D\to\infty} \frac{G}{\Omega_{D+1} r_0^{D+1}}. \tag{D.21}$$

Geometry of (D.18) is a well known geometry and considering any perturbation of this geometry gives us an infinite number of massive two dimensional non-minimally coupled massive scalers.

Bibliography

[1] Panagiota Kanti. **Footprints of higher-dimensional decaying black holes**. *Rom.J.Phys.*, **57**:879–893, 2012. vii, 37

[2] E. S. C. Ching, P. T. Leung, W. M. Suen, and K. Young. **Wave propagation in gravitational systems: Late time behavior**. *Phys. Rev.*, **D52**:2118–2132, 1995. ix, 63, 64

[3] A. Zhidenko R. A. Konoplya. **Quasinormal modes of black holes: from astrophysics to string theory**. *Rev.Mod.Phys.*, **83**:793–836, 2011. ix, 57, 60, 63, 64, 66, 67

[4] M. Shibata and H. Yoshino. **Bar-mode instability of rapidly spinning black hole in higher dimensions: Numerical simulation in general relativity**. *Phys. Rev.*, **D81**:104035, 2010. ix, 71, 82

[5] R. A. Konoplya and A. Zhidenko. **(In)stability of D-dimensional black holes in Gauss-Bonnet theory**. *Phys. Rev.*, **D77**:104004, 2008. ix, 72

[6] Roberto Emparan and Kentaro Tanabe. **Universal quasinormal modes of large D black holes**. *Phys. Rev.*, **D89**(6):064028, 2014. ix, 79, 80

[7] S. Creek, O. Efthimiou, P. Kanti, and K. Tamvakis. **Graviton emission in the bulk from a higher-dimensional Schwarzschild black hole**. *Phys.Lett.*, **B635**:39–49, 2006. ix, 33, 34, 92, 93, 94

[8] David Finkelstein. **Past-future asymmetry of the gravitational field of a point particle**. *Phys. Rev.*, **110**(4):965–967, 1958. 4

[9] R. Penrose. **Gravitational collapse: The role of general relativity**. *Riv. Nuovo Cim.*, **1**:252–276, 1969. [Gen. Rel. Grav.34,1141(2002)]. 4

[10] Matt Visser. **The Kerr spacetime: A brief introduction**. In *Kerr Fest: Black Holes in Astrophysics, General Relativity and Quantum Gravity Christchurch, New Zealand, August 26-28, 2004*, 2007. 5

[11] W. Israel. **Event horizons in static vacuum space-times**. *Phys. Rev.*, **164**:1776–1779, 1967. 8

[12] B. Carter J. M. Bardeen and S. W. Hawking. **The four laws of black hole mechanics**. *Commun. Math. Phys.*, **31**:161–170, 1973. 8

[13] J. D. Bekenstein. **Black holes and entropy**. *Phys. Rev. D*, **7**:2333–2346, 1973. 8, 9

[14] S. W. Hawking. **Particle creation by black holes**. *Commun. Math. Phys.*, **43**:199–220, 1975. 8, 13

[15] Werner Israel. **Event horizons in static vacuum space-times**. *Phys. Rev.*, **164**(5):1776–1779, 1967. 8

[16] Gary T. Horowitz. *'Quantum States of Black Holes' in Black Holes and Relativistic Stars*. University of Chicago Press, Chicago, U.S.A., 1998. 10

[17] Nima Arkani-Hamed, Savas Dimopoulos, and G.R. Dvali. **The hierarchy problem and new dimensions at a millimeter**. *Phys.Lett.*, **B429**:263–272, 1998. 14

[18] Vardan Khachatryan et al. **Search for microscopic black hole signatures at the Large Hadron Collider**. *Phys.Lett.*, **B697**:434–453, 2011. 14

[19] Greg L. Landsberg. **Discovering new physics in the decays of black holes**. *Phys. Rev. Lett.*, **88**:181801, 2002. 15

[20] Roberto Emparan, Manuel Masip, and Riccardo Rattazzi. **Cosmic rays as probes of large extra dimensions and TeV gravity**. *Phys. Rev.*, **D65**:064023, 2002. 15

[21] S.A. Teukolsky and W.H. Press. **Perturbations of a rotating black hole. III - Interaction of the hole with gravitational and electromagnet ic radiation**. *Astrophys.J.*, **193**:443–461, 1974. 17

[22] Richard Brito, Vitor Cardoso, and Paolo Pani. **Superradiance**. 2015. [arXiv: gr-qc /1501.06570]. 17

[23] Steven B. Giddings and Scott Thomas. **High energy colliders as black hole factories: The end of short distance physics**. *Phys. Rev. D*, **65**(056010), 2002. 20

[24] W. T. ZAUMEN. **Upper bound on the electric charge of a black hole**. *Nature*, **247**:530–531, 1974. 21

[25] Robert C. Myers and M. J. Perry. **Black holes in higher dimensional space-times**. *Annals Phys.*, **172**:304, 1986. 21, 34

[26] Roberto Emparan, Gary T. Horowitz, and Robert C. Myers. **Black holes radiate mainly on the brane**. *Phys.Rev.Lett.*, **85**:499–502, 2000. 21

[27] Bruce P. Jensen Nils Andersson. **Scattering by black holes**. 2000. [arXiv:gr-qc/0011025]. 23

[28] Jorge Escobedo. *Greybody factors, Hawking radiation in disgise*. Master's thesis, University of Amesterdam, 2008. 23

[29] Panagiota Kanti and Elizabeth Winstanley. **Hawking radiation from higher-dimensional black holes**. *Fundam.Theor.Phys.*, **178**:229–265, 2015. 28

[30] Vitor Cardoso, Marco Cavaglia, and Leonardo Gualtieri. **Hawking emission of gravitons in higher dimensions: Non-rotating black holes**. *JHEP*, **0602**:021, 2006. 28

[31] Chris M. Harris and Panagiota Kanti. **Hawking radiation from a (4+n)-dimensional black hole: Exact results for the Schwarzschild phase**. *JHEP*, **0310**:014, 2003. 28, 31, 32, 33

[32] A. Neitzke L. Motl. **Asymptotic black hole quasinormal frequencies**. *Adv. Theor. Math. Phys.*, **7**:307–330, 2003. 29, 59

[33] Mirjam Cvetic and Finn Larsen. **Greybody factors for black holes in four-dimensions: Particles with spin**. *Phys.Rev.*, **D57**:6297–6310, 1998. 31

[34] Panagiota Kanti and John March-Russell. **Calculable corrections to brane black hole decay. 2. Greybody factors for spin 1/2 and 1**. *Phys.Rev.*, **D67**:104019, 2003. 31, 32

[35] Panagiota Kanti and John March-Russell. **Calculable corrections to brane black hole decay. 1. The scalar case**. *Phys.Rev.*, **D66**:024023, 2002. 31

[36] Hideo Kodama and Akihiro Ishibashi. **A master equation for gravitational perturbations of maximally symmetric black holes in higher dimensions**. *Prog.Theor.Phys.*, **110**:701–722, 2003. 33

[37] Alan S. Cornell, Wade Naylor, and Misao Sasaki. **Graviton emission from a higher-dimensional black hole**. *JHEP*, **0602**:012, 2006. 33, 34

[38] Daisuke Ida, Kin-ya Oda, and Seong Chan Park. **Rotating black holes at future colliders: Greybody factors for brane fields**. *Phys.Rev.*, **D67**:064025, 2003. 34, 35, 36

[39] Marc Casals, P. Kanti, and E. Winstanley. **Brane decay of a (4+n)-dimensional rotating black hole. II. Spin-1 particles**. *JHEP*, **0602**:051, 2006. 34

[40] G. Duffy, C. Harris, P. Kanti, and E. Winstanley. **Brane decay of a (4+n)-dimensional rotating black hole: Spin-0 particles**. *JHEP*, **0509**:049, 2005. 34

[41] S. Creek, O. Efthimiou, P. Kanti, and K. Tamvakis. **Greybody factors for brane scalar fields in a rotating black-hole background**. *Phys.Rev.*, **D75**:084043, 2007. 34

[42] S. Creek, O. Efthimiou, P. Kanti, and K. Tamvakis. **Greybody factors in a rotating black-hole background. II. Fermions and gauge bosons**. *Phys.Rev.*, **D76**:104013, 2007. 34

[43] Marc Casals, S.R. Dolan, P. Kanti, and E. Winstanley. **Brane decay of a (4+n)-dimensional rotating black hole. III. Spin-1/2 particles**. *JHEP*, **0703**:019, 2007. 34, 36

[44] M. Casals, S.R. Dolan, P. Kanti, and E. Winstanley. **Bulk emission of scalars by a rotating black hole**. *JHEP*, **0806**:071, 2008. 34, 36, 38

[45] S. Creek, O. Efthimiou, P. Kanti, and K. Tamvakis. **Scalar emission in the bulk in a rotating black hole background**. *Phys.Lett.*, **B656**:102–111, 2007. 34, 36

[46] P. Kanti, H. Kodama, R.A. Konoplya, N. Pappas, and A. Zhidenko. **Graviton emission in the bulk by a simply rotating black hole**. *Phys.Rev.*, **D80**:084016, 2009. 34, 36, 38, 39

[47] S.A. Teukolsky. **Rotating black holes - separable wave equations for gravitational and electromagnetic perturbations**. *Phys.Rev.Lett.*, **29**:1114–1118, 1972. 35

[48] Saul A. Teukolsky. **Perturbations of a rotating black hole. 1. Fundamental equations for gravitational electromagnetic and neutrino field perturbations**. *Astrophys.J.*, **185**:635–647, 1973. 35

[49] Panagiota Kanti. **Black holes in theories with large extra dimensions: A review**. *Int.J.Mod.Phys.*, **A19**:4899–4951, 2004. 36

[50] James A. Frost, Jonathan R. Gaunt, Marco O.P. Sampaio, Marc Casals, Sam R. Dolan, et al. **Phenomenology of production and decay of spinning extra-dimensional black holes at hadron colliders**. *JHEP*, **0910**:014, 2009. 39, 117

[51] De-Chang Dai, Glenn Starkman, Dejan Stojkovic, Cigdem Issever, Eram Rizvi, et al. **BlackMax: A black-hole event generator with rotation, recoil, split branes, and brane tension**. *Phys.Rev.*, **D77**:076007, 2008. 39, 117

[52] Torbjorn Sjostrand. **PYTHIA 5.7 and jetset 7.4 physics and manual**. *Comp. Phys. Comm.*, **82**:74, 1994. 40

[53] HERWIG 6.5 release note. [arXiv:hep-ph/0210213]. 40

[54] M. V. Garzelli, M. O'Loughlin, and S. Nafooshe. **Cosmic ray induced micro black hole showers**. In *13th International Conference on Nuclear Reaction Mechanisms Varenna, Italy, June 11-15, 2012*, pages 525–530, 2012. 47

[55] Saeede Nafooshe, Martin O'Loughlin, and Maria Vittoria Garzelli. **Micro Black Hole Production and Evaporation**. *Proceedings of the 4th Conference on Time and Matter - TAM 2013, pp 175 - 181, UNG press (ISBN 978-961-6311-79-3)*, 12 2013. 51

[56] C. V. VISHVESHWARA. **Scattering of gravitational radiation by a Schwarzschild black-hole**. *Nature*, (227):936–938, 1970. 55

[57] R. Ruffini. **Gravitational radiation from a mass projected into a Schwarzschild black hole**. *Phys. Rev.*, **D7**:972–976, 1973. 55

[58] M. Davis, R. Ruffini, W. H. Press, and R. H. Price. **Gravitational radiation from a particle falling radially into a Schwarzschild black hole**. *Phys. Rev. Lett.*, **27**:1466–1469, 1971. 55

[59] M. Davis, R. Ruffini, and J. Tiomno. **Pulses of gravitational radiation of a particle falling radially into a Schwarzschild black hole**. *Phys. Rev.*, **D5**:2932–2935, 1972. 55

[60] Kostas D. Kokkotas and Bernd G. Schmidt. **Quasinormal modes of stars and black holes**. *Living Rev. Rel.*, **2**:2, 1999. 56

[61] Vitor Cardoso. *Quasinormal Modes and Gravitational Radiation in Black Hole Spacetimes*. PhD thesis, Instituto Superior Tecnico, December 2003. 57, 64

[62] **http://lisa.nasa.gov** [online]. 57

[63] **http://wwwcascina.virgo.infn.it** [online]. 57

[64] **http://www.ligo.caltech.edu** [online]. 57

[65] J. M. Maldacena. **The large N limit of superconformal field theories and supergravity**. *Adv. Theor. Math. Phys.*, **2**:231–252, 1998. 58

[66] Alvaro Nunez and Andrei O. Starinets. **AdS / CFT correspondence, quasinormal modes, and thermal correlators in N=4 SYM**. *Phys. Rev.*, **D67**:124013, 2003. 58

[67] Born M. *Atomic physics*. London: Blackie and Son Ltd., 8th edition, 1969. 58

[68] Jacob D. Bekenstein. **Black holes: Classical properties, thermodynamics and heuristic quantization**. In *9th Brazilian School of Cosmology and Gravitation (BSCG 1998) Rio de Janeiro, Brazil, July 27-August 7, 1998*, 1998. [gr-qc/9808028]. 58

[69] J. D. Bekenstein. **The quantum mass spectrum of the Kerr black hole**. *Lett. Nuovo Cim.*, **11**:467, 1974. 58

[70] Hod S. **Bohr's correspondence principle and the area spectrum of quantum black holes**. *Phys. Rev. Lett.*, **81**(4293), 1998. 58, 59

[71] Hans-Peter Nollert. **Quasinormal modes of Schwarzschild black holes: The determination of quasinormal frequencies with very large imaginary parts**. *Phys. Rev.*, **D47**:5253–5258, 1993. 59, 69

[72] L. Motl. **An analytical computation of asymptotic Schwarzschild quasinormal frequencies**. *Adv. Theor. Math. Phys.*, **6**:1135–1162, 2003. 59

[73] Elcio Abdalla, Cecilia B. M. H. Chirenti, and Alberto Saa. **Quasinormal modes for the Vaidya metric**. *Phys. Rev.*, **D74**:084029, 2006. 60

[74] Cheng-Gang Shao, Bin Wang, Elcio Abdalla, and Ru-Keng Su. **Quasinormal modes in time-dependent black hole background**. *Phys. Rev.*, **D71**:044003, 2005. 60, 68

[75] Bin Wang Li-Hui Xue, Zai-Xiong Shen and Ru-Keng Su. **Numerical simulation of quasi-normal modes in time-dependent background**. *Mod.Phys.Lett.*, **A19**(239), 2004. 61

[76] Nils Andersson and Hisashi Onozawa. **Quasinormal modes of nearly extreme Reissner-Nordstrom black holes**. *Phys. Rev.*, **D54**:7470–7475, 1996. 61

[77] Qiyuan Pan Jiliang Jing. **Quasinormal modes and second order thermodynamic phase transition for Reissner-Nordstrom black hole**. *Phys.Lett.B.*, **660**:13–18, 2008. 61

[78] Edward Seidel and Sai Iyer. **Black hole normal modes: a WKB approach. 4. Kerr black holes**. *Phys. Rev.*, **D41**:374–382, 1990. 61

[79] Emanuele Berti, Vitor Cardoso, Kostas D. Kokkotas, and Hisashi Onozawa. **Highly damped quasinormal modes of Kerr black holes**. *Phys. Rev.*, **D68**:124018, 2003. 62

[80] Richard H. Price. **Nonspherical perturbations of relativistic gravitational collapse. 1. Scalar and gravitational perturbations**. *Phys. Rev.*, **D5**:2419–2438, 1972. 62

[81] Carsten Gundlach, Richard H. Price, and Jorge Pullin. **Late time behavior of stellar collapse and explosions: 1. Linearized perturbations**. *Phys. Rev.*, **D49**:883–889, 1994. 62, 66

[82] Carsten Gundlach, Richard H. Price, and Jorge Pullin. **Late time behavior of stellar collapse and explosions: 2. Nonlinear evolution**. *Phys. Rev.*, **D49**:890–899, 1994. 62

[83] R. A. Konoplya and C. Molina. **Late time tails of the massive vector field in a black hole background**. *Phys. Rev.*, **D75**:084004, 2007. 64

[84] Bahram Mashhoon Valeria Ferrari. **Oscillations of a black hole**. *Phys. Rev. Lett.*, **52**(16), 1984. 68

[85] A. Zhidenko. **Quasi-normal modes of Schwarzschild-de Sitter black holes**. *Class.Quant.Grav.*, **21**:273–280, 2004. 68

[86] E. W. Leaver. **An analytic representation for the quasi-normal modes of Kerr black holes**. *Proceedings of the Royal Society of London. Series A*, **402**(1823):285–298, 1985. 68

[87] Masaru Shibata and Hirotaka Yoshino. **Nonaxisymmetric instability of rapidly rotating black hole in five dimensions**. *Phys. Rev.*, **D81**:021501, 2010. 70

[88] R. A. Konoplya, Keiju Murata, Jiro Soda, and A. Zhidenko. **Looking at the Gregory-Laflamme instability through quasi-normal modes**. *Phys. Rev.*, **D78**:084012, 2008. 71

[89] G. 't Hoof. **A planar diagram theory for strong interactions**. *Nuclear Physics B*, **72**:461–473, 1973. 73

[90] Roberto Emparan, Ryotaku Suzuki, and Kentaro Tanabe. **The large D limit of general relativity**. *JHEP*, **1306**:009, 2013. 74, 85, 90, 115

[91] Andrew Strominger. **The inverse dimensional expansion in quantum gravity**. *Phys. Rev.*, **D24**:3082, 1981. 74

[92] Fabrizio Canfora, Alex Giacomini, and Alfonso R. Zerwekh. **Kaluza-Klein theory in the limit of large number of extra dimensions**. *Phys. Rev.*, **D80**:084039, 2009. 74

[93] Herbert W. Hamber and Ruth M. Williams. **Quantum gravity in large dimensions**. *Phys. Rev.*, **D73**:044031, 2006. 74

[94] D. Grumillerc R. Emparan and K. Tanabeb. **Large D gravity and low D strings**. *Phys. Rev.Lett.*, **110**(251102), 2013. 75, 76, 143

[95] Hari K. Kunduri, James Lucietti, and Harvey S. Reall. **Gravitational perturbations of higher dimensional rotating black holes: Tensor perturbations**. *Phys. Rev.*, **D74**:084021, 2006. 77

[96] Roberto Emparan, Ryotaku Suzuki, and Kentaro Tanabe. **Instability of rotating black holes: large D analysis**. *JHEP*, **06**:106, 2014. 77, 78, 80, 82

[97] Roberto Emparan, Ryotaku Suzuki, and Kentaro Tanabe. **Decoupling and non-decoupling dynamics of large D black holes**. *JHEP*, **07**:113, 2014. 79

[98] R. Monteiro H. S. Reall O. J. C. Dias, P. Figueras and J. E. Santos. **An instability of higher-dimensional rotating black holes**. *JHEP*, **05**(76), 2010. 82, 125

[99] Gavin S. Hartnett and Jorge E. Santos. **Non-axisymmetric instability of rotating black holes in higher dimensions**. *Phys.Rev.*, **D88**:041505, 2013. 82, 83

[100] P.C. Vaidya. **The external field of a radiating star in general relativity**. *Current Sience*, **12 (06)**:183, 1943. 95

[101] T. Zannias. **Spacetimes admitting a three-parameter group of isometries and quasilocal gravitational mass**. *Phys. Rev.*, **D41**(10):3252–3254, 1990. 95

[102] Alex B. Nielsen and Dong-han Yeom. **Spherically symmetric trapping horizons, Misner-Sharp mass and black hole evaporation**. *Int. J. Mod. Phys.*, **A24**:5261–5285, 2009. 95

[103] Sijie Gao and Jose P.S. Lemos. **The Tolman-Bondi-Vaidya spacetime: Matching timelike dust to null dust**. *Phys.Rev.*, **D71**:084022, 2005. 95

[104] W.A. Hiscock, L.G. Williams, and D.M. Eardley. **Creation of particles by shell focusing singularities** . *Phys.Rev.*, **D26**:751–760, 1982. 96, 98

[105] Anzhong Wang and Yumei Wu. **Generalized Vaidya solutions**. *General Relativity and Gravitation*, **31**(1):107–114, 1999. 97

[106] Robert P. Geroch. **What is a singularity in general relativity?** *Annals Phys.*, **48**:526–540, 1968. 98

[107] Kayll Lake. **Naked singularities in gravitational collapse which is not self-similar**. *Phys. Rev.*, **D43**(4):1416–1417, 1991. 98

[108] B. Waugh and Kayll Lake. **Double-null coordinates for the Vaidya metric**. *Phys. Rev.*, **D34**(10):2978–2984, 1986. 99, 100, 101

[109] W. G. Unruh. **Collapse of radiating fluid spheres and cosmic censorship**. *Phys. Rev.*, **D31**(10):2693–2694, 1985. 99, 101

[110] Martin O'Loughlin. **A linear mass Vaidya metric at the end of black hole evaporation**. *Phys. Rev.*, **D91**(044020), 2 2015. 100, 101, 102, 103, 111, 140

[111] Li-Hui Xue, Zai-Xiong Shen, Bin Wang, and Ru-Keng Su. **Numerical simulation of quasinormal modes in time dependent background**. *Mod. Phys. Lett.*, **A19**:239, 2004. 107

[112] Shahar Hod. **Wave tails in time dependent backgrounds**. *Phys. Rev.*, **D66**:024001, 2002. 107, 114

[113] Shahar Hod. **How pure is the tail of gravitational collapse?** *Class. Quant. Grav.*, **26**:028001, 2009. 107

[114] Matthew W. Choptuik. **Universality and scaling in gravitational collapse of a massless scalar field**. *Phys. Rev. Lett.*, **70**:9–12, 1993. 115

[115] BR Iyer and CV Vishveshwara. **The Vaidya solution in higher dimensions**. *Pramana-Journal of Physics*, **32**(6):749–752, 1989. 115, 139

[116] SG Ghosh and Naresh Dadhich. **Naked singularities in higher dimensional Vaidya space-times**. *Phys. Rev.*, **D64**(4):047501, 2001. 139